How good is the calibrated steady-state model of the Hollandse Graven catchment for predicting its hydrological system regimes under wet and dry climate conditions?

GEDEFAW TADELE ASNAKEW

January, 2024

SUPERVISORS:
Dr. Yijian Zeng
Dr. Ir. Maciek W. Lubczynski

ADVISOR:
Mostafa Gomaa Daoud

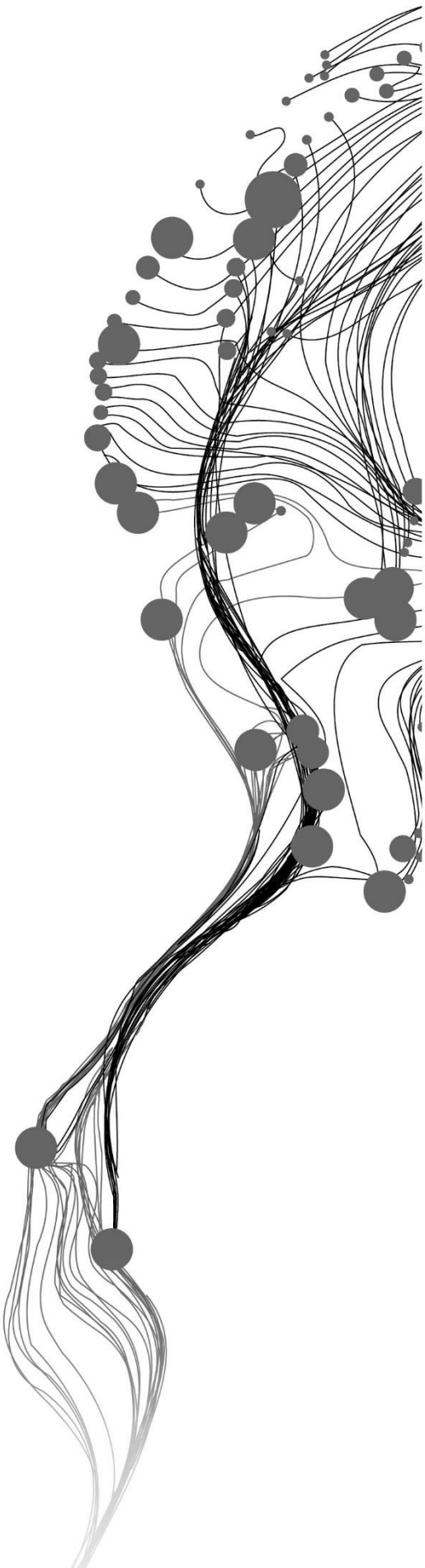

How good is the calibrated steady-state model of the Hollandse Graven catchment for predicting its hydrological system regimes under wet and dry climate conditions?

GEDEFAW TADELE ASNAKEW
Enschede, The Netherlands, January, 2024

Thesis submitted to the Faculty of Geo-Information Science and Earth Observation of the University of Twente in partial fulfilment of the requirements for the degree of Master of Science in Geo-information Science and Earth Observation.
Specialization: Water Resources and Environmental Management

SUPERVISORS:
Dr. Yijian Zeng
Dr. Ir. Maciek W. Lubczynski

ADVISOR:
Mostafa Gomaa Daoud

THESIS ASSESSMENT BOARD:
Dr. Tom H.M. Rientjes (Chair)
Dr. Jacek Gurwin (External Examiner, University of Wroclaw, Poland)

ABSTRACT

A steady-state groundwater flow model for the Hollandse graven catchment, the Netherlands, has been developed using MODFLOW 6. The model was developed to examine its predictive capability of hydrological system regime in a transient state under 2017 wet (834.33 mm. $year^{-1}$) and 2018 dry (650 mm. $year^{-1}$) climatic conditions. Six hydrological years, 2010-2015, of driving forces and groundwater level measurements from 44 piezometers have been used to calibrate the groundwater model with nine hydrological units.

In the steady-state groundwater model calibration, a reasonable agreement between observed and simulated hydraulic heads has been achieved. Mean error (ME) is as low as zero, while mean absolute error (MAE), and root mean square error (RMSE) are of 0.34 and 0.42 meters, respectively. The calibrated steady-state groundwater model was further validated with independent groundwater level datasets from 33 piezometers of the 2016 hydrological year. ME of -0.03, MAE of 0.41, and RMSE of 0.55 meters have been obtained in the model validation.

Driving forces of the wet and dry year and groundwater level measurements from 61 piezometers have been used to test the predictive capability of the calibrated steady-state groundwater model in monthly transient stress period simulations. The model's predictive capability was evaluated using visual observation graphs and error metrics. For the overall simulation period, an ME of 0.45, MAE of 1.08 and RMSE of 1.29 meters have been obtained, and 90.2 % of the piezometers demonstrated an MAE of ≤ 1.71 meters and RMSE of ≤ 1.8 meters. Compared to the dry year, the model's predictive capability is more effective in the wet year simulation. In the wet year, 90.9 % of the piezometers demonstrated an MAE of ≤ 1.89 meters and 96.9% an RMSE of ≤2 meters. In the dry year, however, 84.8% of the piezometers have an MAE of ≤1.89, and 81.8 % an RMSE of ≤ 1.8.

Water balance discrepancies of the whole catchment are found to be as low as 1.81 % and -0.02 % for wet and dry years, respectively. Groundwater gross recharge accounts for 23.69% and 23.42% of precipitation for wet and dry years, respectively. However, while 24.42 % of the gross recharge transforms into net recharge in the wet year, only 1.22% of the gross recharge becomes net recharge in the dry year. Total evapotranspiration accounts 42.95% and 59.45% of the precipitation during wet and dry years, respectively.

Based on the analysis of overall observed versus simulated hydraulic head, water balance discrepancy, and error metrics assessment, it can be concluded that the steady-state calibrated groundwater model of the Hollandse graven catchment can predict the hydrological water regimes under 2017 wet and 2018 dry climatic conditions. Nevertheless, the application of steady-state calibrated groundwater model for transient prediction still encounters challenges in accurately replicating hydraulic heads across stress periods.

ACKNOWLEDGEMENT

Almighty God, I thank you so much for blessing me with the strength to face challenges during those difficult times of my life and for successfully completing my thesis.

I would like to thank the government of the Netherlands for providing me with financial support through the Orange Knowledge Programme (OKP) to study for my master's degree in science at ITC, the University of Twente.

Without the strong patience, continuous support, and encouragement of Dr. Yijian Zeng, my first supervisor, this work would not have successfully ended; I am sincerely thankful and respectful. I would like to express my deep gratitude and respect to Dr. Ir. Maciek W. Lubczynski, my second supervisor, for his valuable research tips, patient explanations on various topics, motivation, and guidance. His polite approach and clear and detailed explanations made it much easier to complete this work.

I am immensely grateful and hold great respect for Mr. Mostafa Gomaa Daoud, my advisor for his exceptional help in resolving the challenges I encountered throughout my journey. His availability for assistance, even outside regular office hours, reflects his incredible dedication to help. I would like to extend my deepest gratitude to Dr. Ir. Rogier van der Velde, my previous first supervisor, for his support, advice, encouragement, and friendly approach throughout our time together.

I am deeply grateful for drs. J.J. Verplanke, ITC programme manager; M.C.F. Metz-Bekkers, student advisor; Arno van Lieshout, and IR.G.N. Parodi, program director of water resources and environmental management, for their continuous administrative-related support during my challenging moments. I extend my heartfelt thanks to each of them.

I am proudly grateful to all my friends for their encouragement and support in various aspects. Your continuous support has meant the world to me, and I appreciate each one of you for being there during every step of my journey.

I am so grateful to Dr. Richard Winston, who generously provided me with the updated versions of ModelMuse, empowering me to tackle groundwater modelling challenges. His prompt and insightful responses to my questions have been invaluable, and I sincerely appreciate his support.

Last but certainly not least, I am at a loss for words to capture my profound love and respect for my family. They are my anchor, most excellent support, and the source of immeasurable joy and strength in my life.

TABLE OF CONTENTS

LIST OF FIGURES

LIST OF TABLES

1. INTRODUCTION

1.1. Background

Groundwater and surface water resources are essential for agricultural, industrial, recreational and other environmental activities with specific water quality standards (Dassargues, 2019). Managing those essential resources with the help of up-to-date tools is necessary for sustainable use. Numerical groundwater models are among the tools that are widely used to address groundwater-related problems. The type of groundwater problems to be solved determines the groundwater model type to be developed. According to Reilly and Harbaugh (2004), there are five main problems that initiate for groundwater modelling. Those five main problems are: basic understanding of the groundwater system, estimation of aquifer properties, understanding the past, understanding the present, and forecasting the future.

Predicting the responses of the aquifer to a specific action is the purpose of the majority of groundwater models (Anderson et al., 2015). Due to man-made or natural phenomena, changes in land use and climate conditions can happen in time. Predictive groundwater models are developed to predict aquifer response to those changes in climate conditions, land use, or pumping rates (Francés et al., 2011). There are studies conducted that focuses on the response of aquifers to the climate change (e.g., Ghazavi and Ebrahimi, 2019), change in recharge and pumping rate (e.g., Awais et al., 2023) and land use and land cover (Van Huijgevoort et al. 2020). Those studies focus on the transient response of aquifers based on transient conditions. However, studies that focus on the transient response of aquifers due to climate and land cover change based on steady-state calibration are limited, as per the assessment of the researcher. Trapp and Geiger (1986), and Moore and Doherty (2021) studied the transient response of aquifers to the change in pumping rates based on steady-state calibration and documented that steady-state calibration could be used for the transient prediction of groundwater resoources. Therefore, predictive groundwater models are important tools in addressing groundwater-related problems, like drought. However, due to their limited capacity in capturing real world complexity, wrong conceptual model, nonrepresentative state variables and unknown distribution of driving forces and parameters make their predictions uncertain (Barnett et al., 2012).

Depending on the purpose of the modelling practice and the nature of connections between surface water and groundwater components, groundwater and surface water predictive models can be developed separately. In areas where there is no significant flux exchange between the two components, only groundwater modelling approach with standard boundary conditions may be adequate (Barnett et al., 2012). Separate modelling practices use standalone models for surface water and groundwater features that only takes one component into consideration. However, due to the fact that groundwater, surface water and

related aquatic ecosystems are interconnected as one management unit, water management practices are shifting towards an integrated hydrological model (Ala-aho et al., 2015). These integrated hydrological models are crucial to add water balance constraints that are absent in single-system models and to understand and capture the interaction between the surface and groundwater systems. In addition to that integrated hydrological models are crucial instruments for the determination of recharge and discharge conditions since it incorporates the major hydrological processes (Spanoudaki et al., 2009). According to Barnett et al. (2012), a modelling approach based on the coupling of surface and groundwater models should be used when surface water dynamics are significantly affected by exchange flows.

Hendriks et al. (2014), conducted research in the Hollands Graven catchment that aims to understand the impact of anthropogenic alterations and climate change on the environmental baseflow needs of streams. The results of their study showed that even though under normal years the baseflow meets the environmental needs of streams, during drought years it is probably insufficient. This indicates that during drought years the exchange between surface water and groundwater becomes reduced while it is higher during wet or normal seasons. The frequent occurrence of drought in the last six years causes a lot of damage in different sectors of the Netherlands like agriculture, industry and nature (Philip et al., 2020; Pouwels et al., 2020). Therefore, there is an urgent need to apply the integrated hydrological modelling to understand the hydrological system regimes in the Netherlands under wet and dry climate conditions, the knowledge of which will support the development of climate adaptation measures to manage drought risks.

1.2. Surface-groundwater interaction processes

It is important to understand the interaction mechanisms between surface water and groundwater to develop the predictive groundwater model. The occurrence of enough amount of precipitation leads to the main processes: infiltration into the unsaturated zone which further may recharge to the phreatic groundwater reservoir, evapotranspiration back to the atmosphere and surface runoff to streams and other water bodies. Depending on the height of groundwater and stream water level, streams may interact with groundwater in three ways: gaining streams, loosing streams and both gaining and loosing streams (Sophocleous et al., 1988; Winter et al., 1999).

Gaining streams refers to streams that gain water from groundwater as the groundwater discharge process because of the altitude of groundwater is higher than the stream surface level. Losing streams are those that lose water as recharge due to the altitude of stream surface water level is greater than that of water table (Figure 1.1). Other streams may lose water at some reaches and gain at others depending on the altitude difference. A major contributor to streams and other surface water bodies can be groundwater while surface water can recharge back to groundwater.

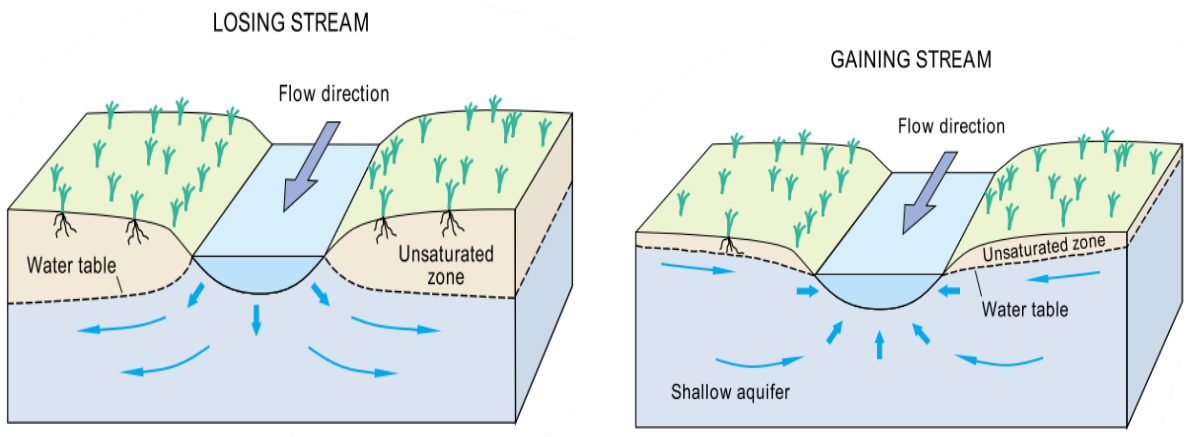

Figure 1.1. Gaining and losing streams that show the interactions between surface water and groundwater Source: (Winter et al., 1999)

In the interaction of losing streams and groundwater, the streams may directly interact with groundwater or first infiltration to the unsaturated zone and then from unsaturated zone recharge to the groundwater.

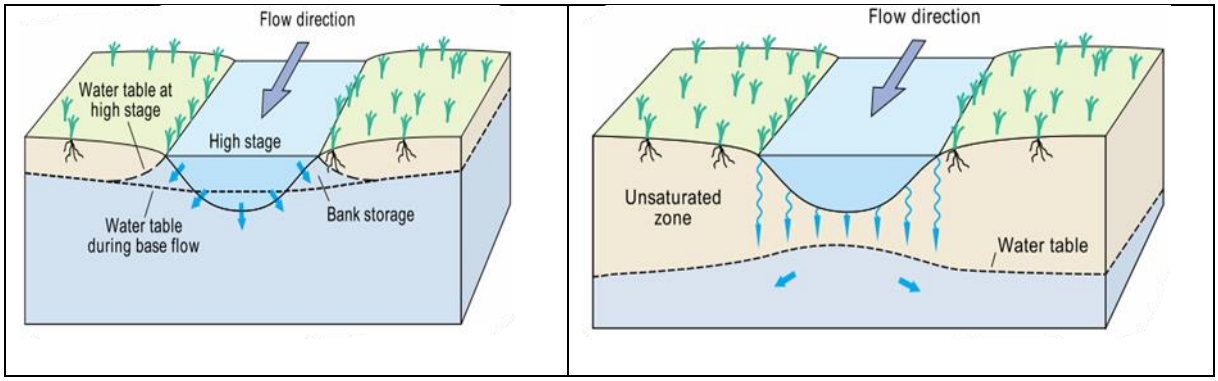

Figure 1.2. Connected streams (left), recharge is the process that connects the two components, whereas in disconnected streams (right) there is infiltration process to the unsaturated zone before recharge to the groundwater. Source: (Winter et al., 1999).

During drought times, the water level of surface water bodies gets lower or even dry if the contribution of groundwater component, baseflow, become lower. The occurrence of drought not only affects the surface water bodies, but it also propagates into the groundwater. As the research of Hendriks et al. (2014), showed, during high drought times, e.g., in 2003 in the Hollandse Graven catchment, streams dry out. The infiltration to the groundwater and the exfiltration to the streams decreases. When the surface water infiltration into the groundwater and vice versa processes are decreased, the water budget of the both the groundwater component and unsaturated zone component decreases. Considering the Hollandse Graven catchment is located in the high sandy region of the Netherlands and more susceptible to drought events, this study will focus on this catchment.

1.3. Hydrological regime, its change and prediction

The concept of hydrological regime can be used for surface water bodies like streams, rivers and wetlands and groundwater systems. Due to various types of interactions between surface water bodies and groundwater systems, the concept of hydrological regime can also be applied in an integrated hydrological modelling approach. Post and Jones (2001), studied the spatio-temporal relationships between streamflow from 18 basins and precipitation. The authors explained the hydrological regime of the basins as the relationships between streamflow outputs and precipitation inputs at various spatio-temporal ranges. Finlayson et al. (2018), explained the hydrological regime of wetlands as the dynamics of inflows, outflows, and storage of the system over space and time. Groundwater regime according to Zhou et al. (2013), is described as the temporal variability of groundwater level and its spatial distribution in response to hydrological stresses and anthropogenic influences. The authors classified the factors or characteristics that cause the spatio-temporal variation of groundwater level into five: land surface features, unsaturated zone attributes, saturated zone attributes, hydrological stresses, and anthropogenic factors. Land use and topography are grouped under land surface features that impact the processes of groundwater recharge and discharge. Geological characteristics of the unsaturated zone and water table depth, on the other hand, are attributes of the unsaturated zone that determine the timing of groundwater response to stresses. Saturated zone attributes are explained by boundary conditions and aquifer properties that can determine the spatio-temporal variation of groundwater level. Hydrological stresses include surface water bodies, precipitation, and evapotranspiration which are the main causes for the groundwater level fluctuations. Anthropogenic factors are those that are introduced by human beings that modify the natural flow of hydrological systems.

Surface and groundwater level changes temporally following the amount of water content that enter and leave the system under consideration. In combination with other factors, as explained above, climate conditions can determine the amount of water that enter and leave the system and hence groundwater level. The effect of climate and land use change on the Veluwe groundwater reservoir of the Netherlands has studied by Van Huijgevoort et al. (2020). The study was conducted for historical and future periods, and it is documented that groundwater level will be higher in the future periods in response to projected increase in winter precipitation; for the historical periods, groundwater recharge was more affected by land use than climate change. Obergfell et al. (2019), conducted research related to groundwater regime change on a phreatic aquifer found under a Pleistocene sand ridge in the eastern Netherlands, close to the present study area. The authors used time series analysis to identify and explain the groundwater regime change between the periods 1982 to 2005; it is documented that groundwater regime change had detected in the mid-1990s. The authors concluded that the detected groundwater regime change didn't show trends with precipitation, evaporation, and land use; it rather was due to dredging works in the Regge river.

Various methods can be used to predict the hydrological regime of a catchment for different stresses. Numerical hydrological models, Artificial Neural Network (ANN) and multiple linear regression (MLR) are among the methods researchers use to predict groundwater level fluctuations. Sahoo and Jha (2013), predicted transient groundwater levels using ANN and MLR methods with the aim to compare their predictive performance. Mohammed et al. (2023), calibrated and validated the groundwater model using groundwater Modelling System (GMS) and compared it with the artificial based models. Though machine learning methods require short time for model construction compared with numerical hydrological modes, they don't represent the complete physical systems for water balance computations (Di Salvo, 2022). MODFLOW is one of the widely used numerical hydrogeological model in the prediction of groundwater resources for different stress conditions (e.g., Awais et al., 2023; Ghazavi and Ebrahimi, 2019). Hence, MODFLOW 6 numerical groundwater model code has been chosen for this research due to its capacity to represent physical systems and its freely available.

The current study focusses on how good a steady-state groundwater model of the Hollandse graven catchment is in predicting its hydrological system regime due to the variations in hydrological stresses, particularly precipitation and evapotranspiration.

2. STUDY AREA

2.1. Location and topography of the study area

Dinkel river is a small meandering river found in the Netherlands and Germany. It is a sand-bed river with the total drainage basin of 643 km² (Wolfert et al., 2002). The current study area (Figure 2.1) is one of the sub-catchments, named Hollandse Graven catchment, of the Dinkel river basin located in the Overijssel province, The Netherlands and covers about 63 km². The study area is found in the Overijssel province and geographically bounded approximately between 483000 m-495000 m northing and 256000 m-265000 m easting, RD New projected coordinate system. The catchment incorporates streams and various land cover types. Most part of the study area is characterized by flat topography with the lowest elevation of 8.58 meters above mean sea level. However the north-western and southern-Eastern part reaches up to 78 meters.

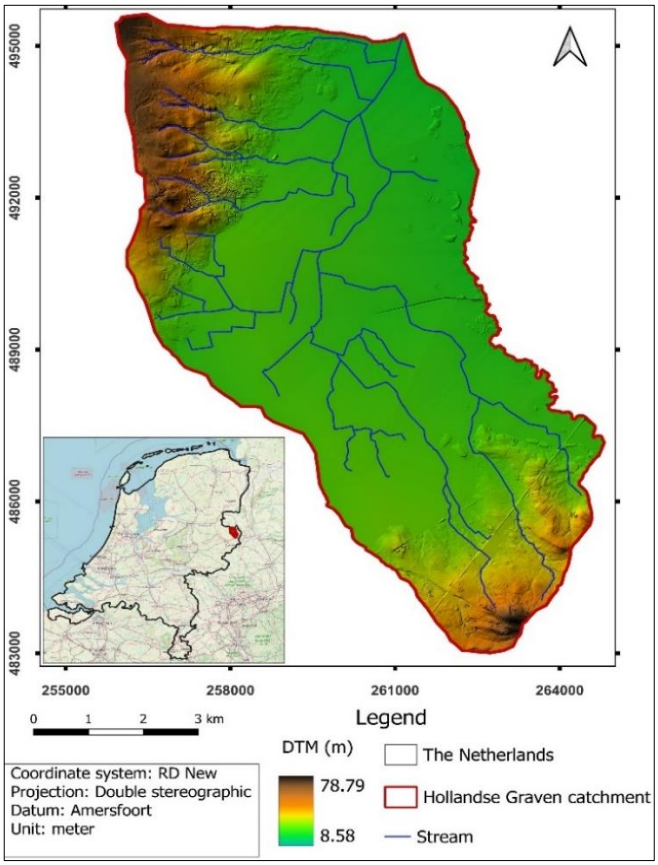

Figure 2.1. Location map of the study area. Note that: the coordinate system, projection, datum, and unit information used here apply to all the maps in this document. Digital Terain Model (DTM) source: AHN- https://www.ahn.nl/

2.2. Climate

Based on the Köppen-Geiger climate classification system, the climate of the Netherlands and hence the Hollandse Graven catchment is characterized by temperate oceanic climate (Cfb) ("Climate Change Knowledge Portal-https://climateknowledgeportal.worldbank.org/," n.d.). The country is characterized by an average monthly precipitation of approximately 40 mm in the month of April to 80 mm in December (Figure 2.2). The mean monthly temperature ranges from 3 °C in January to 18 °C in July and August. According to Hendriks et al. (2014), the Hollandse Graven catchment receives precipitation amount that ranges from 800 to 850 mm per year.

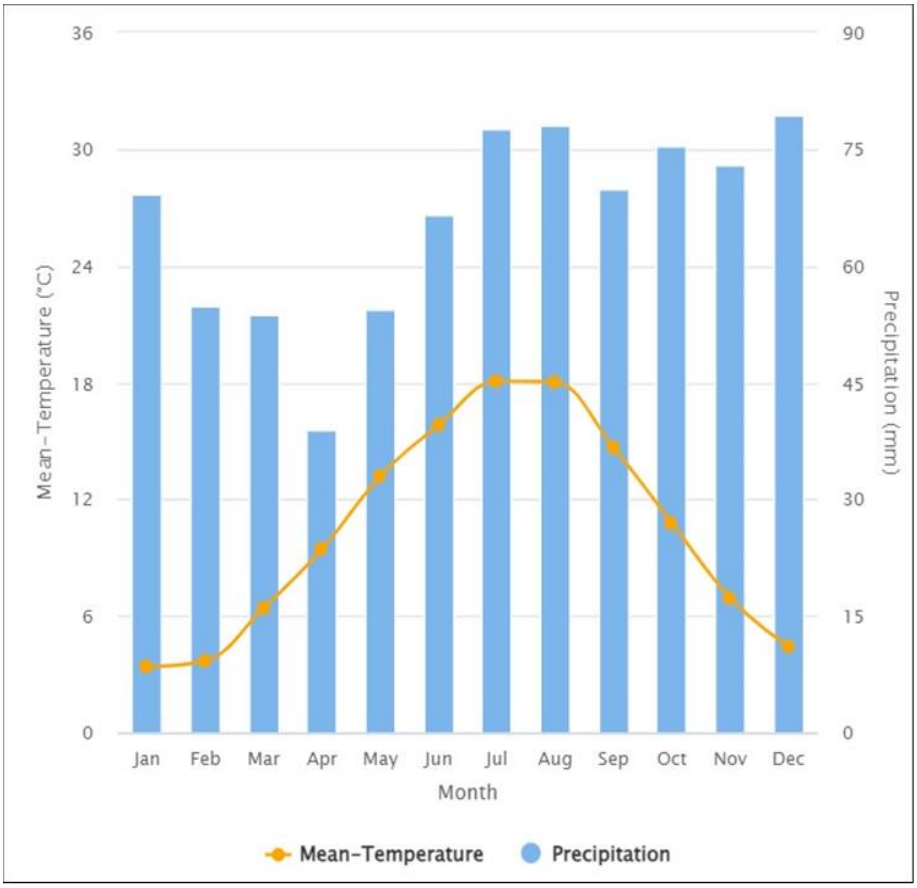

Figure 2.2. Monthly mean-temperature and precipitation of The Netherlands from 1991-2020. Source: https://climateknowledgeportal.worldbank.org/.

2.3. Land cover

CORINE land cover map of 2012 was available that could be used for hydrological studies. However, since it has small number of land cover classes for the Hollands Graven catchment, a land cover map with more classes has been prepared (Figure 2.3) to better conceptualize the system. The land cover map was prepared using the semi-automatic classification plugin (SCP) in Quantum Geographic Information System (QGIS).

Sentinel 2 MultiSpectral Instrument (MSI), 20 m resolution image taken on the 1st of October 2015 was used for the land cover map preparation. Since reference data that represent land cover classes of the study area for the modelling period are required to take spectral signatures, secondary data have been integrated. To take spectral signatures in the classification of the land cover map, the following reference data have been overlaid on the Sentinel 2 image. 1) The 2015 Basic registration of the crop field (BRP) of the Netherlands ("PDOK-https://www.pdok.nl/introductie/-/article/basisregistratie-gewaspercelen-brp-," n.d.) to take spectral signatures for various crops 2) CORINE land cover map ("CORINE Land Cover-https://land.copernicus.eu/en/products/corine-land-cover," n.d.) of 2012 to take spectral signatures for built-up areas, evergreen and deciduous trees and 3) Google earth image and OpenStreetMap to take spectral signatures for water bodies and to support number 2 for built-up areas. Those reference data were overlaid on the sentinel 2 MSI, 20 m resolution image and spectral signatures of each land cover class were taken. There are nine land cover classes in the study area (Figure 2.3), these are: built-up area, bare soil, wheat, corn, heather, grass, deciduous tree, ever green tree, and water. While grass is the dominant land cover, deciduous and evergreen trees are found on the northern, central and southern parts of the catchment.

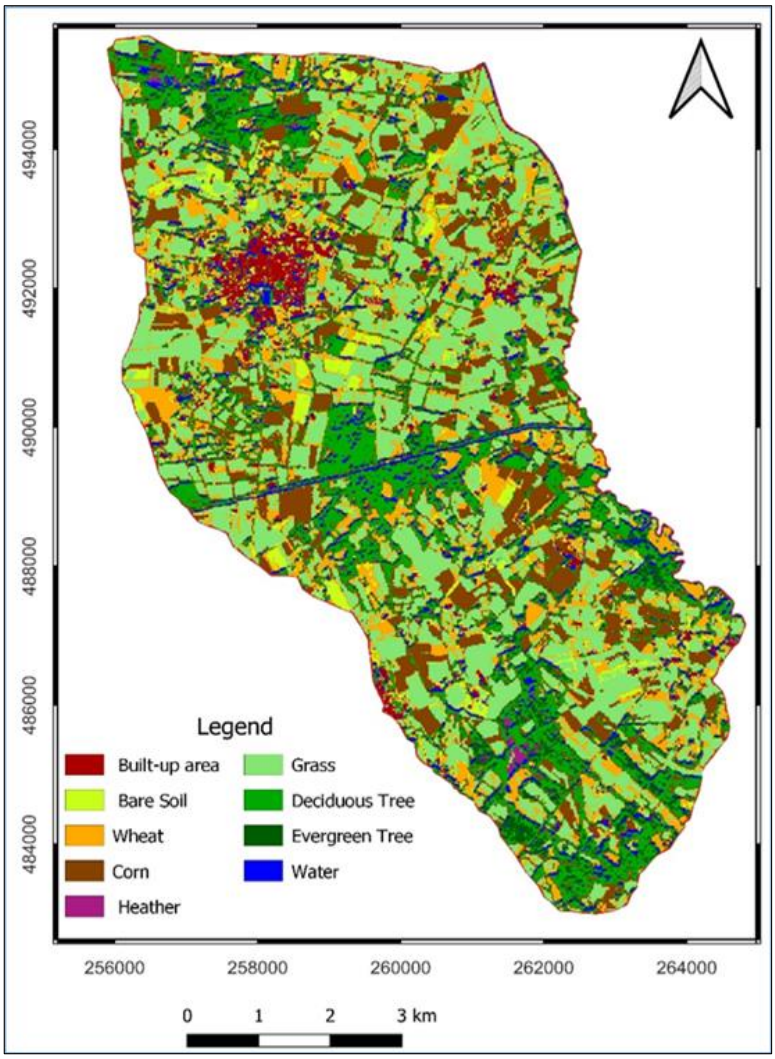

Figure 2.3. Land cover map of the study area

2.4. Soil

The geological and soil nature of an area play an important role in the hydrological modelling since it directly impacts the groundwater recharge. The data for the preparation of the soil map of the study area has been downloaded from ("Soil Physical Units Map - WUR-https://www.wur.nl/nl/show/bodemfysische-eenhedenkaart-bofek2020.htm," n.d.). The 2012 version of Dutch soil physical units map has been used. According Heinen et al. (2022), there are eighteen top- (B01-B18) and eighteen sub-soils (O01 – O18) based on grain size classification which broadly are categorized into major soil types: clay, loess, loam, peat, peaty and sandy soils. Clay and loess soils are those that are characterized by grain size of 25–100 % <2 µm and 50–100 % <50 µm respectively. A soil is categorized as peat if more than 50 % of it is peat in 0–80 cm. Peaty soils on the other hand are soils where less than 50 % of it is peat in 0–80 cm. Sandy soils are soils characterized by a combination of criteria, less than 8 % <2 µm and less than 50 % <50 µm and less than 15 % organic matter. Soils are classified as loam if it is characterized by 8-25 % of it is <2 µm. The dominant soil type in the study area is sandy soil (Figure 2.4). The soil map of the Netherlands represents the thickness of about 0.8 to 1 meter of the upper hydrogeological unit (Heinen et al. (2022); "Soil map of the Netherlands-https://www.tudelft.nl/en/library/collections/map-room/map-collection/thematic-maps/soil-map-of-the-netherlands-150000," n.d.). Since the nature of hydrogeological units below 1 meter can be explained by the hydrogeological units, geological maps are not presented here.

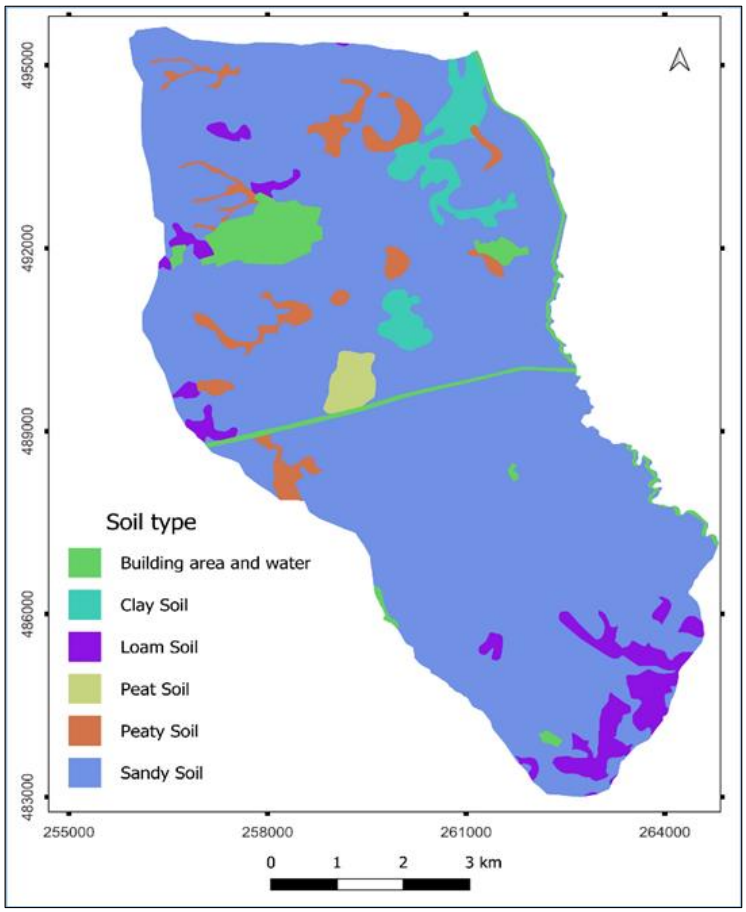

Figure 2.4. Soil map of the study area. Sandy soil covers most of the study area.

2.5. Hydrology and Hydrogeology

Since the lack of significant topographical variations and hard rock systems in the sandy and high drainage catchments of the Netherlands causes high rate of infiltration (Kaandorp et al., 2018), groundwater is the source of water for the majority of streams (Van Der Velde et al., 2011). Streams originate and flow from the northwestern, western, and southern parts of the study area (Figure 2.1) to its outlet, the northern part. Dinkel river flows from south to north along the eastern boundary of the study area. According to Kaandorp et al. (2018), the Springendalse Beek, Roelinksbeek, and Elsbeek catchments, found nearby the current study area, are characterized by the shallow aquifer systems and drained intensively. Kuijper et al. (2012) explained in the documentation of Waterboard Regge and Dinkel (WRD) model that there are extensive watercourse systems, and many streams are altered for the purpose of agricultural activities. Climatic conditions and alterations on the groundwater system decrease the baseflow and probably insufficient during drought times (Hendriks et al., 2014).

Two groundwater models with different scales developed earlier by different parties for the northeastern Netherlands: Interactive planning Water Management Methodology (MIPWA) and WRD groundwater models; the WRD being updated in 2012. The area was represented by different number of hydrogeological units in the MIPWA and old and updated variants of WRD models (Kuijper et al., 2012). The area has been represented with seven and three hydrogeological units in the MIPWA and old, 2004 version, of WRD models respectively. In the 2012 version of WRD groundwater model, the hydrogeological units have been increased. The basis for both hydrogeological groundwater models to consider the number of hydrogeological units is REGIS II. The groundwater level of the study area is characterized by the average highest and average lowest groundwater levels (Figure 2.5) which indicate the groundwater level fluctuations. The average highest and lowest groundwater levels are among the MIPWA groundwater model results which can be accessed at NHI data portal- https://data.nhi.nu/bekijk and it is for the years 2000-2014.

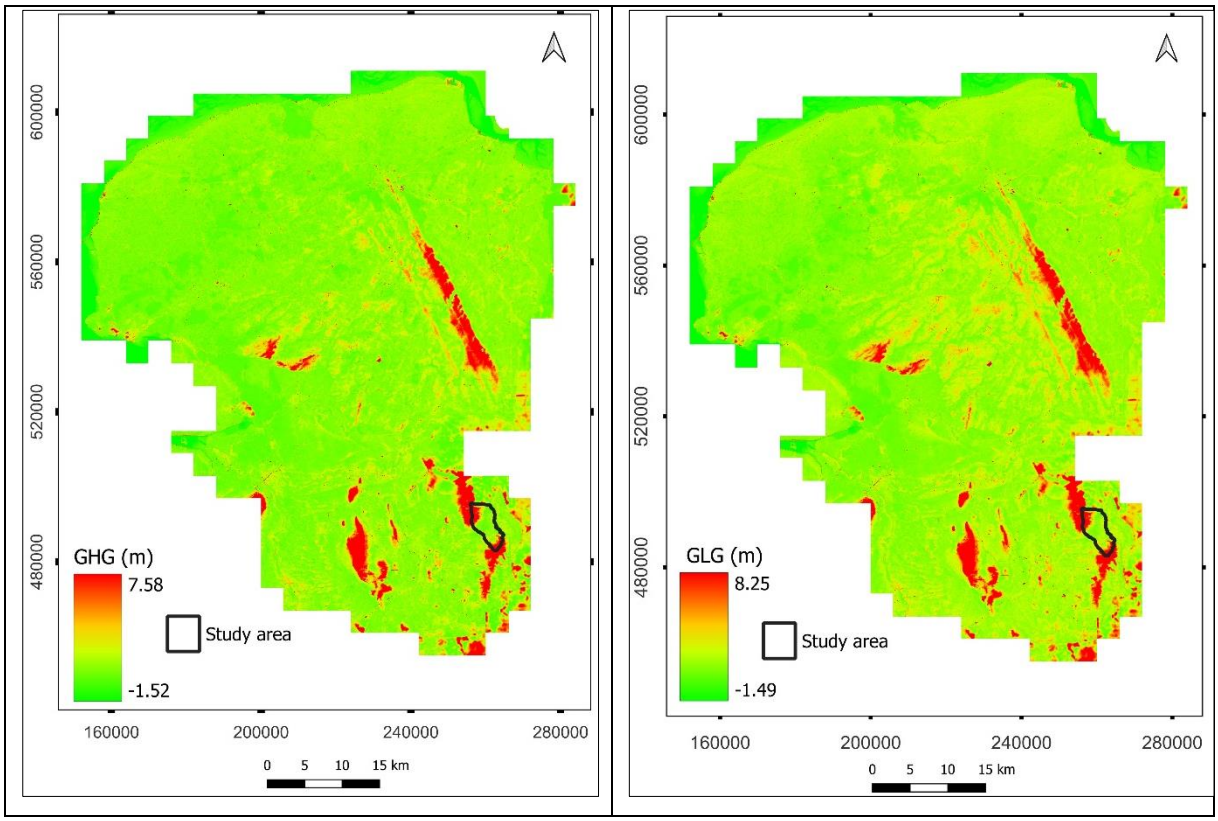

Figure 2.5. Average highest (GHG) and Average lowest (GLG) groundwater levels in meter below ground surface (b.g.s) of the northeastern Netherlands. Source: NHI data portal- https://data.nhi.nu/bekijk.

2.6. Monitoring network

The locations of groundwater piezometers in the study area, precipitation and reference evapotranspiration recording stations around the study area are shown in Figure 2.6, which were used in this research. Groundwater level measurements were accessed from the central point of access for Data and Information of the Dutch Subsurface ("Dinoloket-https://www.dinoloket.nl/," n.d.). Even though more groundwater level monitoring wells are available in the study area, only those that have available data for the intended simulation period, 2010-2015, 2016, 2017 and 2018, are selected and presented in (Figure 2.6). There are 73 monitoring wells in the study area with available data for the selected, calibration, validation and prediction, simulation periods. Some of the groundwater level measurements are available in daily whereas others are in bimonthly. Those records of the groundwater level were adjusted as per the model time discretization.

Precipitation and reference evapotranspiration measurements are available daily and lumped into yearly for the model calibration and monthly for the model prediction to fit with the temporal discretization of this modelling approach. Precipitation and reference evapotranspiration were taken from the manually operated-Denekamp precipitation station and an automated-Twente weather station respectively.

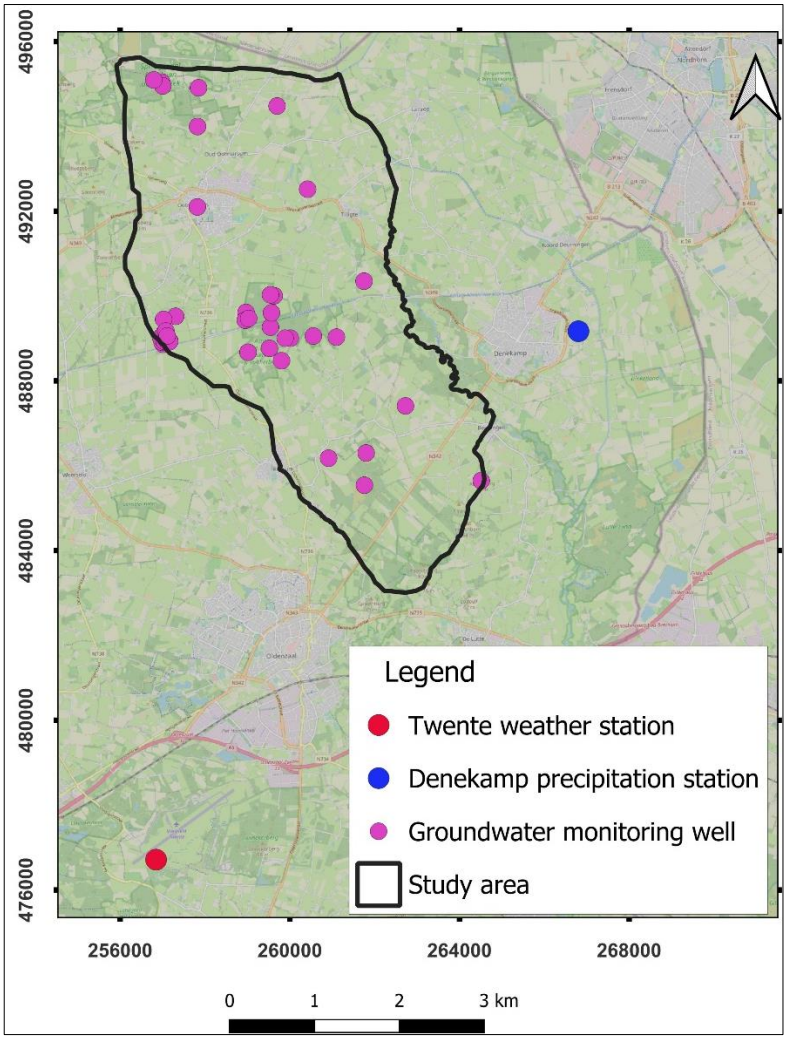

Figure 2.6. Monitoring network for groundwater, precipitation, and reference evapotranspiration records.

3. PROBLEM STATEMENT, OBJECTIVES AND RESEATCH QUSTIONS

3.1. Statement of the problem

The majority of numerical groundwater models, according to Anderson et al. (2015), are developed to predict what a particular action results in the change of hydrological system regime. In management practices, climatic conditions, pumping rates, and land cover changes are among the actions considered when developing predictive groundwater models, which could be in steady or transient states.

Steady-state groundwater models have advantages over their transient counterpart in terms of their less required input data, computational efficiency, and easier model setup. Due to that, calibrated steady-state groundwater models have sometimes been used as predictive tools for transient conditions. Trapp and Geiger (1986), and Moore and Doherty (2021), for example, used steady-state groundwater models to predict the response of groundwater levels for different pumping rates. In both of those models, steady-state model provides proper transient model solution. Moreover, Moore and Doherty (2021) documented that steady-state calibration could be used in decision-support for predicting streamflow and groundwater levels in response to pumping rates. How about the predictive capability of calibrated steady-state groundwater models under climatic condition variations? To answer such questions, it is necessary to take wet and dry climatic conditions into considerations.

The year 2018 has been considered an extreme drought year in the Netherlands (Bakke et al., 2020). On the other hand, the annual precipitation data for the years 2016-2021 taken from the Denekamp precipitation station shows that 2017 was a wet year. These dry and wet years are favourable conditions to test how good a steady-state calibrated groundwater model of Hollandse Grave catchment, the Netherlands, is in predicting its hydrological system regimes under those wet and dry climate conditions. It is to note that the precipitation amounts of 2017 wet is 834.33 mm/year and 2018 dry is 650 mm/year.

3.2. Research objectives

The foremost objective of this research is to examine the predictive capability of calibrated steady-state groundwater model of the Hollande's Graven catchment in predicting its hydrological system regimes.

The specific research objectives:

1. To calibrate a steady-state groundwater model of the Hollande's Graven catchment;
2. To define the hydrogeological water balance of the transient or testing model

3. To compare the transient simulated (predicted from calibrated steady-state model calibration) with the measured hydraulic heads in two predictive, contrasting years, 2017-wet and 2018-dry.

3.3. Research questions

How good is the calibrated steady-state model of the Hollandse Grave catchment for predicting its hydrological system regimes under extreme climate conditions?

Specific research questions:

1. With what optimal model parameter values, the Hollandse graven catchment groundwater model could be calibration?
2. What are the water balance components of the Hollandse graven catchment?
3. How good are the head predictions in the two contrasting years, 2017-wet and 2018-dry and which of the two presents better agreement with the simulated heads?

4. RESEARCH METHODOLOGY

4.1. Methodology flowchart

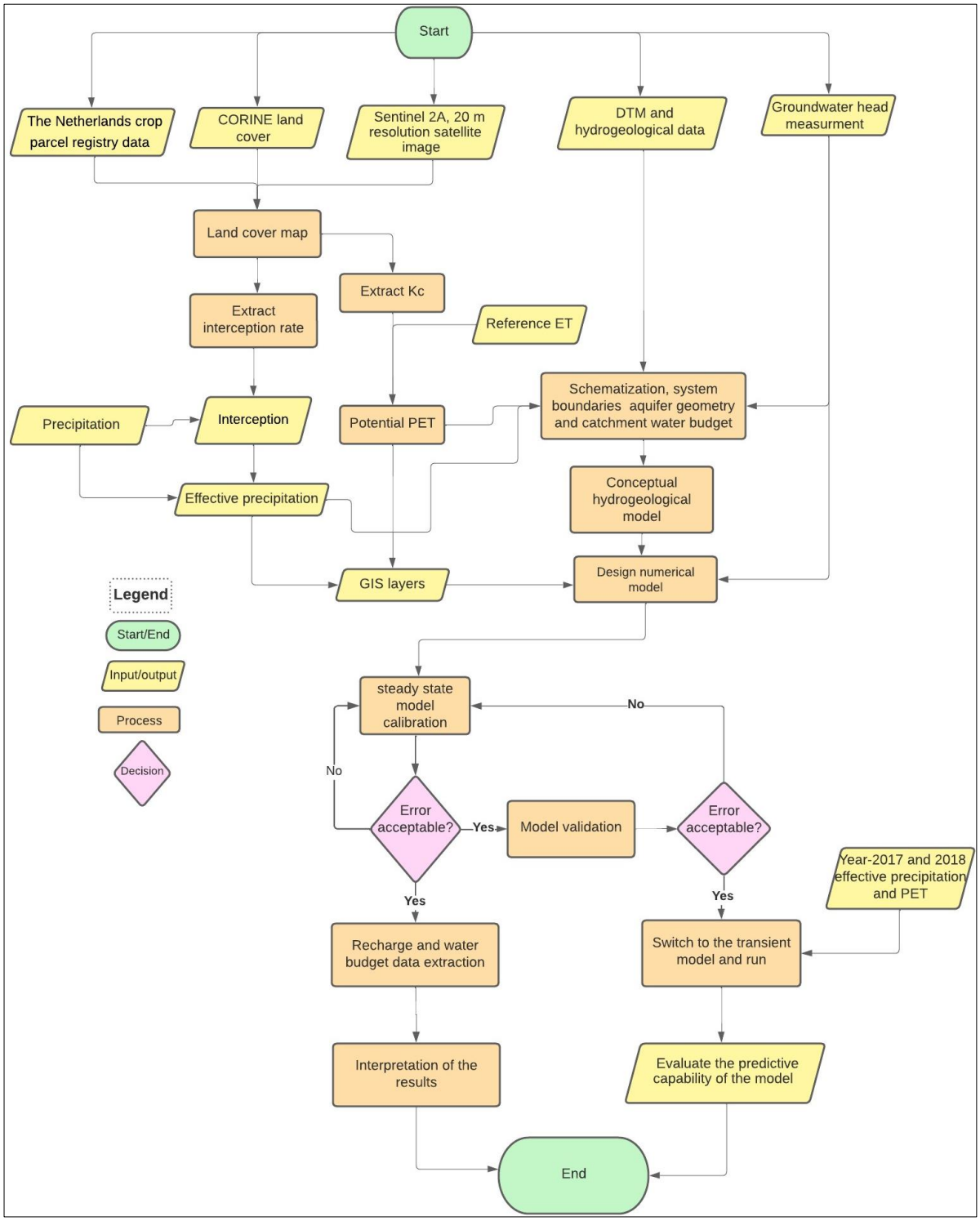

Figure 4.1. Methodology flowchart.

4.2. Data sources

Integrated hydrological models require surface and subsurface data types. As per, various data types have been collected from different sources (Table 4.1). Sentinel II image was used for land cover preparation. The land cover map then has been used as a basis for interception, effective precipitation and potential evapotranspiration (PET) calculation. Topographical data was used for the model top reference. Precipitation on the other hand has been used for effective precipitation calculation. The reference evapotranspiration was used to calculate PET. Soil map was used to determine the distribution of soil types of the study area. Hydrogeological units has been used to represent the geometry of aquifer systems. Groundwater level data has been used to calibrate the model by taking it as a target of calibration and prediction. Groundwater isohypse were used to determine the groundwater flow direction and boundary conditions identification. Shapefiles of the river and streams were also used to define the boundary conditions of the study area. The collected data has arranged and analysed in QGIS, and those data required to the numerical model has been converted to surfer grid files.

Table 4.1. Data types used in this study and their respective sources.

Data type	Source
Digital Terrain Model	https://www.ahn.nl/
Hydrogeological data	https://www.dinoloket.nl/
Hydraulic conductivity	https://www.dinoloket.nl/
Groundwater level	https://www.dinoloket.nl/en/subsurface-data
Groundwater isohypse	https://www.grondwatertools.nl/grondwatertools-viewer
Soil map	https://www.wur.nl/nl/show/bodemfysische-eenhedenkaart-bofek2020.htm
Precipitation and ETo	https://climexp.knmi.nl/selectdailyseries.cgi?id=b8d27b318b493c764dff3ca1a80bd58a
GHG and GLG	https://data.nhi.nu/
Sentinel II image	https://explore.creodias.eu/search
Crop type	https://www.pdok.nl/introductie/-/article/basisregistratie-gewaspercelen-brp-
Built-up area map	https://land.copernicus.eu/en/products/corine-land-cover
Stream, river, and study area	https://www.geoportaaloverijssel.nl/

4.3. Simulation year identification

From the previous works (e.g., Philip et al., 2020), it has been understood that the year 2018 was a drought year and is taken as a reference year for this study. The precipitation records of the years 2018-2021, then was analysed (Figure 4.2) to identify the wet year. The years 2010-2015 has been taken for the model calibration period. The drought year of 2018 was supported by yearly average precipitation measurement comparisons taken from the Denekamp precipitation station. The yearly average precipitation used for calibration, 2010-2015, was compared with the yearly precipitation measurements of 2016, 2017, 2018, 2019, 2020 and 2021. The comparison showed that 2018 and 2017 are the dry and wet years with the

precipitation values of 650 mm. year^{-1} and 834.33 mm. year^{-1} respectively. Hence 2018 is taken as a dry year and 2017 as a wet year for this study. The average yearly reference evapotranspiration data used for calibration and the consecutive six years, 2016-2021, was also compared to see if the identified wet and dry years using precipitation is consistent. The yearly reference evapotranspiration data agrees with the average precipitation comparisons. As shown in the figure below, the precipitation of 2017 is the highest of all the hydrological years and its reference evaporation is the lowest. On the other hand, the precipitation and reference evaporation value of 2018 are the lowest and highest of all the years respectively. This precipitation and PET agreement improves the confidence in identifying wet and dry years for this study. In the Netherlands, the hydrological year starts from the first of April to the 31st of next year which is followed in this modelling activity.

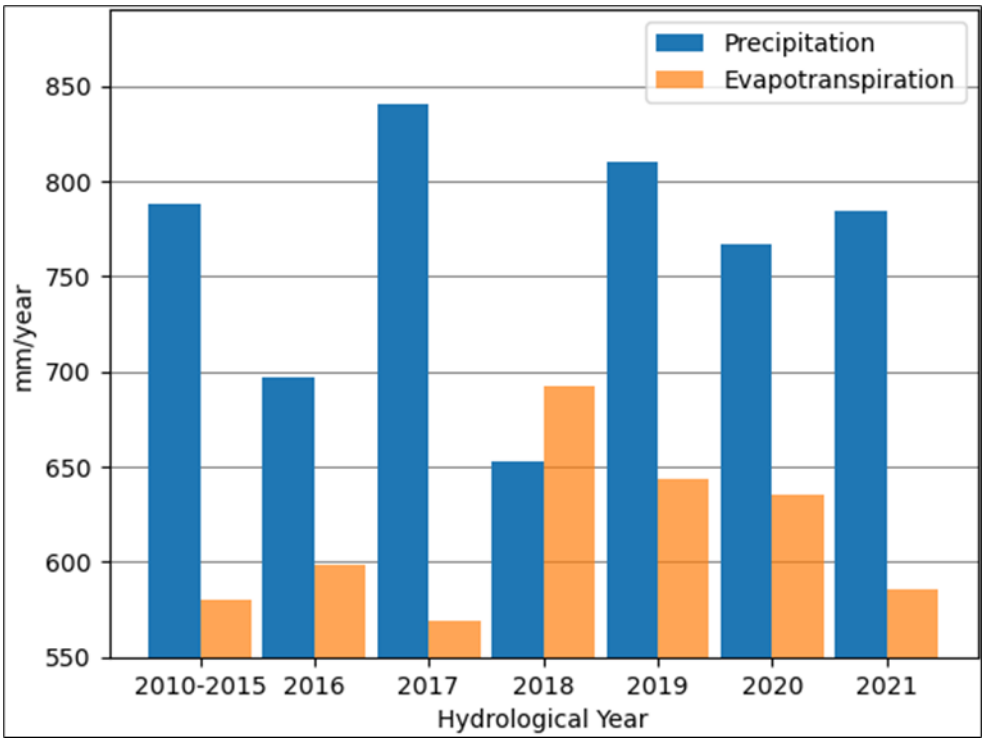

Figure 4.2. Yearly precipitation and reference evapotranspiration records for different years. The record for the years 2010-2015 is taken as yearly average of those six years.

4.4. Groundwater level measurment

Groundwater level measurements has been obtained from Dinoloket-https://www.dinoloket.nl/. Only those monitoring wells that have available data for the intended simulation period, April 2010-2015 for calibration, 2016 for validation, and 2017 and 2018 for model prediction, are selected and presented in Figure 2.6. There are 73 monitoring wells in the study area with available data for the selected calibration, validation, and prediction periods. DINOloket measured the available groundwater level measurement in daily and bimonthly time intervals in the units of meter/day. The groundwater level measurement has been arranged as per the time discretization of the models; all the groundwater level measurements are taken

above mean sea level. Since the numerical groundwater model in ModelMuse has been set with time and length measurement units of day and meter respectively, for each piezometer with available measurement, the average of all the simulation period in the units of meter per day has been taken for model calibration and validation. For model prediction, monthly average groundwater level measurements have been taken.

4.5. Driving forces

In this integrated hydrological modelling approach, precipitation, and PET are considered as driving forces. Those driving forces for this study were taken as spatially homogeneous which were accessed from the respective monitoring networks as described in section 2.6 The monitoring networks being found near by the study area and the study area being relatively small, makes that taking the spatially homogeneous driving forces reasonably acceptable. Effective precipitation and PET are inputs to the numerical model which are derived from precipitation and reference crop evapotranspiration respectively. It is important to note that the calculation of effective precipitation and PET for steady-state model and transient predictive groundwater model follows the same trend, hence the explanation works for both cases. The estimation mechanisms for effective precipitation and PET are described below and the respective maps used for the steady state model are found in Figure 5.1.

4.5.1. Interception and effective precipitation

Interception refers to fraction of the rainfall that does not reach the surface rather falls on to vegetation and evaporates back to the atmosphere. To calculate the effective precipitation, called applied infiltration in MODFLOW 6, it is crucial first to determine that portion of the precipitation intercepted by the land cover classes. Once the land cover map of the study area has been prepared (section 2.3), the interception rate for each land cover class was obtained from the literature (Table 4.2.) Interception map was then calculated (Figure 5.1) based on the precipitation and interception rate of the land cover map. The precipitation for the construction of steady-state groundwater model was taken as average of six years which is equivalent to 2.16 mm/day. For the transient prediction, monthly average precipitation (Figure 5.14) has been taken. Interception of a particular land cover was calculated by multiplying the precipitation with its corresponding fraction of interception.

$$\text{Interception} = \text{Precipitation} * \text{fraction of interception rate} \qquad 4.1$$

The rate of interception depends on the type and the seasonal variation of the land cover. Two considerations have been taken for the calculation of effective precipitation: 1) the fall of deciduous tree leaves at the end of autumn. The interception rates of deciduous trees during winter and summer seasons have been taken as 0 and 13 % respectively. Hence, for the calculation of interception, the average has been taken. 2) the seasonal crop rotations between corn and ryegrass. During the winter season of the Netherlands, cornfields, which have interception rate of 16% are commonly covered with ryegrass (Fan et

al., 2020) which accounts the interception rates of 7.9%. Therefore, in the calculation of interception of the land cover class corn, 11.95 %, average of the two, has been taken.

Since it is assumed as no interception, no PET and no infiltration on the areas where land cover is built-up area, calculations of those terms is taken into consideration. For PET, it's simply taken as the Kc for the built-up area is zero which implies that the PET becomes zero. For the calculation of interception, the interception rate for the built-up area is taken as zero like bare soil and water.

For the calculation of effective precipitation, a technique is applied in such a way that, first the interception map with an interception rate of 100% for the built-up area has been assigned, and others kept to their true value. Then, the effective precipitation was calculated from the 100% interception rate map as: effective precipitation=precipitation-interception. This way, the effective precipitation of the land cover area gets zero.

Table 4.2. Interception rate (%) for each land cover classes of the study area

Land cover	Interception rate (%)	Average interception rate (%)	Source
Built-up area	0	0	-
Bare Soil	0	0	-
Wheat	36	36	(Kozak et al., 2007)
Corn Ryegrass	16 7.9	11.95	(Kozak et al. 2007) ; (Corbett and Crouse, 1968)
Heather	23	23	(Farrick and Price, 2010)
Grass	7.9	7.9	(Corbett and Crouse, 1968)
Deciduous tree	0-13	6.5	(de Jong and Jetten, 2007)
Evergreen tree	17.3	17.3	(Jetten, 1996)
Water	0	0	-

4.5.2. Evapotranspiration

Evapotranspiration is the combination of evaporation from soil, intercepted water and other water bodies and transpiration from trees. Evapotranspiration is mainly affected by three factors: crop type and its characteristics, weather parameters and environmental aspects and management practices (Allen et al., 1998). The numerical model requires PET as an input and one of the methods to calculate it is by multiplying reference crop evapotranspiration with crop coefficient.

4.5.3. Reference crop evapotranspiration

The Makkink based, daily reference crop evapotranspiration data has been obtained from KNMI weather station called Twente weather station (Figure 2.6) which is found approximately nearby to the study area. As described by de Bruin (1987), the Makkink based reference crop evapotranspiration is evapotranspiration

in summertime from well-watered short grass; it is calculated from the observed data on global radiation and air temperature and is expressed as:

$$E_r = C * \frac{s}{s+\Upsilon} * \frac{K\downarrow}{\lambda} \quad 4.2$$

Where E_r is reference crop evapotranspiration (length. Time^{-1}), C is constant which is equal to 0.65, s is slope of the saturation water vapour pressure temperature curve at air temperature (m.bar.K^{-1}), Υ is psychrometer constant, k↓ is global radiation (W.m^{-2}), λ = latent heat of vaporization of water (J.kg^{-1}).

4.5.3.1. Potential evapotranspiration (PET)

PET is the product of reference crop evapotranspiration and crop coefficient factor (Kc). Crop coefficient values varies according to the growth stage of crops; hence the average Kc values has been taken. The Kc initial and end values for the soil represents the wet and dry conditions of the soil. For the calculation of PET, the Kc average has been multiplied by the reference crop evapotranspiration obtained from the Twente weather station. The reference evapotranspiration for the construction of steady-state grundwater model was taken as average of six years which is equivalent to 1.59 mm/day. For the transient prediction, monthly average reference evapotranspiration has been teken (Figure 5.14). The crop coefficient for seasonal crop rotations between corn and ryegrass has also been considered here, average Kc of the two has been taken.

$$PET = Kc * Er \quad 4.3$$

Where Kc is crop coefficient factor

Table 4.3. Time averaged Kc of the land cover classes (Allen et al., 1998)

Land cover	Kc initial	K mid	Kc end	Kc average	Source
Built-up area	0	0	0	0	-
Bare Soil	1.2	0.2	0.15	0.52	(Allen et al., 1998)
Wheat	0.7	1.15	0.25-0.4	0.63	(Allen et al., 1998)
Corn	0.3	1.2	0.35-0.6	0.79	(Allen et al., 1998)
Ryegrass	0.95	1.05	1.0		(Allen et al., 1998)
Heather	0.92	0.92	0.92	0.92	(NISTOR, 2018)
Grass	0.95	1.05	1.0	1.0	(Allen et al., 1998)
Deciduous tree	0.9	0.8	0.3	0.67	(Allen et al., 1998)
Evergreen tree	1.0	1.0	1.0	1.0	(Allen et al., 1998)
Water	1.05	1.05	1.05	1.05	(Allen et al., 1998)

4.6. Rooting depth

Extinction depth- the depth at which evapotranspiration ceases - is also required in the numerical model of MODFLOW 6 code. The rooting depth for each land cover class has been obtained from the literature as shown in Table 4.4. The average rooting depth have been taken for the two, corn and ryegrass, seasonally rotating crops to have a consistence conceptualization with interception rate and crop coefficient.

Table 4.4. Rooting depth (m) for each land cover class

Land cover	Rooting depth (m) range	Average rooting depth (m)	Source
Built-up area	0	0	-
Bare Soil	0.5	0.5	
Wheat	1.5-1.8	1.65	(Allen et al., 1998)
Corn Ryegrass	1-1.7 0.6-1	1.1	(Allen et al., 1998)
Heather	1.4	1.4	(Foxx et al., 1984)
Grass	0.6-1	0.8	(Allen et al., 1998)
Deciduous tree	3.32	3.32	(Foxx et al., 1984)
Evergreen tree	3.36	3.36	(Foxx et al., 1984)
Water	0	0	-

4.7. Coceptual hydrogeological model

Conceptual hydrogeological model is critical for the development of numerical hydrogeological model. Anderson et al. (2015), explained that, as the conceptual hydrogeological model represents good approximation of the field condition, reasonable forecasts can be obtained from the numerical model, which is developed from the conceptual model. The author also pointed out that Hydrostratigraphy, system boundaries, general groundwater flow direction, sources and sinks of water, estimates of hydrogeological parameters and field-based groundwater budget are the main components of the conceptual model.

4.8. Schematization

Schematization of the hydrological system (Figure 4.3) represents the simplified processes of the problem domain. Here the system is schematized as saturated zone, unsaturated zones and surface features like stream and river. The processes representing the exchange of water between the atmosphere, unsaturated zone, saturated zone and rivers and stream have also been shown. Though no information has been found, as per the knowledge of the researcher, explaining the hydrological connections the Dinkel river has with the groundwater system, it is assumed that the river and groundwater are hydraulically connected. During

wet years like 2017, the unsaturated zone, found between the river and streams and the saturated zone, could be completely saturated.

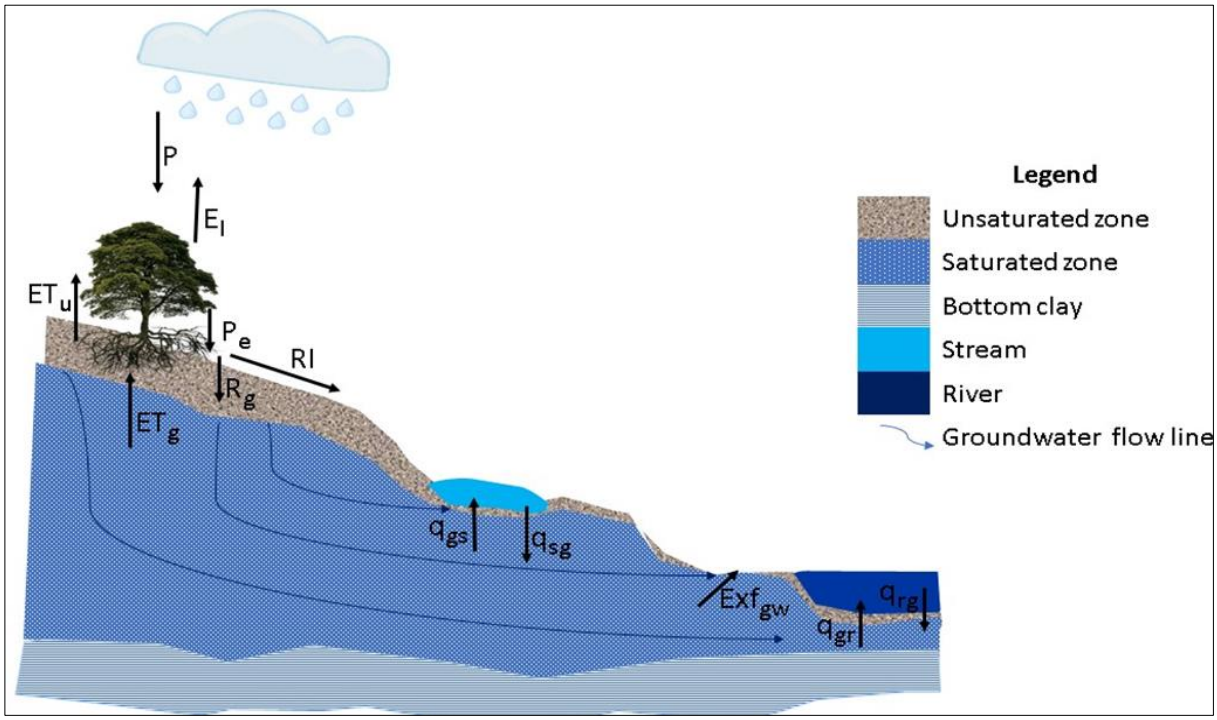

Figure 4.3. Schematization of the system zones and processes

4.9. Hydrogeological units

The Netherlands' stratigraphy is classified based on various classification methods, like: age, depositional setting, stratigraphic group and hierarchical classification mechanisms. The upper, middle, and lower North Sea groups are some of the groups in the hierarchical classification. ("DINO counter-Stratigraphic Nomenclator-https://www.dinoloket.nl/stratigrafische-nomenclator,"n.d.). However, an important classification of the subsurface for this research is based on the hydrostratigraphic nature of the subsurface.

The geological survey of The Netherlands (TNO) has developed four basic subsurface models: Digital Geological Model (DGM-deep), DGM , Regional hydrological model (REGIS II) and GeoTOP (Stafleu et al., 2019). The authors explained that GeoTOP covers up to 50 meter below mean sea level and is a voxel 3D raster. DGM-deep maps the subsurface down about the depth of 7 kilometre while DGM is up to 500 meters deep. DGM is used as a framework for the construction of REGIS II hydrological model. REGIS II model is the hydrogeological model where the subsurface is classified into hydrogeological units of water bearing and poorly permeable layers; it is a de facto standard which is used for the groundwater models construction (Stafleu et al., 2019). This model has also been used as a basis for the identification of hydrogeological units of the study area. The model can be requested in the form of GIS file at Dinoloket-https://www.dinoloket.nl/. Nine hydrogeological units have been identified (Table 4.5) using this model.

Hydrogeological units which have similar hydrogeological characteristics, e.g., if both are clays or sands, have been grouped together. The subsurface is characterised by alternating clay and sand hydrogeological units. The names for the abbreviations (Table 4.5) in REGIS II hydrogeological model are: HL = Holocene, BX = Boxtel formation, DR =Drenthe formation, DRGI = Gieten member of the Drenthe formation (glacial till), DT = Ice-pushed ridges, RU = Rupel formation and DO = Dongen formation. The letters: z = aquifer, k = aquitard and c refers to complex hydrogeological units (Zaadnoordijk et al., 2019). The two hydrogeological units, HLc and DTc, are defined as neither clay nor sand. According to Pokhrel et al. (2023), the Holocene complex consists of fine to medium sand and clay. Since sandy soils cover the majority of the study area and Holocene complex is the uppermost hydrogeological unit, it has been grouped together with Boxtel sand 2 (BXz2) in this study. On the other hand, Zaadnoordijk et al. (2019), described the Ice-pushed ridges as the hydrogeological units that mostly consists of sandy sediments. Therefore, Ice-pushed ridges in this study are grouped with Drenthe formation sand 3 (DRz3). DOk1 called Dongen clay in the study area has a thickness that ranges from 9.18 to 181.82 meters, and it is this hydrogeological unit used as a bottom boundary of the model.

Table 4.5. Hydrogeological units (HU) of the study area.

Code in REGIS II	Code-geological material in this work	Remark
HLc	HU1-sand	HLc is not defined as clay or sand. Since sand soil covers large area, it's
BXz2		grouped with BXz2 in this study.
BXk1	HU2-clay	
BXz3	HU3-sand	
BXk2	HU4-clay	
BXz4		Three of them are sandy units, one over the other, hence they are
DRz1	HU5-sand	merged and represented by the 5th hydrogeological unit
DRz2		
DRGIk1	HU6-clay	
DRz3	HU7-sand	Even though DTc is characterized by the presence of both sand and
DTc		clay, it is merged with sand here because its majority is sand.
RUk1	HU8-clay	
DOz2	HU9-sand	
DOk1	This is the bottom boundary of the model. It covers the entire study area with the minimum thickness of 9.18 meter. It is not modelled in this work rather taken as bottom boundary	

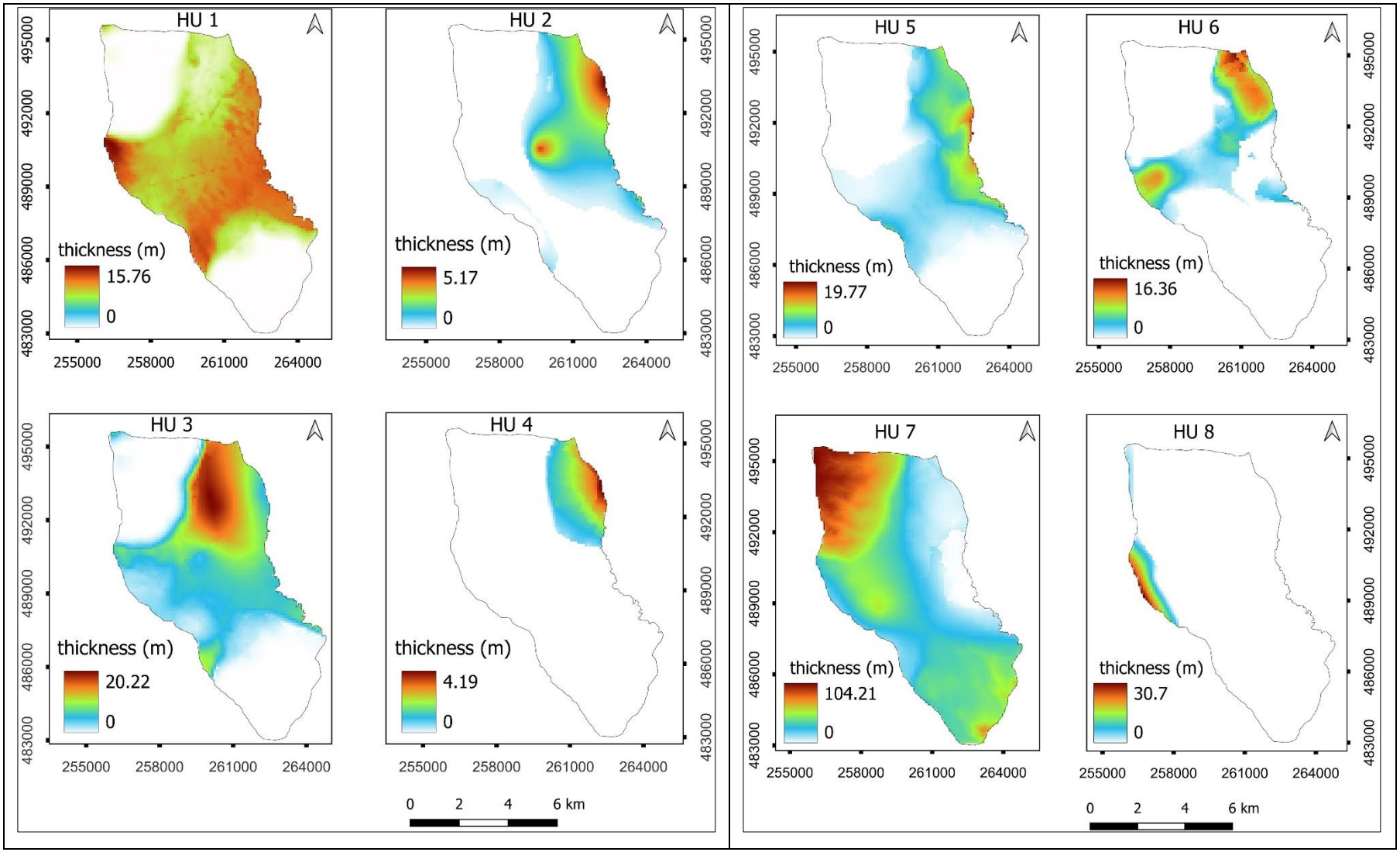
HU 1
thickness (m)
15.76
0
HU 2
thickness (m)
5.17
0
HU 3
thickness (m)
20.22
0
HU 4
thickness (m)
4.19
0
HU 5
thickness (m)
19.77
0
HU 6
thickness (m)
16.36
0
HU 7
thickness (m)
104.21
0
HU 8
thickness (m)
30.7
0
255000
258000
261000
264000
483000
486000
489000
492000
495000
0 2 4 6 km

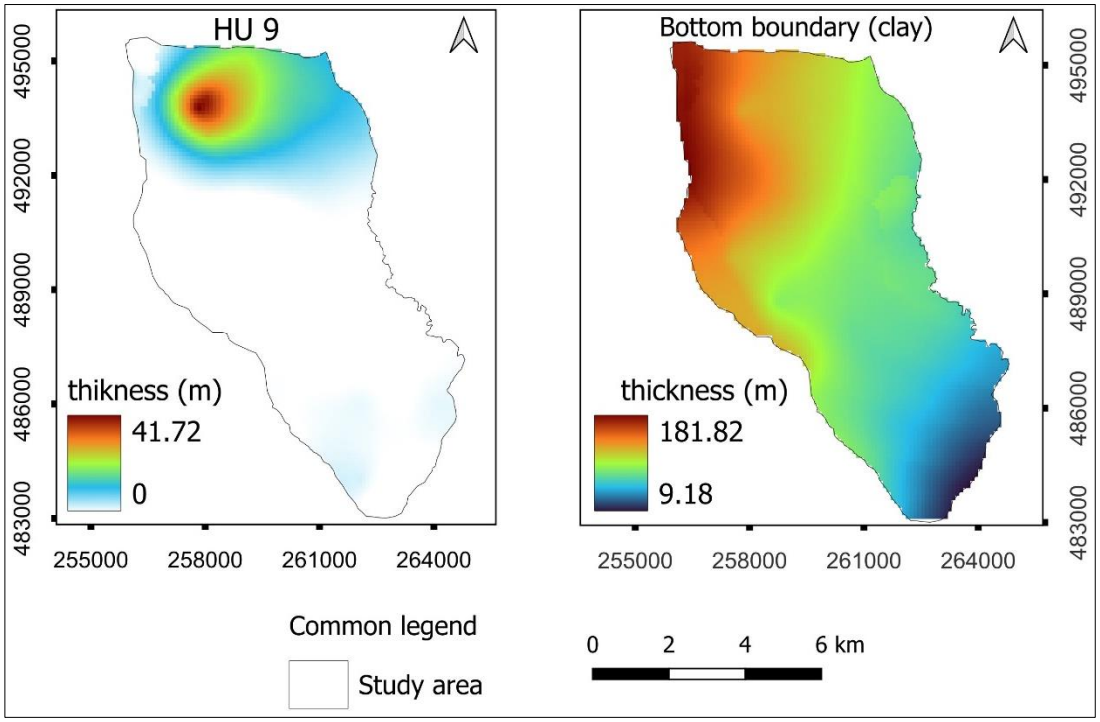

Figure 4.4. The nine hydrogeological units of the study area and their corresponding thicknesses. It shows that none of the hydrogeological units entirely cover the study area. The bottom clay unit is presented to show that the bottom no flow boundary is thick enough.

4.10. System Boundaries

Hydraulic features like groundwater divide, impermeable rock units and physical features like surface water bodies can be used as boundary conditions of the system (Anderson et al., 2015). To identify the boundary conditions of the Hollandse graven catchment, Waterboard Regge and Dinkel (WRD) groundwater model (Figure 4.5), groundwater isohypse taken from the groundwater tools-viewer Groundwater-https://www.grondwatertools.nl/gwsinbeeld/ of the DINOloket , average GHG and GLG of the MIPWA NHI -https://data.nhi.nu/ groundwater model , steams and Dinkel river (Figure 4.6) and impermeable hydrogeological unit called Dongen clay (Figure 4.4) was taken into consideration. The groundwater isohypse were downloaded which were calculated for the hydrological year 2012 and first model layer of the National Hydrological Model (LHM) of the Netherlands. In the WRD model developed by Kuijper et al. (2012), it is indicated that flow along the northern boundary is east to west. The authors described that there is no watershed divide along northern boundary. For the northern part of the Water board Regge and Dinkel area (red line in Figure 4.5), the authors placed a fixed head boundary at some distance away from the model catchment boundary. As shown from the groundwater isohypse (Figure 4.6), however, it is identified that the northern boundary of the current study area, a small part of the larger north side of the WRD mode, is no flow boundary (marked by red lines in Figure 4.6). This could be due to the WRD model was developed for political boundary, but the current study area is some distance away from the Netherlands-German political boundary.

As used for the northern boundary, boundary conditions of the southern and western part of the Hollandse Graven catchment are identified based on groundwater contour lines with the concept of the streamlines (groundwater divide). Since groundwater flows parallel to streamlines and no water crosses them, streamlines can form no flow boundary conditions (Anderson et al., 2015).

Based on this assumption, no flow boundary conditions have been assigned to the northern, southern and western side of the study area which are outlined in red lines in Figure 4.6. Streams originate at the northwestern and southern part of the catchment which are the elevated part of the study area. Since all the streams originate inside the study area, streams also support the assignment of no flow boundary for the indicated bound of the study area. To the eastern side of the study area, Dinkel river is found, that flows from south to north relative to the orientation of the study area. The river has been taken as the catchment boundary represented with river package.

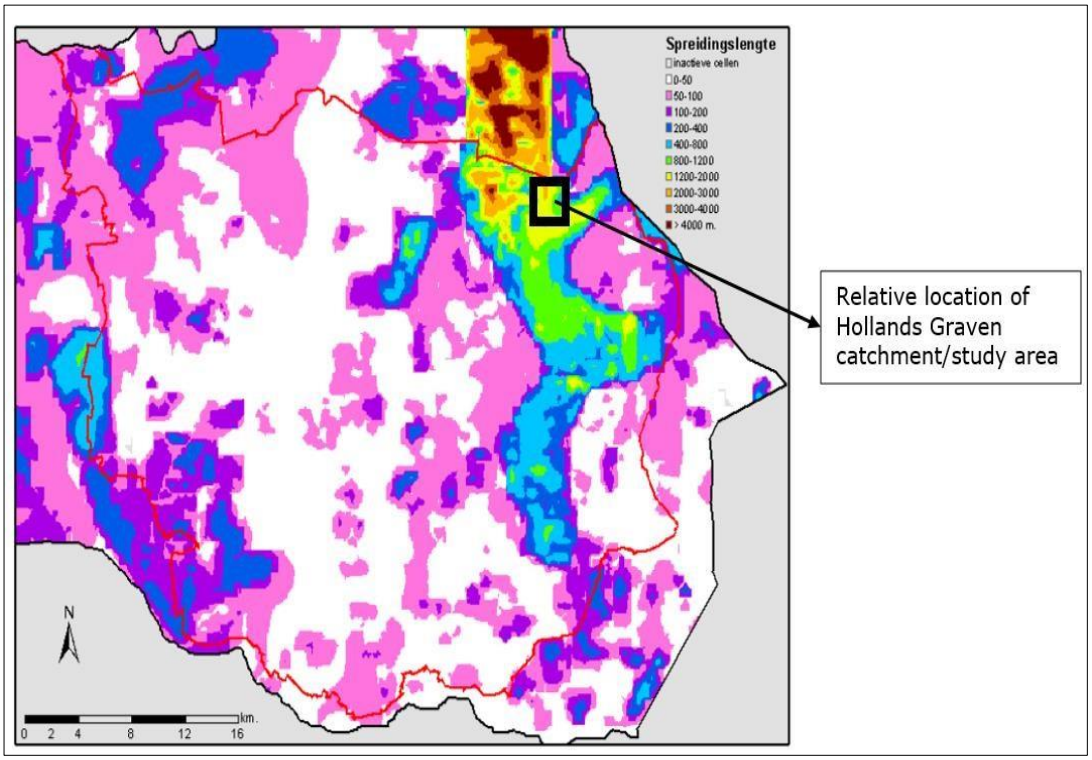

Figure 4.5. Spread length of the WRD model; the red line indicates the WRD model area, and the black indicates the location of boundary conditions of the model. Image source: (Kuijper et al., 2012).

The impermeable hydrogeological unit called Dongen clay (DOk1), covers the entire study area with the thickness ranging 9.18 to 181.82 meters. It is this impermeable hydrogeological unit used as the bottom no flow boundary of the Hollandse graven groundwater model.

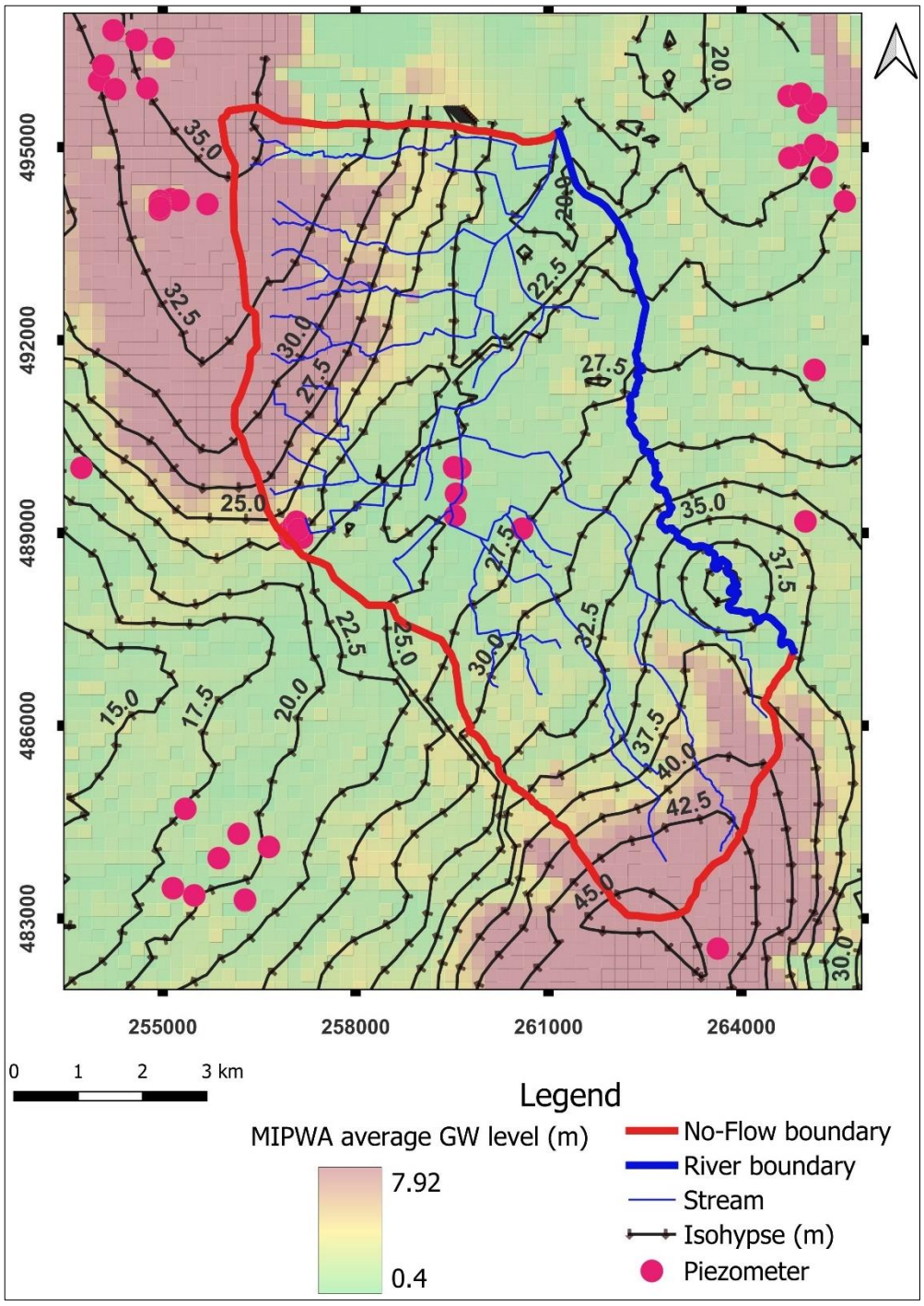

Figure 4.6. The no-flow and river perimeter boundaries of the Hollandse graven catchment. Arrows indicate the groundwater flow direction, generated from groundwater isohypse. While the MIPWA average (average of GHG and GLG) groundwatr level is in meters below the ground surface, isohypse represent above mean sea level.

4.11. Groundwater flow direction

The groundwater flow direction of the catchment is determined from the isohypse groundwater lines obtained from groundwater tools-viewer (https://www.grondwatertools.nl/) of the DINOloket and the groundwater level map of the MIPWA (https://data.nhi.nu/.) model results. The regional groundwater flow pattern in the study area shows that (shown by arrows in Figure 4.6) the groundwater flows to the central part from the elevated northwest and southeast areas and then to the northeastern part, to the downstream side of the river.

4.12. Water balance components

The inflows and outflows of the model can be determined from the model boundary conditions which is discussed in the system boundary's part. The water budget components can be classified into saturated and unsaturated zones where surface water components are considered as part of the unsaturated zone. The general equation for water budget of catchment is expressed as:

$$\text{Inflow} = \text{Outflow} \pm \Delta \text{ Change in storage} \quad 4.4$$

Change in storage for the steady state model is zero, hence inflow and outflow components of the steady model become equal. The change in storage, ΔS, for the monthly prediction transient model is taken as the sum of unsaturated, ΔSu, and saturated, ΔSg, zones storage changes.

$$\Delta S = \Delta Su + \Delta Sg \quad 4.5$$

In the Hollandse Graven catchment, the main inflows to the groundwater system are precipitation and groundwater inflow to streams and river whereas outflows are evapotranspiration, stream discharge at the catchment outlet and groundwater outflow via the river boundary. It is important to note that the assumption in this modelling approach is that the built-up area part of the land cover classes receives precipitation, but it neither infiltrated nor intercepted, rather directly routed to the sewerage system. Hence, the amount of precipitation that the built-up area received has been considered as an outflow, its volumetric amount has been obtained by multiplying the area of the built-up area by precipitation. Therefore, the general inflow and outflow terms for the Hollandse graven groundwater system are expressed as:

$$P + q_{sg} + q_{rg} = ET + q_{gs} + q_{gr} + Exf_{gw} + RI + q_{sw} \quad 4.6$$

Where: P=Precipitation, q_{sg} and q_{rg} are stream and river water seepage to the groundwater system respectively. ET=Total evapotranspiration, q_{gs} and q_{gr} are groundwater seepage to streams and river respectively, Exf_{gw} = groundwater exfiltration to the land surface, RI and q_{sw} are rejected infiltration and precipitation water on built-up area that directly flow to the sewerage system.

Precipitation can be partitioned into two main parts: interception, and effective precipitation and is expressed as:

$$\mathrm{P} = P_e + E_I \quad 4.7$$

Where P_e and E_I represent effective precipitation and plant interception respectively. Once it reaches the land surface, effective precipitation is partitioned into infiltration and rejected infiltration, each proportion being dependent on the value of vertical hydraulic conductivity.

$$P_e = I + RI \quad 4.8$$

Where I and RI are infiltration and rejected infiltration respectively.
The exchange between groundwater and river could be found by the formula:

$$qR = q_{gr} - q_{rg} \quad 4.9$$

Where qR represents river groundwater exchange
Total evapotranspiration (ET) is the summation of surface, unsaturated zone, and saturated zone ET components.

$$\mathrm{ET} = E_s + E_{ss} \quad 4.10$$

Where Es is surface evapotranspiration, and E_{ss} is subsurface evapotranspiration. Es can be expressed as:

$$E_s = E_I + E_{ow} \quad 4.11$$

Where E_{ow} is the open water evaporation and considered as negligible in the Hollands' Graven catchment. Ess can be expressed as:

$$E_{ss} = ET_g + ET_u \quad 4.12$$

Where ETu is the unsaturated zone evapotranspiration and ETg, the saturated zone evapotranspiration. Total stream discharge (q) is the summation of runoff components: rejected infiltration and groundwater exfiltration, and baseflow.

$$\mathrm{q} = RE^s + qB = \left(RI + Exf_{gw}\right) + qB \quad 4.13$$

Where RE^s, Exf_{gw} and $_{qB}$ are direct runoff and baseflow. Baseflow is expressed as:

$$qB = (q_{gs} - q_{sg)} + (q_{gr} - q_{rg}) \quad 4.14$$

The unsaturated zone water balance of the model, which incorporates the surface water components, is expressed as:

$$P_e = RI + ET_u + R_g \pm \Delta S_u \quad 4.15$$

Where Rg is the gross recharge
The saturated zone water balance is expressed as:

$$R_g + q_{sg} + q_{rg} = ET_g + Exf_{gw} + q_{gs} + q_{gr} \pm \Delta S_g \quad 4.16$$

According to Daoud et al. (2022) and Hassan et al. (2014), the net groundwater recharge of a catchment is calculated as:

$$R_n = R_g - ET_g - Exf_{gw} \quad 4.17$$

4.13. Numerical model

According to Anderson et al. (2015), the groundwater flow mathematical model incorporates a governing equation, boundary conditions and initial, for transient model, conditions. The governing equation represents the processes involved within the problem domain whereas boundary and initial conditions represent processes at the boundaries of the model domain and the initial head respectively. For transient groundwater flow in three dimensions under heterogeneous and anisotropic conditions, the governing equation is given by:

$$\frac{\partial}{\partial \mathrm{x}}\left(Kx\,\frac{\partial \mathrm{h}}{\partial \mathrm{x}}\right)) + \frac{\partial}{\partial \mathrm{y}}\left(Ky\,\frac{\partial \mathrm{h}}{\partial \mathrm{y}}\right) + \frac{\partial}{\partial \mathrm{z}}\left(Kz\,\frac{\partial \mathrm{h}}{\partial \mathrm{z}}\right) = Ss\left(\frac{\partial \mathrm{h}}{\partial \mathrm{t}}\right) - W \quad 4.18$$

Where: Kx, Ky and Kz refers to the hydraulic conductivity [LT^{-1}] along the x, y and z axes respectively, h is the hydraulic head [L], Ss= specific storage [L^{-1}], t is the time [T] and W is sink or source of water [T^{-1}]. Under steady state conditions, the change in head over time, $\left(\frac{\partial \mathrm{h}}{\partial \mathrm{t}}\right) = 0$. Therefore, the groundwater flow governing equation for steady state condition is expressed as:

$$\frac{\partial}{\partial \mathrm{x}}\left(Kx\,\frac{\partial \mathrm{h}}{\partial \mathrm{x}}\right)) + \frac{\partial}{\partial \mathrm{y}}\left(Ky\,\frac{\partial \mathrm{h}}{\partial \mathrm{y}}\right) + \frac{\partial}{\partial \mathrm{z}}\left(Kz\,\frac{\partial \mathrm{h}}{\partial \mathrm{z}}\right) + W = 0 \quad 4.19$$

MODFLOW 6 groundwater code has been used to simulate the numerical groundwater model. In MODFLOW 6, the groundwater flow governing equation, is discretised using control-volume finite-difference (CVFD) method. Since Newton-Raphson method can avoid cell drying and rewetting and improve s solution convergence (Langevin et al., 2017), it has been activated.

4.13.1. Software and graphical user interface

Even though different versions of MODFLOW are designed for various typical hydrological problems, a control volume finite difference (CVFD) formulation based-MODFLOW 6 incorporates most functionalities of MODFLOW-2005, MODFLOW-USG, MODFLOW-NWT and MODFLOW-LGR for groundwater flow modelling (Langevin et al., 2017); hence, MODFLOW 6 has been used for this study.
The groundwater flow modelling software-MODFLOW 6 requires either graphical user interface like ModelMuse or programming language for pre-and post-processing applications. In the construction of numerical groundwater models, graphical user interfaces are widely used environments since they provide level of ease (Bakker et al.,2016). The latest and unreleased version of ModelMuse has been used.

4.13.2. Grid design and spatial discretization

In MODFLOW 6, two basic unstructured grid discretization packages are available: the discretization by vertices (DISV) and the general unstructured discretization package (DISU) (Langevin et al., 2017). The selected graphical user interface-ModelMuse supports the discretization by vertices (DISV) package which uses a quadtree polygon grid discretization technique (Winston, 2019) around the area of interest. Therefore, for the better representation of the streams and piezometers, the DISV package has been used. The model is dicritized into cells of 100 x 100 meters grid. For better conceptualization and representation, refinements around the streams and piezometers then have been used. The refinements around the streams and piezometers have a grid resolution of 25 x 25 meters.

4.13.3. Temporal discretization

To achieve the objective of the research, a steady-state model has to be first developed. As such, the base model was steady-state for the daily average of six hydrological years, from April 2010 to 31st of March 2015. Before testing the base model for transient conditions, it has been validated with a steady-state condition using the daily average groundwater level data of 2016 hydrological year. For the transient predictive groundwater model, a monthly time step has been used. Twenty-four stress periods were defined and each stress period has a length equivalent to the number of days of the corresponding month. The transient model has been run for the wet and dry years of 2017 and 2018, respectively.

4.13.4. Hydraulic and sorage properties

According to Langevin et al. (2017), in MODFLOW 6, the horizontal (Kh) and vertical (Kv) hydraulic conductivities between adjacent cells is calculated by the Node Property Flow Package (NPF). NPF calculates the saturated zone hydraulic conductivities while the unsaturated zone flow package (UZF) is used to calculate the hydraulic conductivities of the unsaturated zone cells along the horizontal and vertical directions. The horizontal hydraulic conductivity for the hydrological units of the study area have been obtained from the REGIS II hydrological model. It is that value taken as an initial horizontal hydraulic conductivity and later has been adjusted during the calibration of the steady-state model. The vertical hydraulic conductivity values have been first assigned for each hydrogeological unit as Kh/10 and later adjusted during the model calibration.

Since storage parameters: specific storage and specific yield are required for the monthly transient groundwater model prediction, storage package was activated during the transient simulation. Because field measured value of specific yield and confined storativity cannot be obtained, as per the researcher data assessment, reasonable values representing sand and clay from the literature have been taken (Anderson et al., 2015) documented that from 297 specific yield analysis of medium sand, the arithmetic mean was found to be 0.32 and from 27 specific yield analysis of clay, the arithmetic mean was found to be 0.06. It is also explained that the specific storage of loose sand and stiff clay ranges from 1 x 10^{-3} to 4.9 x 10^{-4} m^{-1} and 2.6 x 10^{-3} to 1.3 x 10^{-3} $m^{-1,}$ respectively. As explained in section 4.9 , the hydrogeological units of the current

study area are characterized by clay and sand units. Thus, a specific storage value of 0.001 m^{-1} and 0.0026 m^{-1} have been assigned for sand and clay hydrogeological units, respectively. For the specific yield, 0.25 was assigned for sand and 0.06 for clay hydrogeological units.

4.13.5. External boundary conditions

External boundary condition here is to mean the boundary condition that defines hydraulic connections between the Hollandse graven catchment and the external hydrological system. As shown in Figure 4.6, the connections the Hollandse graven catchment have with the external system has been conceptualized with two boundary conditions: no-flow and river boundary conditions.

4.13.5.1. No flow boundary

The no-flow boundary condition as explained in section 4.10 is defined using groundwater isohypse. In terms of surface water features, streams, all the streams originate in the study area and flow to the catchment outlet. Therefore, most part of the study area is surrounded by the no-flow boundary condition.

4.13.5.2. River package (RIV)

Depending on the head gradient between the river and groundwater regime, water can flow from the river to the groundwater system or vice versa. The eastern side of the study area (Figure 4.6), has been represented with river boundary and was simulated with the river package, which is one of the stress packages of MODFLOW 6. According to Langevin et al. (2017), the river package simulates only the river-aquifer seepage; it doesn't simulate surface water flow in the river.

The river package requires the user to define the river stage, hydraulic conductance of the river-aquifer interconnection and river bottom. The river stage was taken as the Digital Terrain Model (DTM). The hydraulic conductance was assigned to be dependent on the vertical hydraulic conductivity so that it becomes spatial variable. It was defined as vertical hydraulic conductivity (Kv)*0.5. the river bottom was defined as river top minus 6.5 (River Top-6.5).

$$q_{gr} = C_{rc}(h_{aq} - h_r) \qquad if\ h_{aq} > R_{bot} \qquad 4.20$$

$$q_{rg} = C_{rc}(h_r - h_{aq}) \qquad if\ h_{aq} \leq R_{bot} \qquad 4.21$$

Where:

q_{gr}	Groundwater leakage to river cell	[$m^3.day^{-1}$]
q_{rg}	River cell leakage to groundwater	[$m^3.day^{-1}$]
C_{rc}	Riverbed conductance	[$m^2.day^{-1}$]
h_{aq}	Head of the aquifer cell	[m]

h_r	Water level (stage) in the river	[m]
R_{bot}	Bottom elevation of the river	[m]

4.13.6. Internal boundary

Internal boundary conditions here are to mean those that are used to define the hydraulic connections between the groundwater regime with the surface and unsaturated components of the system.

4.13.6.1. Steam Flow Routing (SFR) package

Steam Flow Routing (SFR) package was used to simulate stream water and the exchange of water between the streams of the Hollandse graven catchment and its groundwater. In the SFR package of MODFLOW 6, the rate of volumetric inflow and outflows are equal, hence there is no storage of water in the surface channels of the streams (Langevin et al., 2017). In the SFR package, flow across the stream bed can be calculated in two methods: active reaches and simple routing reaches. A simple routing reach option that uses a user-specified stream stage (Langevin et al., 2017) was used in the current study, where the model top has been taken as the stream stage. The active reaches method of flow across the stream bed calculation, on the other hand, calculates stream depth as a function of flow using Manning's equation.
Towards which system water flows between a stream reach and aquifer depends on the hydraulic head of the aquifer cell and the stage of the stream reach and is computed as:

$$q_{gs} = \frac{k_b * L_b * W_b}{b_b} * (h_{aq} - h_b) \qquad \text{if } h_{aq} > h_b \tag{4.22}$$

$$q_{sg} = \frac{k_b * L_b * W_b}{b_b} * (h_b - h_{aq}) \qquad \text{if } h_{aq} > h_b \tag{4.23}$$

Where:

q_{gs}	Groundwater leakage to stream reach	[$m^3.day^{-1}$]
q_{sg}	Stream reach leakage to groundwater	[$m^3.day^{-1}$]
k_b	Hydraulic conductivity of the stream reach	[$m.day^{-1}$]
L_b	Length of stream reach	[m]
W_b	Width of stream reach	[m]
b_b	Bed thickness of stream reach	[m]
h_{aq}	Head of the aquifer cell	[m]
h_b	Stream reach stage	[m]

Stream reach length, reach width, stream gradient, bed top, bed thickness, bed hydraulic conductivity, stream stage, and Manning's roughness coefficient are required to be defined for the SFR package. The stream reach length has been defined automatically in ModelMuse using the default formula ' ObjectIntersectLength' in such a way that the stream reach length is measured from the refined model cell that a stream segment crosses. The hydraulic gradient, on the other hand, has been calculated using the length of the segment and the Digital Terrain Model (DTM) pixel values taken at the up and downstream ends of the stream segment. The stream reach width and stream bed thickness were assigned as 0.4 and 0.5 meters, respectively. The stream bed top was assigned as model top minus 3.5 meters. The stream bed hydraulic conductivity was assigned as a function of vertical hydraulic conductivity/1.5. The Manning's roughness coefficient was assigned as 0.035. The stream and river width initial value assignments were based on informations obtained from Hendriks et al.(2014) and simple filed observation.

4.13.6.2. Unsaturated Zone Flow (UZF) package

The hydrological characteristics and the thickness of the unsaturated zone can determine the timing and rate of aquifer recharge. UZF package of MODFLOW 6 simulates recharge to the aquifer, unsaturated zone ET, and saturated zone ET (Langevin et al., 2017). The UZF package is a package where the effective precipitation, potential evapotranspiration, and rooting depth data are handled. The downward vertical flow of water through the unsaturated zone where evaporation is assumed to be instantaneously removed from the soil profile can be explained by simplifying Richards's equation, as follows:

$$\frac{\delta\theta}{\delta t} + \frac{\delta K}{\delta z} + i_{ET} = 0 \qquad 4.24$$

Where:

θ	Volumetric water content of the unsaturated zone	($L^3.L^{-3}$)
t	Time	(T)
K	Vertical unsaturated hydraulic conductivity as a function of water content	($L.T^{-1}$)
z	Distance in the vertical direction	(L)
i_{ET}	Unsaturated evapotranspiration rate per unit depth	$L.T^{-1}.\ L^{-1}$)

The Brooks-Corey equation expresses the vertical unsaturated hydraulic conductivity in terms of water content and saturated hydraulic conductivity as shown in equation 4.25. The infiltration rate, which was in the units of ($m.day^{-1}$) specified by the user in the form of effective precipitation is then changed into water content ($m^3.m^3$) in the UZF package using the formula:

$$K(\theta) = K_{sat} * [\frac{\theta - \theta_{resid}}{\theta_{sat} - \theta_{resid}}]^{\varepsilon} \qquad 4.25$$

$$\theta_{qa} = \left[\frac{q_a}{K_{sat}}\right] 1/\varepsilon * [\theta_{sat} - \theta_{resid}] + \theta_{resid} \qquad 0 < q_a < K_{sat} \qquad 4.26$$

$$\theta_{qa} = \theta_{sat} \qquad q_a > K_{sat} \qquad 4.27$$

Where:

K_{sat}	Saturated vertical hydraulic conductivity	($L.T^{-1}$)
θ_{qa}	Corresponding water content to the specified infiltration rate	($L^3.L^{-3}$)
θ_{sat}	Saturated water content	($L^3.L^{-3}$)
θ_{resid}	Residual water content	($L^3.L^{-3}$)
q_a	Infiltration rate	($L.T^{-1}$)
ε	Brooks-Corey exponent	(-)

The rooting depth (d_{ext}), a depth where evapotranspiration ceases to occur was defined by assigning the root length for each of the nine land cover classes from the literature (Table 4.4). In addition to the potential evapotranspiration, effective precipitation, and rooting depth (d_{ext}) , UZF package requires the assignment of other parameters. Surface depression depth (d_{surf}), was assigned a value of 0.001 meter, saturated vertical hydraulic conductivity (K_{sat}), was assigned to be dependent on the vertical hydraulic conductivity as Kv * 0.65, residual water content (θ_{resid}) and extinction water content (θ_{ext}) were assigned the same value of 0.015. Saturated water content (θ_{sat}) and initial water content were assigned 0.45 and 0.016 respectively.

4.13.6.3. Water Mover (MVR) Package

The process of rejected infiltration can happen in two ways: the presence of a shallow water table and the smaller hydraulic conductivity of the unsaturated zone than the infiltration rate (Langevin et al., 2017). The Mover package is used to move the available water between the packages (Langevin et al., 2017). The application of MVR package requires the providers and receivers; in this modelling practice, the Mover package was activated to transfer the rejected infiltration and groundwater exfiltration from the upslope areas (providers, UZF cells) to the downslope nearest streams (receivers, SFR reaches).

4.14. Model calibration

To calibrate the steady state groundwater model of the Hollandse graven catchment, trial and error approach has been employed. Average measured groundwater levels have been interpolated and used as initial hydraulic head for the steady-state model calibration. The hydraulic conductivity values of hydrogeological units, taken from the REGIS II hydrogeological model was used as a reference for each hydrogeological unit, except the topmost layer (HLc) and, ice-pushed ridges (DTc) (Table 4.5), which were not given. Since both HLc and DTc were grouped into other hydrogeological units, the hydraulic conductivity values of those units have been taken. To calibrate the model, most of the hydrogeological units were partitioned into different zones of hydraulic conductivity which can be observed from the hydraulic conductivity map (Figure

5.4). During the calibration of the steady-state model, the following considerations have been taken: 1) a soil map, was imported into ModelMuse to identify areas covered with clay soils for the first hydrogeological unit to assign the logical values to those clay units 2) a range for clay and sand hydrostratigraphic units were kept while changing the values of hydraulic conductivity. 3) To maintain the natural behaviour of gradual change of hydraulic conductivity values between hydraulic conductivity zones, the reference hydraulic conductivity, obtained from the REGIS II model of the respective hydrogeological units was adjusted. Since groundwater head measurements are available in the study area, the calibration targets in this modelling activity were taken as groundwater heads. A total of 44 piezometer groundwater level measurements were used to calibrate the steady-state groundwater model. The following table shows the initial calibration parameters of the packages used.

Table 4.6. Steady-state model calibration parameters initial values

parameter	Description	Dependency	Initial value	Unit	Package
K_h	Horizontal hydraulic conductivity		K_h *from REGIS II*	m.day^{-1}	NPF
K_v	Vertical hydraulic conductivity	K_h	$K_h/10$	m.day^{-1}	NPF
K_{sat}	Vertical saturated hydraulic conductivity	K_v	$K_v * 0.8$	m.day^{-1}	UZF
K_b	Stream bed hydraulic conductivity	K_v	K_v	m.day^{-1}	SFR
θ_{resid}	Residual water content		0.03	m^3.m^{-3}	UZF
θ_{sat}	Saturated water content		0.5	m^3.m^{-3}	UZF
θ_i	Initial water content		0.04	m^3.m^{-3}	UZF
θ_{ext}	Extinction water content		0.03	m^3.m^{-3}	UZF
d_{surf}	Surface depression depth		0.1	m	UZF
C_{rc}	Riverbed conductance	K_h	$K_h * 0.5$	m^2.day^{-1}	RIV

4.14.1. Error assessment

An efficient way of model assessment, according to Anderson et al. (2015), is to use visual observations of simulated and observed values and use error matrices together. In this modelling approach, mean error (ME), absolute mean error (MAE) and root mean square error (RMSE) were used for steady state and MAE and RMSE for predictive transient groundwater model assessment in addition to the visual observed and simulated graph. There is no standard value for ME, MAE and RMSE to say the model is sufficiently calibrated or not. The steady-state model in this groundwater modelling was set to be calibrated if ME<0.2, MAE<0.3 and RMSE<0.5.

$$ME = \frac{1}{n}\sum_{i=1}^{n}(h_m - h_s)_i \quad 4.28$$

$$MAE = \frac{1}{n}\sum_{i=1}^{n}|(h_m - h_s)_i \quad 4.29$$

$$RMSE = \left[\frac{1}{n}\sum_{i=1}^{n}(h_m - h_s)_i^2\right]0.5 \quad 4.30$$

Where:

n	the number of targets	
h_m	Measured head	m
h_s	Simulated head	m
$\bar{h}_m$	Mean of measured head	m

4.15. Model validation

Groundwater regime predictions resulting from calibrated but unvalidated groundwater models will be more uncertain than those validated (Anderson and Woessner, 1991). For steady-state model validation, groundwater piezometers with measurements for the 2016 hydrological year were selected. The groundwater level measurements of those piezometers were then arranged as per the time discretization of the steady-state model. Then from the results of model run, simulated and observed heads were compared as shown in Figure 5.9. A total of 35 piezometer groundwater level measurements were used to validate the steady-state groundwater model of the Hollandse graven catchment.

4.16. Model prediction

In the study area, there are 33 and 61 available piezometers with groundwater level measurements for the 2017 and 2018 hydrological years, respectively. To run the 2017 wet and 2018 dry transient predictive groundwater model, which has a monthly time step, the following steps were followed:

- Piezometers with groundwater level measurements for the 2017 wet and 2018 dry hydrological year were selected and arranged to monthly average head.
- Daily measurements of precipitation and reference evapotranspiration for the 2017 wet and 2018 dry years were adjusted into monthly values.
- Effective precipitation was calculated, the method of calculation is described in section 4.5.1, from land cover interception rate and the monthly average precipitation data of the 2017 wet and 2018 dry years.
- PET was calculated, for method of calculation, section 4.5.2, from the crop coefficient and monthly average reference evapotranspiration data of the two years.
- The calibrated steady-state model was copied and switched to a transient mode with 24 stress periods of monthly time step.

- The storage package was activated, and the specific storage and specific yield values were assigned to each hydrogeological unit.
- The steady-state head observations were removed from the switched model, and the prepared head, effective precipitation, and PET were imported into the transient model and assigned to the respective packages.
- The calculated hydraulic head of the calibrated steady-state model was used as an initial hydraulic head for the transient predictive groundwater model simulation. As in the steady-state model, appropriate results were extracted after running the predictive transient groundwater model.

5. RESULTS AND DISCUSSION

5.1. Driving Forces

5.1.1. Interception and effective precipitation

As described in section 4.5.1, interception was calculated using precipitation and interception rate of the land cover classes obtained from the literature (Table 4.2); the spatial distribution of land cover classes has been presented in the land cover map of the study area (Figure 2.3). The highest interception rate value is 0.78 mm/day, which represents the land cover wheat with the interception rate of 36%. The lowest interception rate on the other hand, has been found to be 0 mm/day which represents the land covers classes: water, soil and built-up area where the inteception rate value is taken as zero. Since effective precipitation is expressed as precipitation minus interception, it is observed that on those areas where interception value is higher, the value of effective precipitation is lower and those areas with low interception rates show high effective precipitation. For the interception map, water, soil and built-up areas have zero interception rates (Table 4.2), so that when the nine land cover classes are grouped based on the interception rate values, seven land cover classes with distinct values of interception have been obtained (Figure 5.1). However, for the effective precipitation, while water and soil have 100% effective precipitation, equivalent to the precipitation, the built-up area continues to have zero effective precipitation or infiltration because all the water goes to the sewerage system. So eight land cover classes with distinct values of effective precipitation have been found.

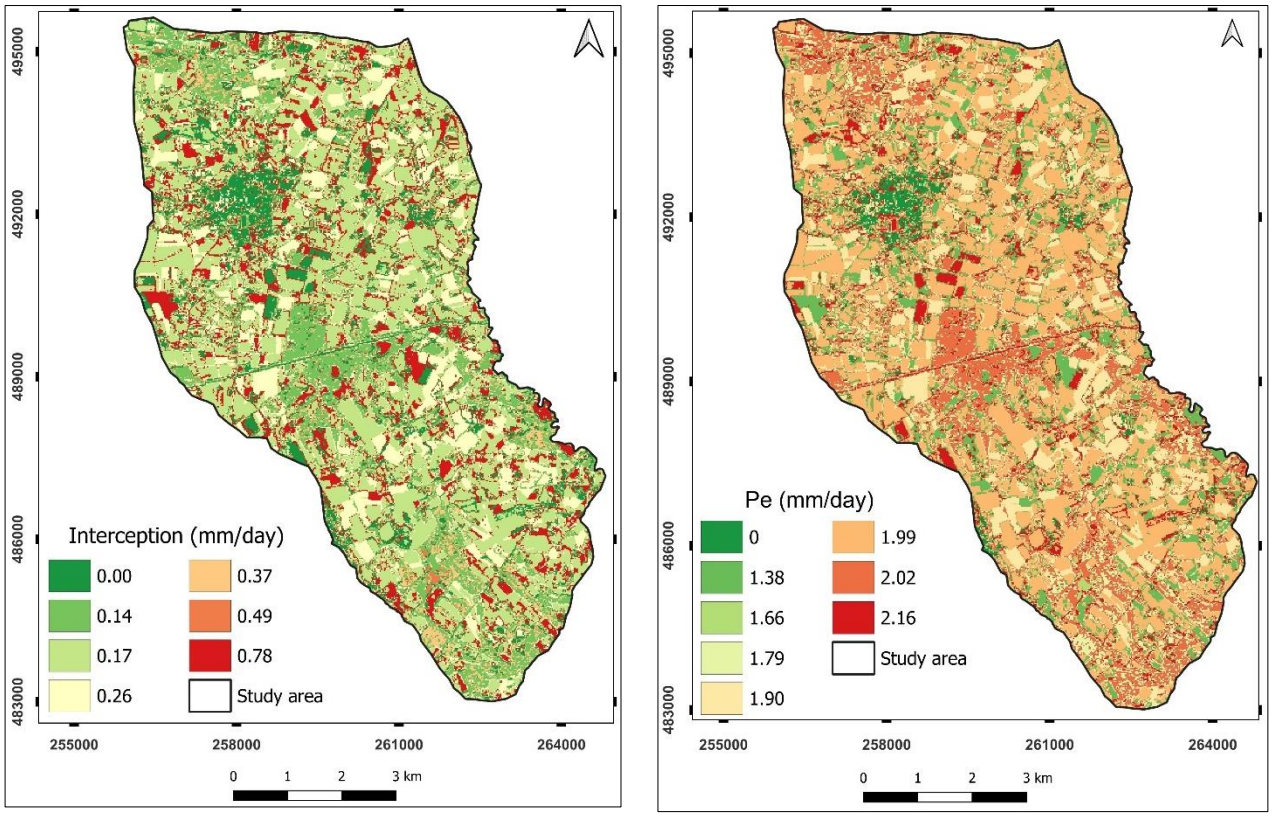

Figure 5.1. Interception and effective precipitation (Pe) of the study area used for the steady-state model calibration.

5.2. Potential evapotranspiration (PET)

Crop coefficient and rooting depth maps have been presented in

Figure 5.2. There are eight distinct values of crop coefficient and rooting depth. That is because grass and evergreen trees have the same value, 1, of crop coefficient, and for the rooting depth, water and built-up area have the same, 0 meter, values. The crop coefficient values of the land cover class range from 0 for built-up areas to 1.05 for water bodies. The values of rooting depth on the other hand, ranges from 0 meter for water and built-up area to 3.36 meters for evergreen trees. In this research, the two parameters used to calculate PET are the crop coefficient and reference crop evapotranspiration. The calculated PET is explained by the crop coefficient of the land cover map because reference crop evapotranspiration is taken as spatially uniform, like precipitation. The highest PET is 1.67 m/day which is for water bodies, due to the high crop coefficient of 1.05, whereas the lowest one is 0 mm/day, for built-up areas.

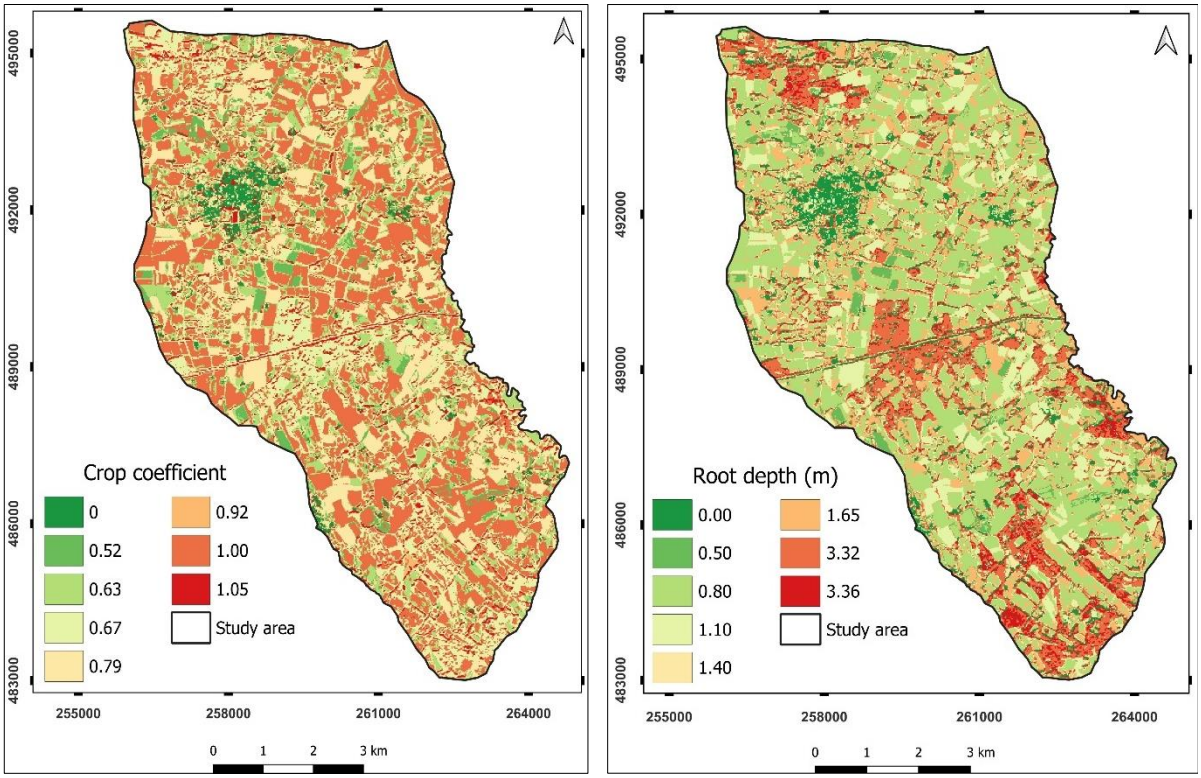

Figure 5.2. Crop coefficient and rooting depth used for the steady-state model calibration.

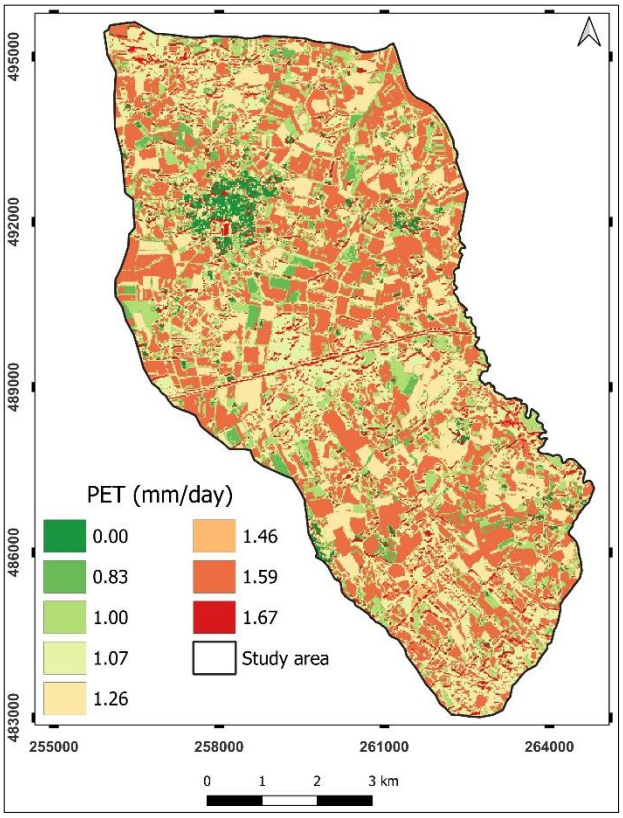

Figure 5.3. PET which is used for the steady-state model calibration.

5.3. Steady-state model calibration results

5.3.1. Parameter values

With the trial-and-error method of head target calibration, a range of values for parameters of various packages have been found and presented in Table 5.1. The horizontal hydraulic conductivity ranges from 0.00013 m.day^{-1} for the 8th hydrogeological unit (HU8), which is clay, to 98.21 m.day^{-1} for the first and 3rd hydrogeological units (HU1 and HU3), which are sand. Vertical hydraulic conductivity has been calibrated in such a way that it varies spatially depending on the horizontal hydraulic conductivity. It was expressed in terms of the horizontal hydraulic conductivity as $K_h/8$. The value of vertical saturated hydraulic conductivity ranges from 0.000016 m.day^{-1} to 12.27 m.day^{-1}. It varies with the vertical hydraulic conductivity and was calibrated as Kv*0.65. Stream bed hydraulic conductivity was also assigned to be dependent on the vertical hydraulic conductivity assigned as Kv/1.5.

Table 5.1. Calibrated steady-state model parameter values.

parameter	Description	Dependency	Found by	Range of calibrated value	Unit	Package
K_h	Horizontal hydraulic conductivity		Calibrated	0.00013-98.21	m.day^{-1}	NPF
K_v	Vertical hydraulic conductivity	K_h	$K_h/8$	0.000016-12.27	m.day^{-1}	NPF
K_{sat}	Vertical saturated hydraulic conductivity	K_v	$K_v * 0.65$	0.00053-7.98	m.day^{-1}	UZF
K_b	Stream bed hydraulic conductivity	K_v	$K_v/1.5$	0.00054-8.2	m.day^{-1}	SFR
θ_{resid}	Residual water content		Adjustment	0.015	m^3.m^{-3}	UZF
θ_{sat}	Saturated water content		Adjustment	0.45	m^3.m^{-3}	UZF
θ_i	Initial water content		Adjustment	0.016	m^3.m^{-3}	UZF
θ_{ext}	Extinction water content		Adjustment	0.015	m^3.m^{-3}	UZF
d_{surf}	Surface depression depth		Adjustment	0.001	m	UZF
C_{rc}	Riverbed conductance	K_h	$K_v * 0.5$	0.041-543.08	m^2.day^{-1}	RIV

5.4. Hydraulic conductivity distribution

The spatial distribution of calibrated horizontal and vertical hydraulic conductivity values have been presented (Figure 5.4 and Figure 5.6). For a better representation of the maps, the horizontal and vertical hydraulic conductivity maps, see the legends, of the 9th hydrogeological unit (HU9) are presented together (Figure 5.5). The distribution of the hydraulic conductivity can be viewed in two ways: spatial distribution

within each hydrogeological unit and the hydraulic conductivity distribution between the nine hydrogeological units. From the nine hydrogeological units (HU1 to HU9), the first, third, fifth, seventh, and ninth are sand units and the rest units are clay. The maximum hydraulic conductivity is found from the first and third sand hydrogeological units with a value of 98.21 $m.day^{-1}$. The distribution of hydraulic conductivity within the first hydrogeological unit can be expressed as high around the central part of the study area and low on the northern and southern elevated parts of the study area. Since the spatial distribution of clay soil (Figure 2.4) has been taken into consideration for the calibration of the first hydrogeological unit, typical clay hydraulic conductivity values have been found.

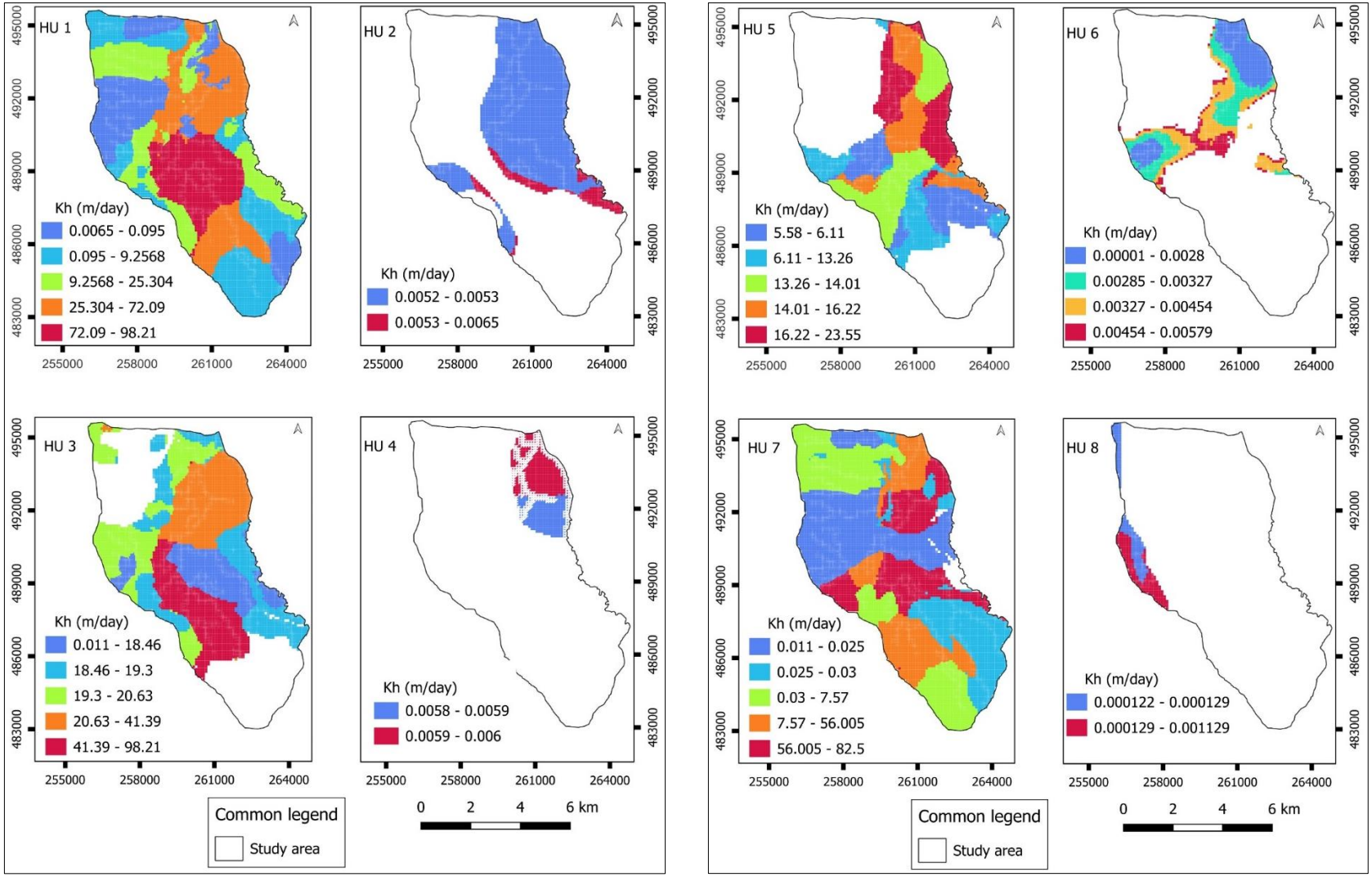

Figure 5.4. Horizontal hydraulic conductivity map of the calibrated steady-state model for the hydrogeological units HU1 to HU8. See for the 9th hydrogeological unit.

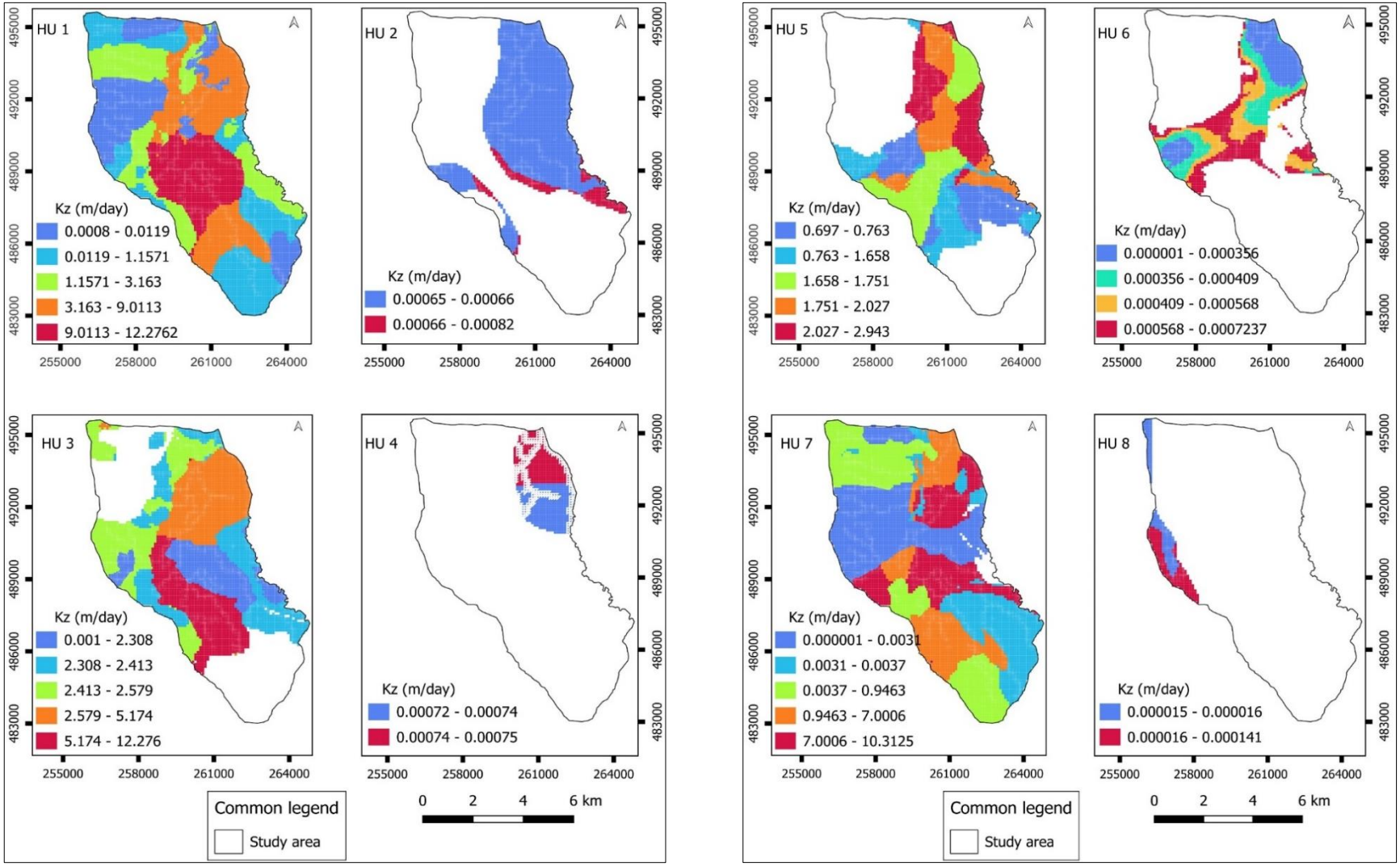

Figure 5.5 Vertical hydraulic conductivity map of the calibrated steady-state model for the hydrogeological units HU1 to HU8. See for the 9th hydrogeological unit.

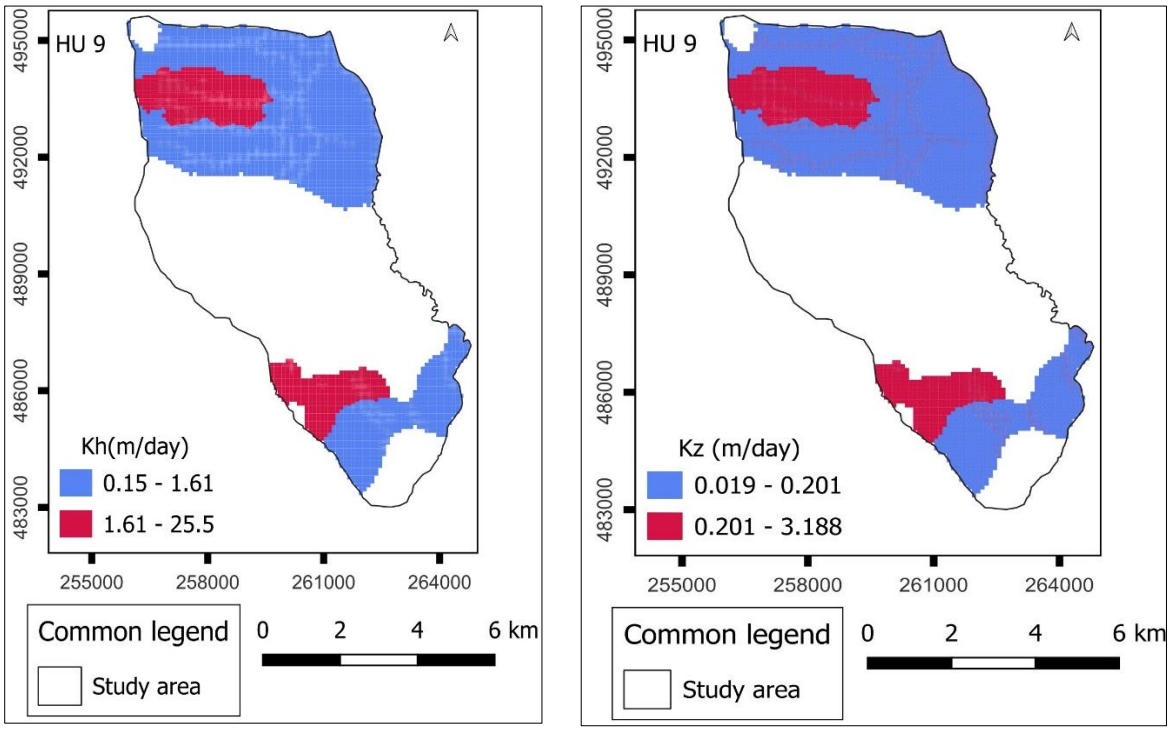

Figure 5.6. Horizontal and vertical hydraulic conductivity distribution map of the calibrated steady state model for the 9th hydrogeological unit (HU9).

5.5. Visual observations and error assessment

The observed and simulated hydraulic head are comapred in Figure 5.7, which shows good agreement with a correlation coefficient of 0.99. Groundwater level measurements from 44 piezometers have been used to calibrate the model. From the 44 measured groundwater level data, the maximum and minimum hydraulic head values are 50.57 and 19.15 meters, respectively; there is a 31.42 meter difference between the highest and lowest hydraulic head values in the study area. Though there are no standard residual error values to say the fit between the measured and simulated heads are in an acceptable range, residuals from the calibration of 44 piezometers are all less than one (Table 5.2). The maximum residual of the calibrated model is -0.94 meters whereas the minimum residuals are ± 0.01. The maximum residual error could be due to the high hydraulic head variations, 31.42 meter, in the study area.

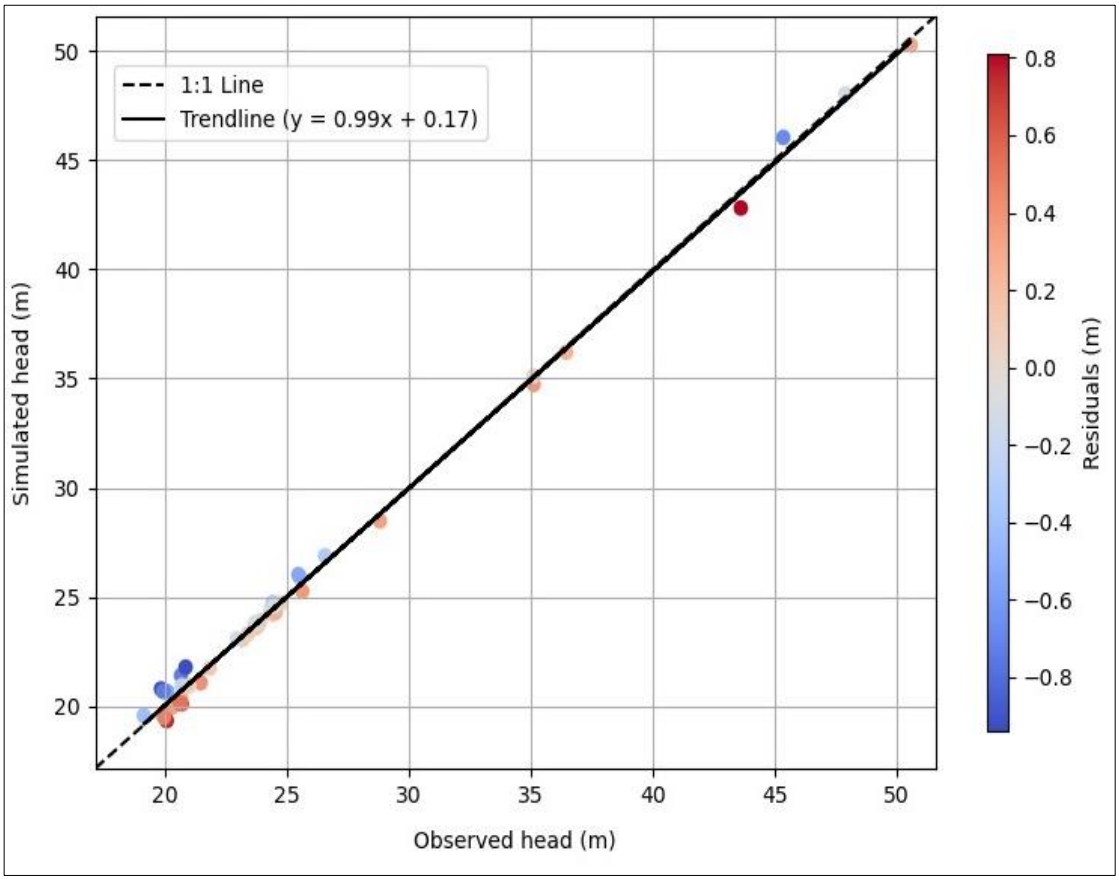

Figure 5.7. Observed versus simulated groundwater head for the calibrated steady-state model.

Figure 5.7 show that the model is able to replicate the groundwater head of the study area well. The spatial distribution of the residual errors map has also been presented in Figure 5.8 The high and low values of residuals are distributed in the entire model area; there is no specific area where residuals are large. This indicates that there is no specific area where the calibration misfit of the steady-state model is high. The unclustered distribution of high and low values of residuals around the specific area is an indirect indication of a reasonable model calibration.

Table 5.2. Piezometers used to calibrate the steady-state model and corresponding residuals.

Piezometer ID	X-coordinate	Y-coordinate	Observed head (m)	Simulated head (m)	Residuals (m)
B28F0172	257825	493996	35.12	34.73	0.39
B28F0207	256980	495040	45.35	46.03	-0.68
B28F0312	259700	494480	21.85	21.74	0.11
B28F0354	257309	489522	24.43	24.23	0.20
B28F0461	257822	492100	36.45	36.20	0.25
B29A0154	261750	490350	20.68	20.44	0.24
B29A0157	261100	489031	21.48	21.08	0.40
B29C0186	261760	485540	28.82	28.48	0.34

B29C0291	262728	487410	25.55	25.89	-0.34
B28F1439	257005	494953	43.61	42.80	0.81
B28F1440	257018	489021	24.33	24.29	0.04
B28F1441	257038	489111	24.35	24.44	-0.09
B28F1442	256794	495094	47.89	48.02	-0.13
B28F1443	257847	494909	35.11	35.12	-0.01
B28F1491	259016	488674	20.67	21.41	-0.74
B29A0046	260420	492518	19.15	19.57	-0.42
B29A0851	260014	489006	20.71	20.11	0.60
B29C0118	264514	485647	50.57	50.26	0.31
B29C0214	260915	486177	25.48	26.02	-0.54
B28F0373	259521	488767	20.70	20.94	-0.24
B28F0374	259545	489266	20.30	19.96	0.34
B28F0380	259568	489604	19.97	19.59	0.38
B28F0381	259633	490006	20.09	19.34	0.75
B28F0382	259545	490028	19.97	19.50	0.47
B28F0384	258968	489614	20.11	20.67	-0.56
B28F0387	258950	489429	19.85	20.79	-0.94
B28F0390	259030	489470	19.94	20.68	-0.74
B28F0393	259805	488475	20.86	21.79	-0.93
B28F0394	259890	489005	20.64	20.12	0.52
B28F0395	257013	488863	23.76	23.60	0.16
B28F0396	256988	488913	23.94	23.92	0.02
B28F0397	256956	489024	24.77	24.73	0.04
B28F0398	257027	489022	24.55	24.29	0.26
B28F0399	257037	489123	24.43	24.75	-0.32
B28F0400	257083	488981	23.73	23.72	0.01
B28F0401	257169	488942	23.19	23.05	0.14
B28F0402	257024	489449	26.57	26.89	-0.32
B28F0403	257041	488934	23.84	23.71	0.13
B28F0404	257119	488924	23.42	23.32	0.10
B28F0405	257169	488925	22.96	23.09	-0.13
B28F0406	257080	489174	24.49	24.58	-0.09
B28F0407	257108	489056	23.71	23.82	-0.11
B29A0172	260557	489057	21.01	20.94	0.07
B29C0268	261800	486300	25.64	25.27	0.37
		ME	0.00		
		MAE	0.34		
		RMSE	0.42		

The error metrics: ME, MAE, and RMSE for the calibrated steady-state model were calculated. ME is zero, whereas the MAE and RMSE values are 0.34 and 0.42, respectively. Since ME can provide a measure of bias in model prediction, zero ME could imply that on average the predictions are not too high nor too low. Furthermore, both MAE and RMSE are less than 0.5, hence the model has been taken as sufficiently calibrated for the intended purpose which is testing its predictive capability under wet and dry conditions.

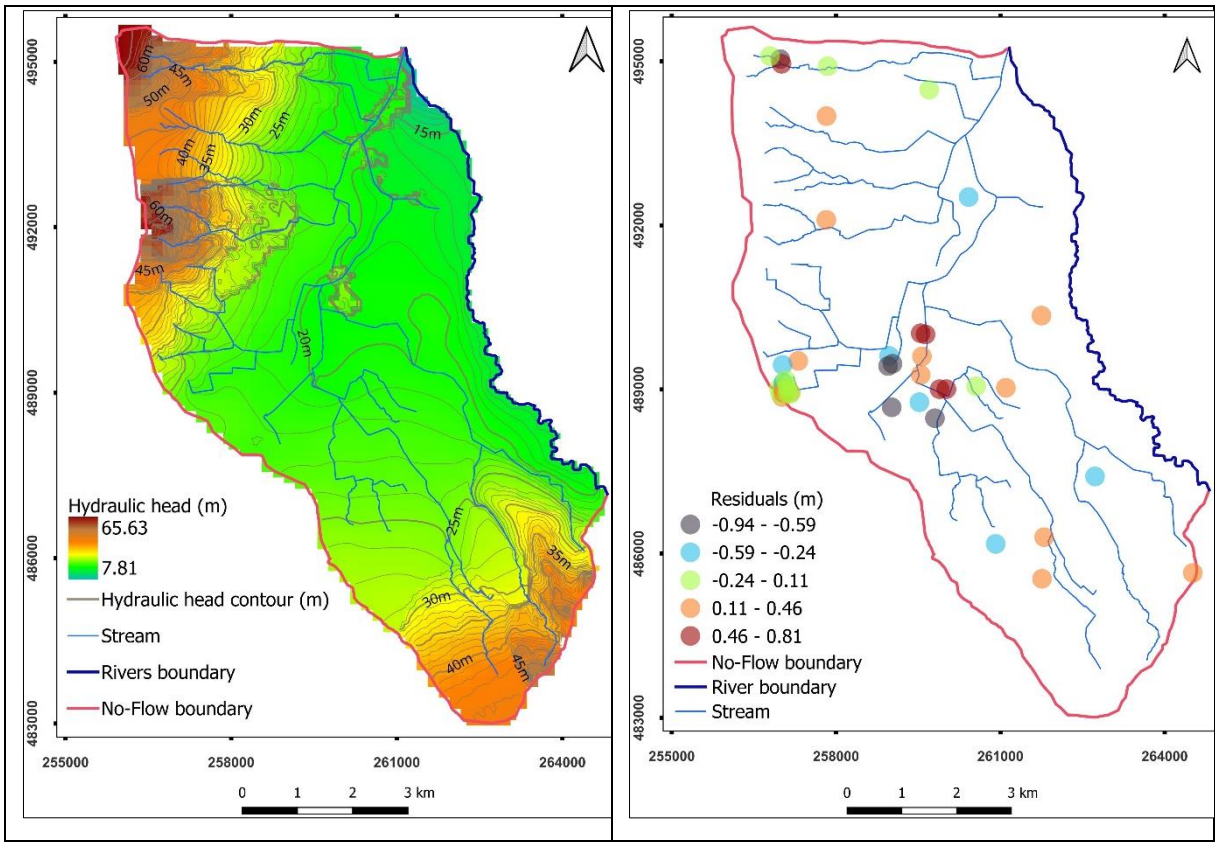

Figure 5.8. Spatial distribution map of hydraulic head and residuals after steady-state model calibration

5.6. Groundwater model validation

The calibrated steady-state model has been validated with 35 independent groundwater level measurements of the hydrological year, 2016. As shown in Figure 5.9, the observed and simulated heads match well to the extent that resembles the calibrated model. The coefficient, 0.98, of the linear regression line also shows a strong relationship between observed and simulated heads. ME of -0.03, MAE of 0.41, and RMSE of 0.55 have been obtained with the maximum residual error of 1.22 meters in the validated model. It is at this stage the calibrated steady-state model was taken as sufficiently calibrated and assessed and ready to be evaluated for its predictive capability for the hydrological regimes of the Hollandse graven catchment.

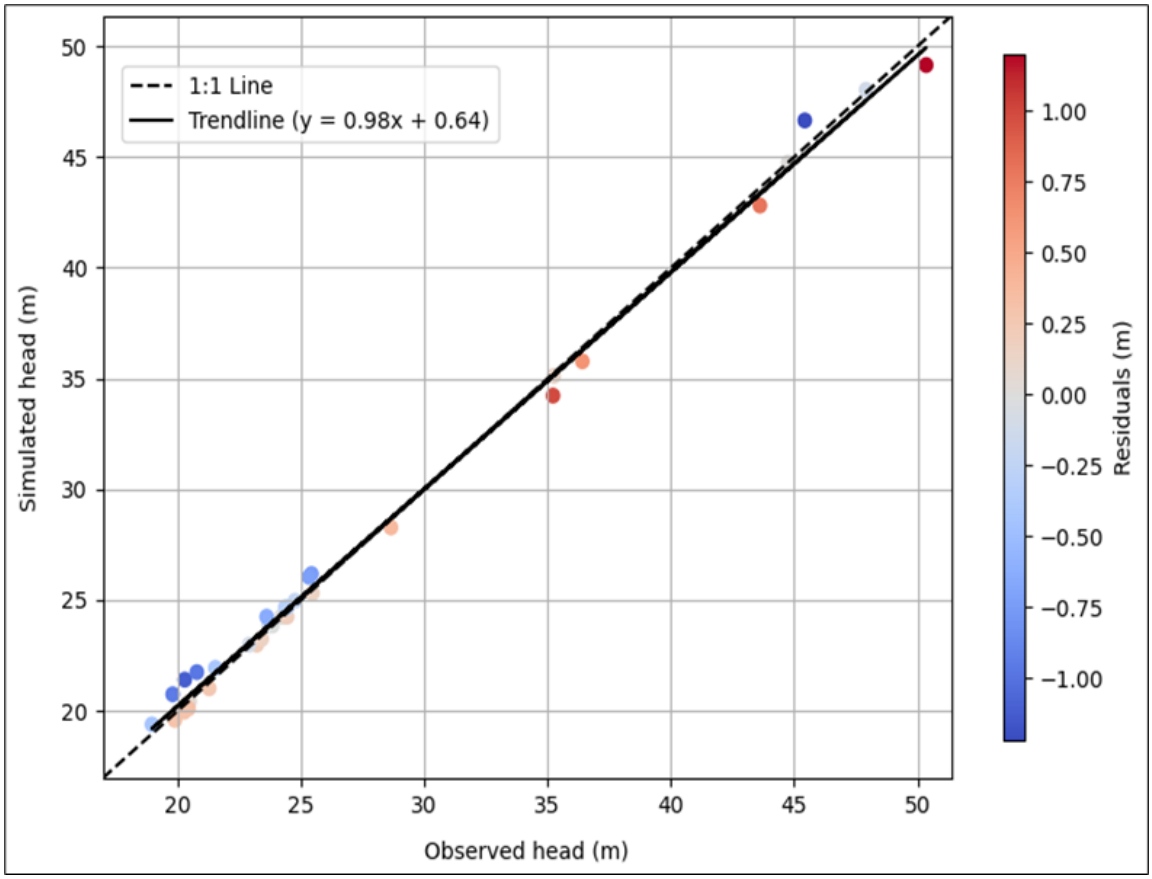

Figure 5.9. plot of model validation observed and simulated head.

Table 5.3. Piezometers and their 2016 mean annual groundwater level (meter/day) which were used to validate the model.

X-coordinate	Y-coordinate	Piezometer ID	Observed head (m)	Simulated head (m)	Residual (m)
257825	493996	B28F0172	35.22	34.23	0.99
256980	495040	B28F0207	45.43	46.65	-1.22
259700	494480	B28F0312	21.53	21.94	-0.41
257309	489522	B28F0354	24.37	24.42	-0.05
257822	492100	B28F0461	36.41	35.78	0.63
261750	490350	B29A0154	20.49	20.44	0.05
261100	489031	B29A0157	21.28	21.02	0.26
261760	485540	B29C0186	28.65	28.28	0.37
262728	487410	B29C0291	25.43	26.18	-0.75
257005	494953	B28F1439	43.61	42.81	0.80
257018	489021	B28F1440	24.20	24.25	-0.05
257038	489111	B28F1441	24.26	24.25	0.01
256794	495094	B28F1442	47.91	48.03	-0.12

257847	494909	B28F1443	35.25	35.12	0.13
259016	488674	B28F1491	20.29	21.41	-1.12
260420	492518	B29A0046	18.96	19.39	-0.43
260014	489006	B29A0851	20.44	20.11	0.33
264514	485647	B29C0118	50.35	49.15	1.20
260915	486177	B29C0214	25.33	26.05	-0.72
263460	484282	B29C1563	44.75	44.75	0.00
259545	489266	B28F0374	20.26	19.96	0.30
259568	489604	B28F0380	19.89	19.59	0.30
258950	489429	B28F0387	19.80	20.75	-0.95
259805	488475	B28F0393	20.78	21.75	-0.97
256956	489024	B28F0397	24.76	24.97	-0.21
257027	489022	B28F0398	24.44	24.25	0.19
257037	489123	B28F0399	24.45	24.67	-0.22
257083	488981	B28F0400	23.69	23.85	-0.16
257169	488942	B28F0401	23.21	22.99	0.22
257041	488934	B28F0403	23.84	23.85	-0.01
257119	488924	B28F0404	23.41	23.25	0.16
257169	488925	B28F0405	22.90	22.99	-0.09
257080	489174	B28F0406	24.36	24.67	-0.31
257108	489056	B28F0407	23.61	24.25	-0.64
261800	486300	B29C0268	25.47	25.32	0.15
		ME	-0.03		
		MAE	0.41		
		RMSE	0.55		

5.7. Groundwater model prediction

After the steady-state groundwater model was calibrated, assessed, and validated, the model was switched to the transient mode as described in section 4.16. Using the observed and simulated results of the hydraulic head and water budget components, the predictive capability of the steady-state-calibrated model under 2017 wet and 2018 dry climatic conditions has been evaluated. There are twenty-four stress periods in the two years of monthly transient simulation. This monthly transient simulation was run with groundwater level measurements from 61 piezometers (Table 5.4). Of the 61 piezometers, all of them have available groundwater level measurements for the dry year 2018 and 33 of them have available measurements for the wet year 2017.

Table 5.4. Piezometers and their monthly average (meter/day) groundwater level data used for the model prediction. ME, MAE and RMSE for each piezometer are also presented. Stress periods 1-12 and 13-24 represents for 2017 wet and 2018 dry years respectively and the first stress period represents April 2017.

Piezometer	X-coordinate	Y-coordinate	Stress periods																						ME	MAE	RMSE
			1	2	3	4	5	6	7	8	9	10	11	12	13	14	15	16	17	18	19	20	21	22	23	24			
B28F0172	257825	493996	35.14	35.05	34.97	34.91	34.87	34.86	34.92	34.93	35.13	35.39	35.41	35.42	35.48	35.37	35.26	35.15	35.03	34.95	34.87	34.81	34.83	34.94	35.07	35.14	2.09	2.09	2.11
B28F0207	256980	495040	45.44	45.38	45.25	45.19	45.15	45.18	45.24	45.28	45.39	45.55	45.57	45.53	45.54	45.47	45.37	45.18	45.07	45.07	45.07	45.12	45.17	45.24	45.33	45.41	0.45	0.70	0.85
B28F0312	259700	494480	21.78	21.53	21.2	21.16	21.23	21.46	21.81	22	22.35	22.51	22.2	22.03	22.04	21.75	21.44	21.07	20.81	20.77	20.75	20.87	21.28	21.96	22.17	22.24	1.40	1.45	1.54
B28F0354	257309	489522	24.58	24.39	23.92	24.06	24.1	24.39	24.66	24.74	24.83	24.86	24.73	24.7	24.66	24.43	23.97	23.64	23.48	23.53	23.48	23.77	24.43	24.75	24.75	24.76	1.21	1.28	1.35
B28F0461	257822	492100	36.46	36.36	36.29	36.41	36.5	36.51	36.53	36.46	36.6	36.74	36.61	36.43	36.44	36.37	36.33	36.24	36.16	36.14	36.19	36.21	36.36	36.53	36.58	36.57	2.16	2.16	2.21
B29A0154	261750	490350	20.72	20.46	20.11	20.12	20.15	20.36	20.72	20.84	21.13	21.25	21.03	20.9	20.89	20.55	20.23	19.9	19.76	19.72	19.68	19.8	20.17	20.78	21	21.07	1.43	1.56	1.61
B29A0157	261100	489031	21.54	21.23	20.83	20.86	20.93	21.05	21.48	21.76	22.11	22.18	21.97	21.82	21.74	21.32	20.93	20.6	20.4	20.3	20.24	20.33	20.68	21.32	21.88	21.98	0.37	0.54	0.65
B29C0186	261760	485540	29.25	28.96	28.19	28.05	28.03	28.05	28.33	28.88	29.43	29.44	29.4	29.39	29.35	28.98	28.3	27.78	27.66	27.65	27.66	27.66	27.66	28.93	29.73	29.29	2.38	2.41	2.51
B29C0291	262728	487410	25.59	25.37	25.04	25.01	24.99	25.11	25.4	25.53	25.92	26.07	25.96	25.9	25.78	25.48	25.19	24.89	24.74	24.64	24.56	24.57	24.87	25.38	25.69	25.8	1.68	1.72	1.85
B28F03precipitation	258780	488660															19.76	19.58	19.49	19.48	19.47	19.58	19.89	20.53	20.66	20.7	-0.91	0.91	1.05
B28F1439	257005	494953	43.62	43.55	43.48	43.57	43.57	43.62	43.64	43.66	43.69	43.7	43.67	43.68	43.64	43.55	43.5	43.35	43.48	43.5	43.53	43.59	43.65	43.66	43.66	43.68	1.22	1.22	1.23
B28F1440	257018	489021	24.57	24.34	23.76	23.71	23.7	23.82	24.33	24.6	24.72	24.73	24.7	24.69	24.64	24.33	23.87	23.5	23.21	23.15	23.11	23.35	23.7	24.4	24.67	24.69	1.32	1.40	1.50
B28F1441	257038	489111	24.51	24.44	23.88	24.14	24.12	24.36	24.49	24.51	24.52	24.53	24.53	24.52	24.52	24.39	23.91	23.39	23.21	23.24	23.23	23.54	24.26	24.5	24.49	24.49	1.38	1.47	1.58
B28F1442	256794	495094	47.88	47.85	47.83	47.82	47.81	47.82	47.84	47.84	47.87	47.9	47.9	47.9	47.9	47.89	47.89	47.85	47.83	47.83	47.83	47.84	47.85	47.85	47.85	47.86	0.80	0.91	0.94
B28F1443	257847	494909	35.27	35.22	35.15	35.18	35.17	35.2	35.24	35.26	35.32	35.38	35.37	35.34	35.33	35.28	35.23	35.1	35.11	35.13	35.13	35.17	35.21	35.26	35.29	35.32	1.61	1.63	1.78
B28F1491	259016	488674	20.63	20.47	20.7	20.74	20.82	20.14	20.57	20.64	20.69	20.7	20.68	20.65	20.64	20.44	20.73	20.31	20.18	20.2	20.21	20.4	20.03	20.57	20.65	20.67	-0.72	0.72	0.88
B29A0046	260420	492518	19.09	18.91	18.67	18.7	18.76	18.93	19.22	19.31	19.55	19.64	19.42	19.26	19.23	18.99	18.79	18.51	18.39	18.4	18.41	18.53	18.87	19.3	19.42	19.46	0.22	0.31	0.38

B29A0187	261090	489520															20.38	20.09	19.91	19.88	19.87	20.04	20.47	21.02	21.18	21.22	0.30	0.41	0.55
B29A0851	260014	489006	20.61	20.49	20.09	20.14	20.17	20.34	20.57	20.65	20.72	20.73	20.69	20.66	20.63	20.5	20.15	19.57	19.41	19.47	19.54	19.87	20.3	20.58	20.66	20.66	0.24	0.44	0.48
B29C1563	263460	484282	45	44.96	44.45	44.24	44.02	44.07	44.61	44.86	45.05	45.06	45.04	45.02	45.02	44.94	44.46	43.72	43.62	43.63	43.64	43.65	43.69	44.06	44.88	44.99	1.77	1.79	2.12
GMW000000013874	259077	490054																		18.18	18.22	18.47	19.33	19.86	19.96	19.98	-1.11	1.11	1.35
GMW000000020093	259306	490368															18.71	18.34	18.07	18.07	18.13	18.34	19.03	19.56	19.62	19.65	-0.94	0.94	1.14
GMW000000020099	259751	490365															18.89	18.51	18.27	18.26	18.32	18.55	19.16	19.86	19.88	19.88	-0.20	0.63	0.68
GMW000000020100	259024	487915															20.59	20.42	20.25	20.2	20.15	20.29	20.72	21.35	21.5	21.54	-0.82	0.84	1.01
GMW000000020101	259736	488114															20.55	20.39	20.28	20.29	20.29	20.44	20.77	21.13	21.21	21.26	-1.16	1.16	1.22
GMW000000020104	258430	489348															19.91	19.73	19.67	19.77	19.82	20.06	20.39	20.52	20.5	20.51	-0.69	0.69	0.79
GMW000000020105	258527	488909															20.14	20.05	19.95	19.93	19.9	19.98	20.36	20.69	20.73	20.77	-0.47	0.52	0.62
GMW000000020106	259427	490936															18.63	18.2	17.92	18.21	18.3	18.45	18.77	18.95	18.93	18.96	-1.57	1.57	1.60
GMW000000020108	258452	490758															20.58	20.51	20.54	20.61	20.6	20.66	20.81	20.89	20.91	20.93	-0.69	0.69	0.73
GMW000000020110	258073	489205															20.34	20.17	20.17	20.29	20.34	20.58	21	21.21	21.21	21.21	-0.45	0.57	0.68
GMW000000020111	258604	490036															19.55	19.34	19.14	19.14	19.16	19.36	19.94	20.28	20.28	20.27	-1.17	1.17	1.27
GMW000000020113	260209	489027															20.06	19.76	19.57	19.59	19.61	19.89	20.4	21.02	21.14	21.22	-0.11	0.58	0.63
GMW000000020114	260947	489190															20.5	20.21	20.01	19.97	19.95	20.13	20.69	21.58	21.81	21.8	-0.03	0.59	0.66
GMW000000020115	260755	488944															18.67	18.47	18.25	18.19	18.17	18.36	18.88	19.68	19.9	19.97	-2.22	2.22	2.30
GMW000000020116	260894	489993															19.92	19.71	19.58	19.58	19.59	19.77	20.34	20.77	20.79	20.81	0.32	0.42	0.57
GMW000000020117	260031	487911															21.07	20.88	20.73	20.71	20.69	20.8	21.17	21.6	21.7	21.77	-1.27	1.27	1.33
GMW000000020118	260227	488636															20.31	20.06	19.94	19.95	19.96	20.16	20.55	20.74	20.78	20.83	-1.38	1.38	1.42

GMW000000020295	258678	488041															20.61	20.45	20.27	20.18	20.1	20.1	20.35	20.81	21.41	21.6	-0.55	0.73	0.79
GMW000000020296	258247	488657															20.28	20.15	20.04	20.02	19.98	20.08	20.5	21.07	21.17	21.17	-0.57	0.72	0.82
GMW000000020298	258554	488223															20.27	20.12	19.94	19.86	19.8	19.85	20.15	20.82	21.17	21.22	-0.70	0.80	0.92
GMW000000020299	258340	488498															20.05	19.86	19.66	19.64	19.64	19.77	20.18	20.7	20.77	20.79	-0.90	0.90	1.08
GMW000000020300	258758	488100															20.65	20.65	20.65	20.65	20.65	20.64	20.64	21.03	21.45	21.52	-0.37	0.49	0.54
GMW000000020302	258909	488387															20.12	20.11	20.11	20.11	20.11	20.11	20.14	20.75	21.16	21.22	-0.64	0.70	0.79
GMW000000020304	260946	488602															20.98	20.76	20.5	20.41	20.36	20.45	20.81	21.38	21.83	21.93	-0.77	0.79	0.91
GMW000000020305	261149	489062															20.91	20.72	20.55	20.46	20.37	20.44	20.79	21.49	21.99	22.08	0.17	0.42	0.56
GMW000000020306	260408	488015															21.82	21.57	21.27	21.11	21.01	20.97	21.06	21.48	21.92	21.18	-0.99	0.99	1.05
B28F0374	259545	489266	20.34	20.24	19.74	20.1	20.18	20.17	20.35	20.38	20.38	20.37	20.36	20.37	20.36	20.22	19.73	19.35	19.15	19.1	19.14	19.72	20.1	20.39	20.36	20.4	0.18	0.43	0.46
B28F0380	259568	489604	19.91	19.64	19.28	19.53	19.44	19.74	20.03	20.08	20.16	20.12	20.03	20.11	20.07	19.74	19.34	19.15	19.08	19.11	19.13	19.33	19.81	20.14	20.04	20.1	0.18	0.37	0.41
B28F0387	258950	489429	19.88	19.74	19.31	19.53	19.79	19.77	19.89	19.91	19.92	19.92	19.9	19.91	19.89	19.73	19.31	18.88	18.75	18.88	18.92	19.46	19.73	19.87	19.87	19.89	-0.85	0.85	0.93
B28F0393	259805	488475	20.97	20.67	20.24	20.46	20.65	20.61	20.89	20.96	21.06	21.05	21.04	21.04	21.01	20.75	20.29	20.01	19.93	19.92	19.92	20.19	20.55	20.94	21.01	21.05	-0.75	0.75	0.83
B28F0397	256956	489024	24.98	24.69	24.01	24.47	24.09	24.41	24.96	24.99	25.02	25	25	25.01	25	24.65	24.05						23.97	24.98	24.98	25	1.30	1.51	1.61
B28F0398	257027	489022	24.61	24.41					24.42	24.68	24.76	24.74	24.7	24.77	24.74	24.67								24.65	24.68	24.72	1.39	1.51	1.71
B28F0399	257037	489123	24.54	24.45	23.87	24.48	24.05	24.44	24.51	24.5	24.55	24.54	24.52	24.54	24.54	24.33	23.78	23.07	23.1			23.45	24.31	24.52	24.51	24.52	1.12	1.31	1.42
B28F0400	257083	488981	23.82	23.62						23.82	23.98	23.97	23.92	23.99	23.96	23.9								23.76	23.9	23.95	1.03	1.25	1.34
B28F0401	257169	488942	23.3	22.84	22.07				23.28	23.34	23.37	23.34	23.3	23.34	23.34	22.88	22.17							23.35	23.35	23.36	0.86	0.95	1.05
B28F0403	257041	488934	24.01	23.53	22.89		22.64	22.82	23.57	23.94	24.08	24.11	24.05	24.11	24.1	23.67	22.78						23.7	23.88	24.08	24.09	1.00	1.15	1.27
B28F0404	257119	488924	23.51	23.03	22.36		22.48	22.71	23	23.44	23.77	23.76	23.67	23.78	23.74	23.18	22.36						22.57	23.3	23.62	23.73	0.93	0.99	1.12

B28F0405	257169	488925	23.24	22.87	21.79	21.6	21.41	21.75	23.01	23.2	23.25	23.26	23.23	23.26	23.23	22.79	21.88	21.21	20.28	20.13	20.06	20.65	21.16	23.23	23.24	23.26	0.17	0.81	0.97
B28F0406	257080	489174	24.68	24.37	23.69	24.13	23.8	24.22	24.64	24.72	24.75	24.75	24.7	24.74	24.71	24.36	23.69	23.16	22.69	22.73	22.63	23.31	24	24.71	24.71	24.73	1.06	1.19	1.34
B28F0407	257108	489056	23.86	23.71	23.05	23.66	23.15	23.6	23.85	23.89	23.92	23.89	23.83	23.89	23.89	23.61	23.05	22.45	21.93	21.87	21.72	22.41	23.22	23.89	23.87	23.89	0.56	0.89	0.99
B29C0268	261800	486300	25.39	25.36	25.26	25.29	25.16	25.56	25.69	25.88	26.04	26.11	26.07	26.11	25.73	25.6	25.32	25.48	24.25	24.24	24.07	24.18	25.11	25.62	25.71	25.86	0.48	0.67	0.71

5.7.1. Water budget of the predictive transient groundwater model

As presented in Table 5.5 for 2017 wet year and Table 5.6 for 2018 dry year, the main water balance components (all in mm. year^{-1}) for each zone have been separated and presented. In the configuration of transient groundwater models, effective precipitation is partitioned into gross recharge, unsaturated zone evapotranspiration and unsaturated zone storage using the UZF package (El-Zehairy et al., 2018) while the remaining is rejected infiltration. As such, the input to the land surface and the unsaturated zone is taken as effective precipitation, whereas unsaturated zone evapotranspiration, rejected infiltration, gross recharge and unsaturated zone storage change are outputs.

In the surface and unsaturated zone, the effective precipitation for the wet 2017 and dry 2018 years accounts 709.12 mm year^{-1} and 552.46 mm year^{-1}, respectively (Table 5.5 and Table 5.6). In both wet and dry years, unsaturated zone evapotranspiration accounts the highest percentage: 33.99% and 53.18% of their respective effective precipitation respectively. The higher percentage of unsaturated zone evapotranspiration in 2018 is most possibly due to the drought event. While unsaturated zone storage change is the second highest with 30.48 % of effective precipitation for the wet year, gross recharge is the second highest output with 27.56 % of effective precipitation for the dry year. This variation in the unsaturated storage change could be due to the higher effective precipitation during the wet year. Gross recharge in the wet year is the third highest output components that covers 27.87% of the effective precipitation whereas, unsaturated zone storage change for the dry year holds the third position of the output components converting 13.44% of effective precipitation. Rejected infiltration covers the remaining, lowest of all output components in both wet and dry years.

Gross recharge, stream and river seepage to the groundwater and groundwater storage are the main inputs to the saturated zone in both wet and dry years. On the other hand, groundwater evapotranspiration, groundwater exfiltration and groundwater seepage to streams and river are the main outputs. In both wet and dry years, stream seepage to the groundwater covers the highest fraction of the total inputs to the saturated zone with 41.15% for the wet and 46.43% for the dry years. However, it is the groundwater seepage to streams that covers the highest portion of the total outputs in both wet and dry years with 69.63% and 64.57% of the total outputs respectively. This indicates that the interactions between groundwater and streams is high. In both dry and wet years, gross recharge is the second highest input to the saturated zone with 38.67% and 35.87% of the total input to the saturated zone for wet and dry years respectively. It is observed that groundwater exfiltration is the second highest output components of the saturated zone in both wet and dry years with 27.83% and 32.82% of their respective total output respectively. The groundwater exfiltration in the dry year (139.38 mm. year^{-1}) however, is greater than the wet year (136.95 mm. year^{-1}) and this could be due to the lower aquifer total storage change in the dry year (-30.81 mm. year^{-1}) than the wet year (-136.74 mm. year^{-1}) which could create more available water for groundwater exfiltration. Groundwater evapotranspiration only covers 2.53 % and 2.59% of the total saturated zone outputs for wet and dry years respectively. This low proportion of the groundwater evapotranspiration could

be due to either the water needs of evapotranspiration is satisfied by the unsaturated zone or the water table is below the rooting depth of the land cover classes. Another observation is that groundwater seepage to river is almost negligible and river seepage to the groundwater is almost constant in both wet and dry years. This could be due to either the groundwater level being found below the river bottom or inappropriate river level and bottom assignments since no measured data available.

Table 5.5. Water budget for the 2017 wet year (mm. year^{-1})

Zone	P	P_e	q_{sw}	E_I	ETu	ET_g	RI	Exf_{gw}	q_{gs}	q_{sg}	q_{gr}	q_{rg}	R_g	ΔSu	ΔSg	ΔS	In	out	In-out	Discrepancy
Surface and unsaturated zone		709.12			241.06		54.27						197.66	-216.14			709.12	709.13	0.01	0.00
Saturated zone						12.45		136.95	342.60	202.45	0.01	31.67	197.66		79.40		511.18	492.01	19.17	3.82
Whole catchment	834.33		20.39	104.82	241.06	12.45	54.27	136.95	342.60	202.45	0.01	31.67				-136.74	1068.45	1049.29		1.81

Table 5.6. Water budget for the 2018 dry year (mm. year ^{1})

Zone	P	P_e	q_{sw}	E_I	ETu	ET_g	RI	Exf_{gw}	q_{gs}	q_{sg}	q_{gr}	q_{rg}	R_g	ΔSu	ΔSg	ΔS	In	out	In-out	Discrepancy
Surface and unsaturated zone		552.46			293.81		32.16						152.26	-74.23			552.46	552.46	0.00	0.00
Saturated zone						11.01		139.38	274.20	197.06	0.01	31.72	152.26		43.41		424.45	424.6	-0.15	-0.04
Whole catchment	650.00		15.88	81.66	293.81	11.01	32.16	139.38	274.20	197.06	0.01	31.72				-30.81	878.78	878.92	-0.14	-0.02

Comparisons of yearly average water balance components for the 2017 wet and 2018 dry year has been presnted in Figure 5.10. Since effective precipitation is dependent on the precipitation and interception rate, and interception rate is the same for both years but, precipitation. As such, the 2017 wet year has higher effective precipitation than the 2018 dry year. Precipitated water that directly routed to the sewarage system is also higher in the wet year. In both 2017 wet and 2018 dry years, unsaturated zone evapotranspiration is the major contributer for total evapotranspiration. On the other hand groundwater evapotranspiration is very small. The evapotranspiration water demand is initially met by removing water from the unsaturated zone; the remaining water demand then is fulfilled by utilizing groundwater depending on the position of the rooting depth and groundwater table (El-Zehairy et al., 2018; Langevin et al., 2017). Therefore, the small amount of groundwater evapotranspiration is possibly due to the majority of evapotranspiration water demand in the Hollandse graven catchment is satisfied with water from the unsaturated zone. While interception and unsaturated zone evapotranspiration are higher in dry year than wet year, the groundwater evapotranspiration is slightly higher in the 2017 wet year than the 2018 dry year (see Table 5.5 and Table 5.6 for specific figure). The higher unsaturated zone evapotranspiratiion in the dry year is due to the higher reference evapotranspiration which leads to higher PET during the 2018 dry year than the contrasting 2017 wet year (Figure 4.2). However, the slightly higher groundwater evapotranspiration in the 2017 wet year than the 2018 dry year is unexpected and it would be probably due to the model unable to calculate reliable groundwater evapotranspiration values.

Rejected infiltration in the 2017 wet year is higher than the contrasting 2018 dry year and this is because of the higher precipitation during the wet year. The vertical hydraulic conductivity has already been adjusted and if the effective precipitation is greater, which increases with increasing precipitation, than the vertical hydraulic conductivity, that portion of water will be rejected. Groundwater exfiltration is approximately the same value in both 2017 wet and 2018 dry years, however the groundwater exfiltration during the dry year is slightly greater than the wet year (see Table 5.5 and Table 5.6 for specific figure) which is difficult to explain in relation to conceptualization. The higher groundwater exfiltration during the dry year than the wet year could be due to the model being uncalibrated for the transient conditions or lower aquifer total storage change in the dry year. As expected gross recharge and net recharge are higher in 2017 wet year than the 2018 dry year and this is due to the higher precipitation in the wet year which leads to higher effective precipitation which in turn causes higher gross recharge and net recharge.

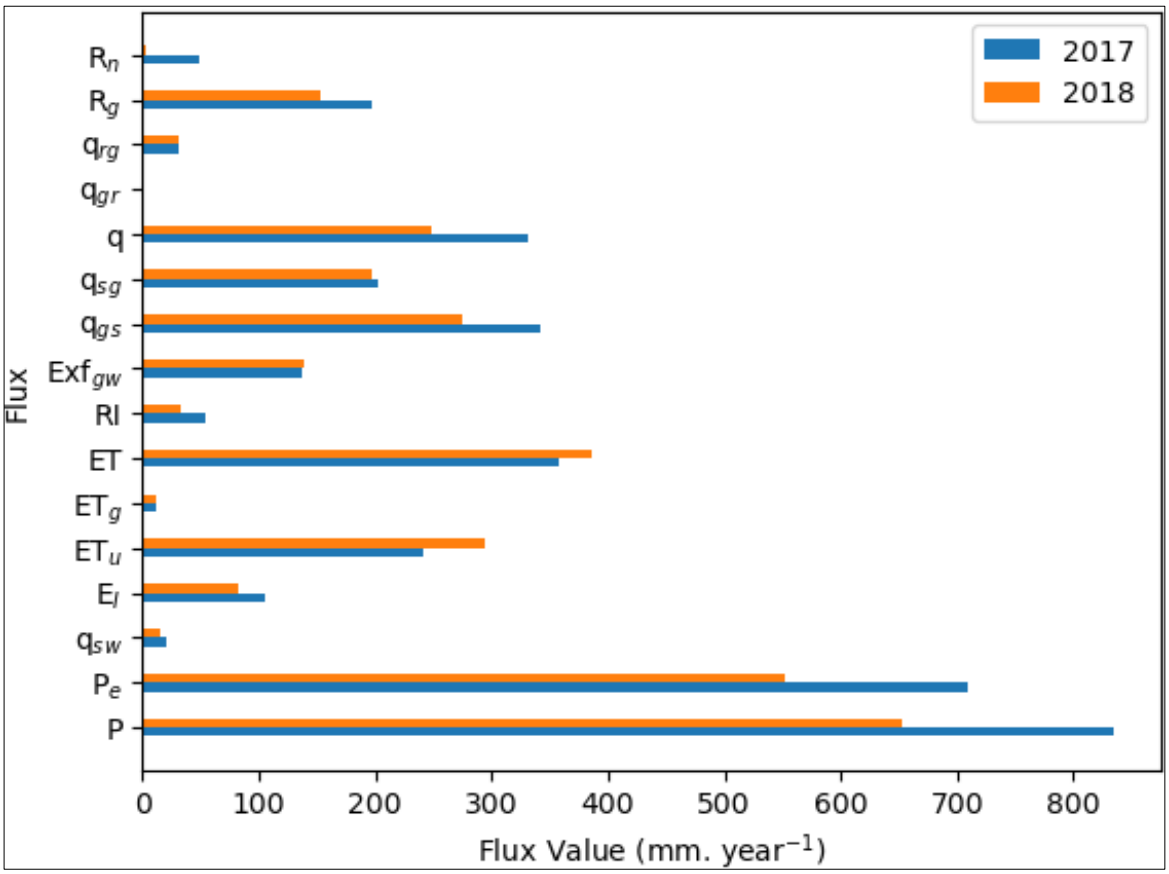

Figure 5.10. Comparison of water balance components of the 2017 wet and 2018 dry years.

5.7.2. Overall model predictive capability

The observed and simulated heads for the entire simulation period have been presented in visual observations (Figure 5.11Figure 5.11). From the visual observations, the simulated and observed heads show a good match with 0.95 coefficient of a regression line. Though some piezometers have more than 3 meters of residuals, the graph depicts that the model has been able to capture the overall hydraulic head variability. The overall ME, MAE and RMSE metrics errors have been calculated and found; ME of 0.45, MAE of 1.08, and RMSE of 1.29 meters. Though elevation variations within the catchment could matter, Daoud et al. (2022) and Hassan et al. (2014), took RMSE ≤ 1 as an acceptable error metric for transient groundwater model calibration. Taking the model being calibrated in steady-state conditions and tested for a transient mode without transient calibration into consideration, -1.25 ≤ ME ≤1.25, MAE ≤ 1.7, and RMSE ≤ 2.0 meters have been taken as acceptable model predictions in this study. Hence, based on the calculated ME, MAE and RMSE, the overall predictive capability of the Hollandse graven steady-state calibrated groundwater model is taken as acceptable.

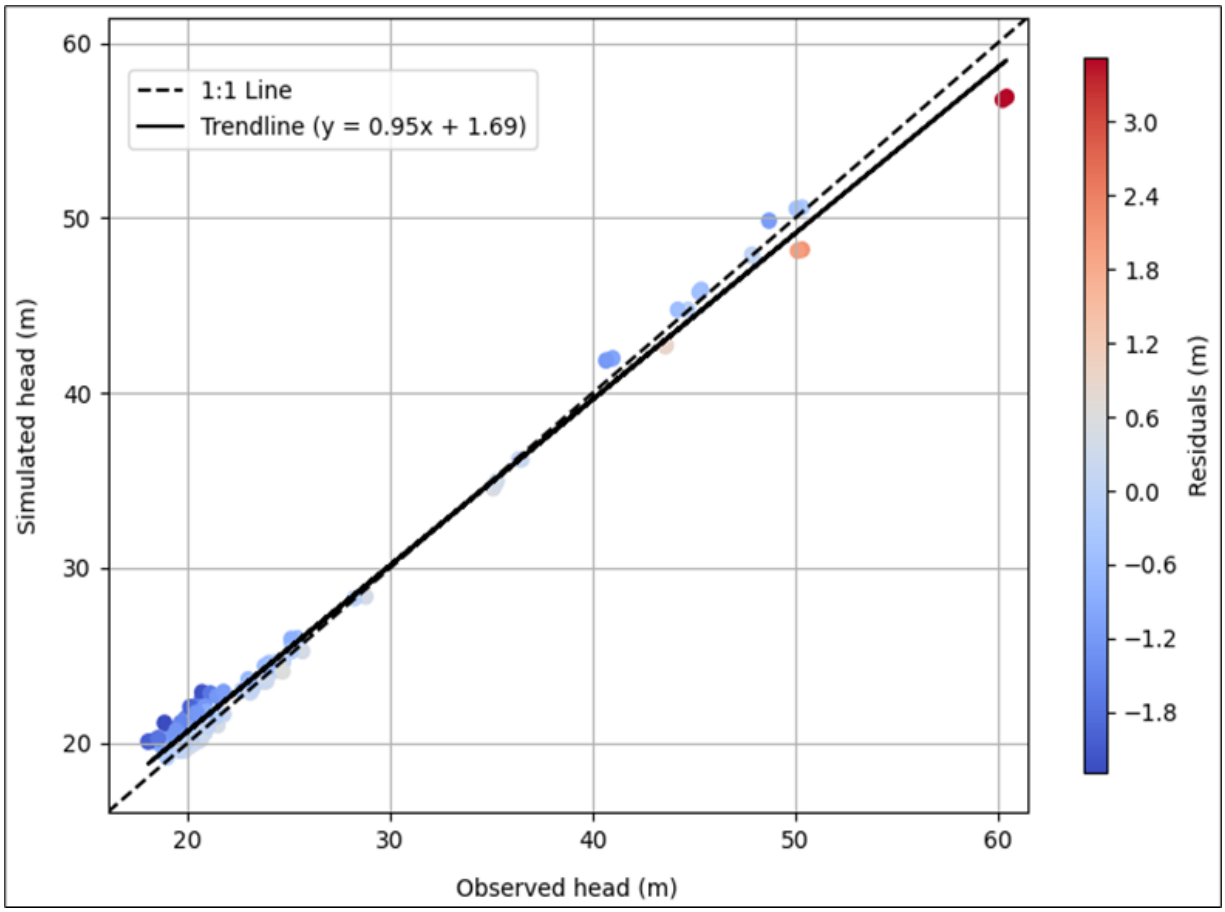

Figure 5.11. Observed versus simulated hydraulic head for the entire transient simulation period with 61 piezometers.

The ME, MAE and RMSE for each of the 61 piezometers which are used to test the model in transient mode simulation have been calculated and presented in Table 5.4 and Figure 5.12. From the 61 piezometers, the minimum ME is found to be -0.03 meter while the minimum MAE and RMSE are 0.31 and 0.38 meters respectively. On the other hand, the maximum ME is 2.38 and maximum MAE and RMSE are 2.41 and 2.51 meters respectively.

To better understand the model prediction bias from the distribution of a histogram of ME, non-uniform bin width approach, considering negative, zero and positive ME values, has been implemented in the construction of a histogram for ME (Figure 5.12). It is observed from the ME histogram that 28 (45.9%) piezometers have ME < 0, with 33 (54.1%) piezometers ME >0 and no piezometer with ME $= 0$. Piezometers with positive ME are greater than those with negative ME by five which indicates that on average, predictions are lower than the actual hydraulic heads; the model underestimates the hydraulic head. This could be due to the lack of measured storage parameter. From the MAE and RMSE histograms, 36 (59.1%) piezometers have MAE of ≤ 1.01 meters whereas 34 (55.7%) piezometers have RMSE of ≤ 1.09 meters; 55 (90.2%) piezometers have an MAE of ≤ 1.71 meters and an RMSE of ≤ 1.8 meters, which is taken as an acceptable value in this modelling exercise for the prediction model without transient calibration conducted.

From the total of 61 piezometers used for the transient groundwater model testing, it is calculated that 73.77% demonstrated the ME of -1.25 ≤ ME ≤ 1.25 (Table 5.4) and 90.20 % with MAE and RMSE of ≤1.71 and ≤ 1.80 meters (Table 5.4 and Figure 5.12) respectively. Important point to note here is that these values of error metrices have been obtained while incorporating 17 extra piezometers for the prediction that have not been used in the model calibration; 44 piezometers have been used to calibrate the steady-state groundwater model (Table 5.2). Therefore, from the overall ME, MAE and RMSE analysis, it can be concluded that a steady-state calibrated model of the Hollandse graven catchment could be used for the prediction of its hydrological water regimes under 2017 wet and 2018 dry climatic conditions.

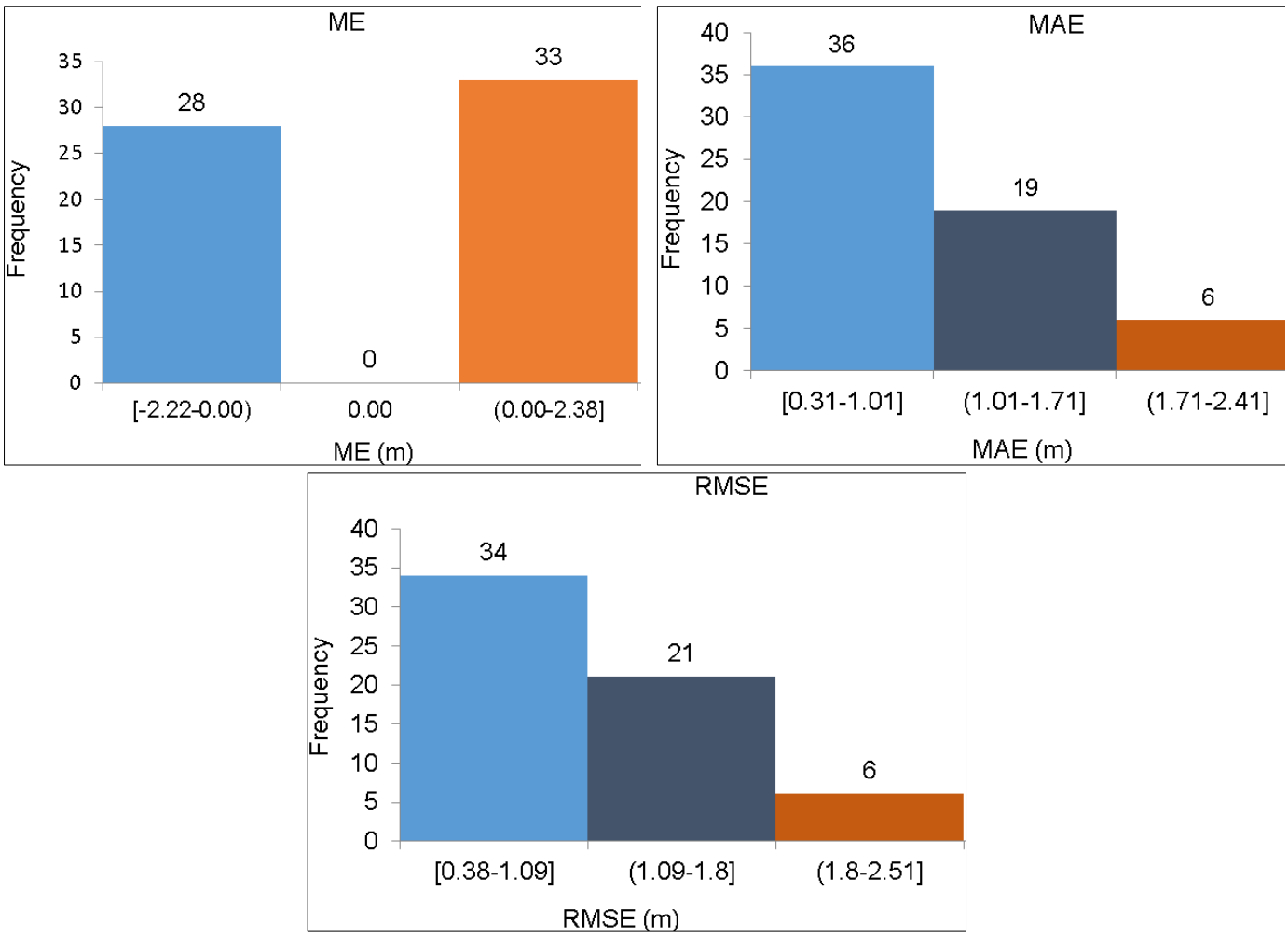

Figure 5.12. A histogram illustrating the range of ME, MAE and RMSE values for all the 61 piezometers used in model testing.

To understand how the transient testing model replicates the observed hydraulic head for the temporal variations, 7 piezometers have been selected (Figure 5.13) based on the spatial distribution and availability of observed hydraulic heads for all stress periods.

Based on the precipitation and reference ET data, the stress periods can be generalized into two parts: 1) Stress periods where reference ET is greater than precipitation; stress periods, 1-3 and 13-19 are typical examples (Figure 5.14). Though reference ET on those stress periods generally is higher, at some stress periods, precipitation and reference ET are comparable, both high or low, and on others, reference ET is much higher than precipitation. 2) Stress periods where precipitation is greater than reference ET. Typical stress periods of such type include 4-10 and 21-24. Again, there are stress periods where reference ET is high, though generally less than precipitation, and stress periods where precipitation is much higher than reference ET. The observed versus simulated hydraulic head graphs (Figure 5.14) show trends based on those two generalizations.

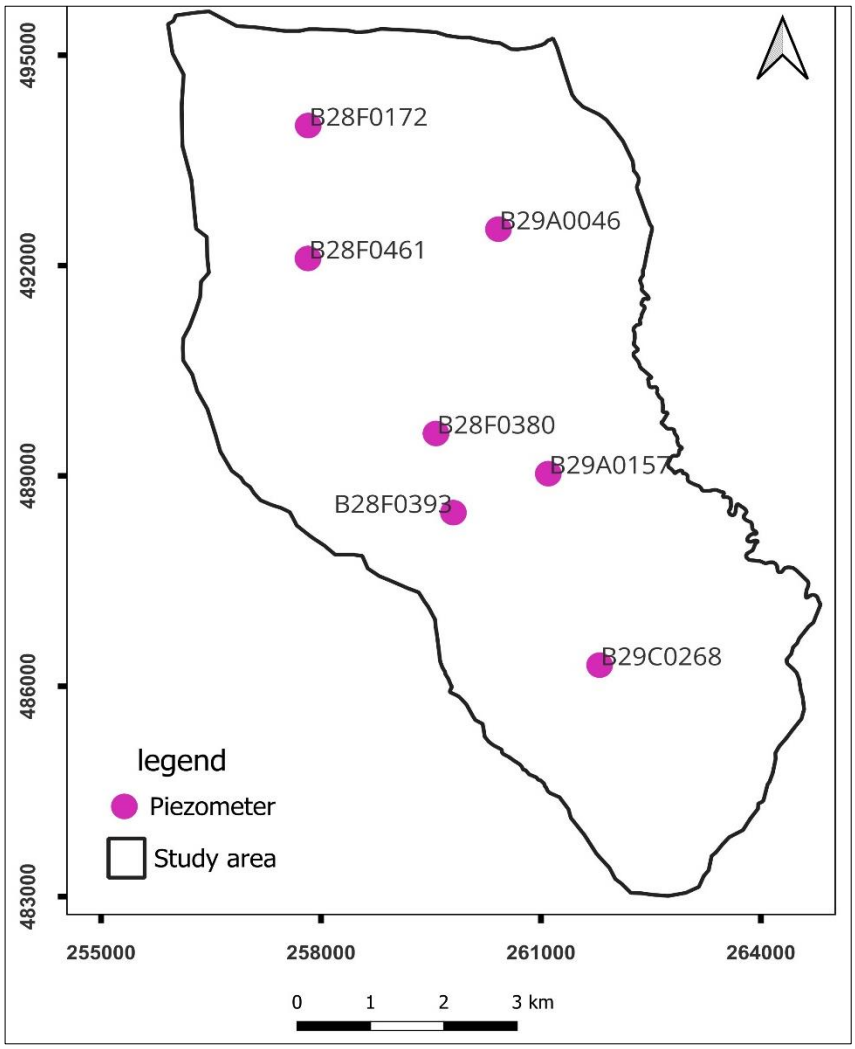

Figure 5.13. Location of the seven selected piezometers based on spatial distribution and availability of measured hydraulic head for the whole stress period.

From the global trend observation, the testing model in most of the piezometers captures the general temporal variability of the hydraulic head. However, while some piezometers, e.g., B29A0046, show distinct variations in simulated head changes between stress periods, others, e.g., B29C0268, exhibited subtle changes. The observed versus simulated hydraulic head of piezometer B28F0461 diverge from the first to the last stress period, regardless of the variations in precipitation and reference ET; while the observed head slightly changes with the forcings, the simulated head continuously decreases as the stress period increases. This could possibly be the piezometer being located within the region of the built-up area (see the land cover map, Figure 2.3) where the built-up area is conceptualized as having no effective precipitation (Figure 5.1).

Though precipitation increases from the first to the next 2 stress periods, reference ET also increases, and reference ET is greater than precipitation on stress periods 1-3. Due to the higher ET and its increasing trend from stress periods 1-3, the observed and simulated head decreases from stress periods 1 -3 in most

of the selected piezometers. The relatively higher hydraulic head in the first stress period while both precipitation and reference ET are low could be due the influence of initial hydraulic head of the transient testing model, which is the steady-state's calculated hydraulic head. This decreasing trend of the observed versus simulated head is also observed at higher reference evapotranspiration stress periods 13-19.
Stress periods 4-10 and 21-24 are characterized by higher precipitation than reference evapotranspiration and generally show higher values of observed and simulated hydraulic heads in most of the selected piezometers. Precipitation at stress period 4 is the highest of all time however, both simulated and observed heads do not show the highest peaks in the corresponding stress period. This could be due to the comparatively higher reference evapotranspiration that results in high unsaturated zone and groundwater evapotranspiration.

To explain peaks and troughs of the simulated hydraulic head, in almost all piezometers, there is a slight peak at the 11th stress period where both precipitation and reference evapotranspiration are low. This could be due to 1) the cumulative precipitation of the stress periods 7-10 where precipitation is high and reference ET is low. Such a combination of high precipitation and low reference ET is again observed at stress periods 21-24, but the stress period next to that is not part of this model to generalize. 2) discrepancy, which could be attributed to the model being uncalibrated for transient conditions. It is important to note that the assigned specific yield and specific storage are not obtained from the measurement which could contribute for inappropriate response to the forcings. Another observation is that, at some piezometers, e.g., B29A0046, the simulated head gets higher than the observed head at some stress periods, while the observed is greater in most stress periods. That happens next to the high reference evapotranspiration at stress periods 14-16. This could be due to the temporal discrepancy or some localized unconceptualized hydrological processes around those areas at the time of those stress periods that could decrease the measured hydraulic head.
Generally, though the steady state calibrated groundwater model captures the global temporal variability, it gets difficulties in replicating the hydraulic head for each stress period. Errors in model conceptualization and parametrization, variability in subgrid-scale altitude, unrepresented aquifer hetrogenity and unaccounted water extraction according to Daoud et al. (2022) and Hassan et al. (2014) are the likely reasons that cause discrepancies in the simulated heads of calibrated groundwater models. In addition to those reasons, the model being uncalibrated for transient conditions could probably took the prior position for the simulated head discrepancies observed in the current testing model. Aquifer heterogeneity in terms of storage parameters have not been conceptualized since it has been assigned the same value for the same hydrogeological units.

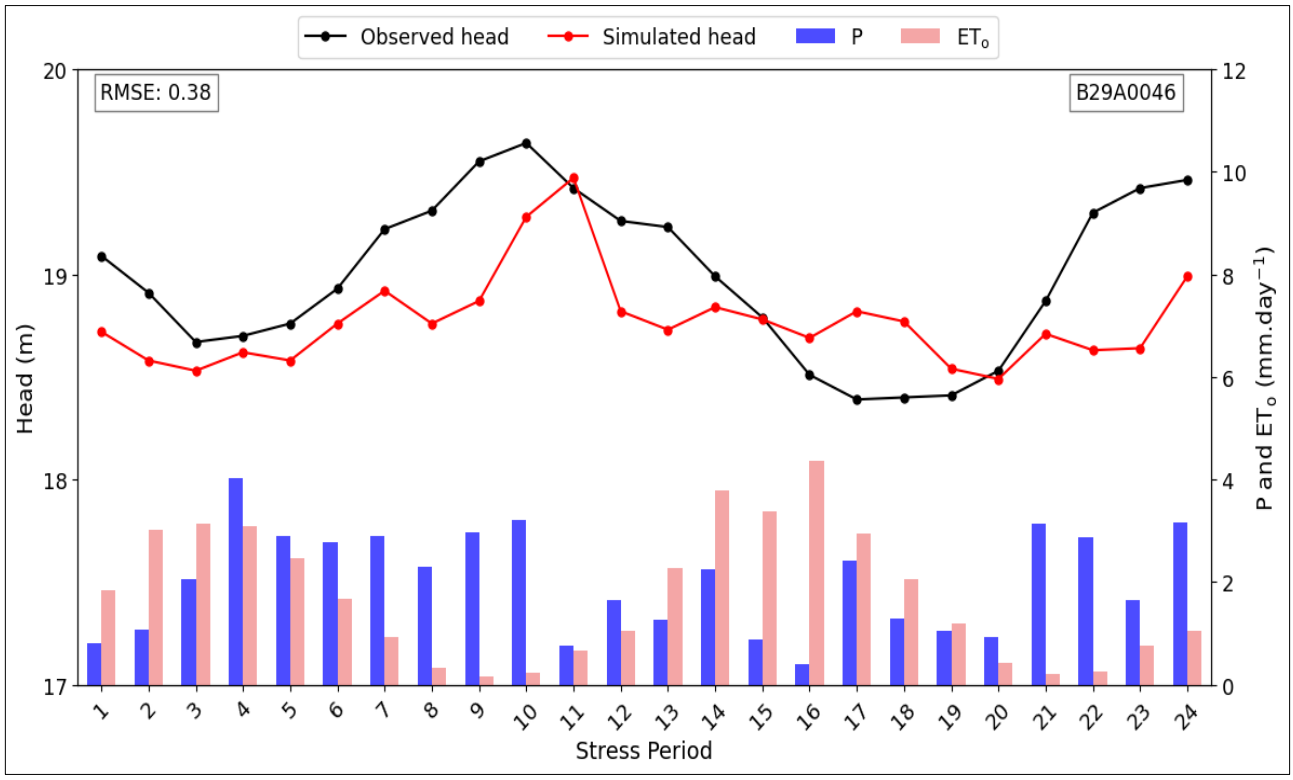
Observed head
Simulated head
P
ET$_o$
RMSE: 0.38
B29A0046
Head (m)
P and ET$_o$ (mm.day^{-1})
Stress Period

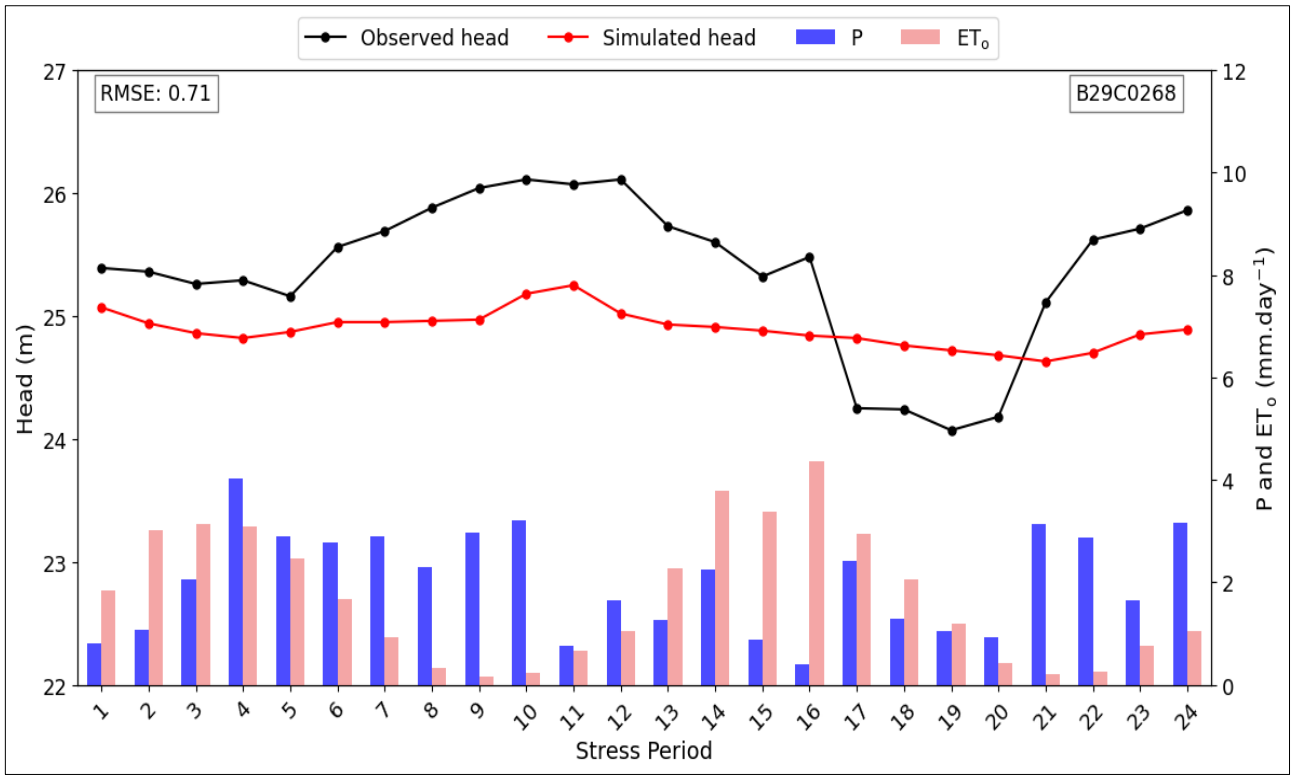
Observed head
Simulated head
P
ET$_o$
RMSE: 0.71
B29C0268
Head (m)
P and ET$_o$ (mm.day^{-1})
Stress Period

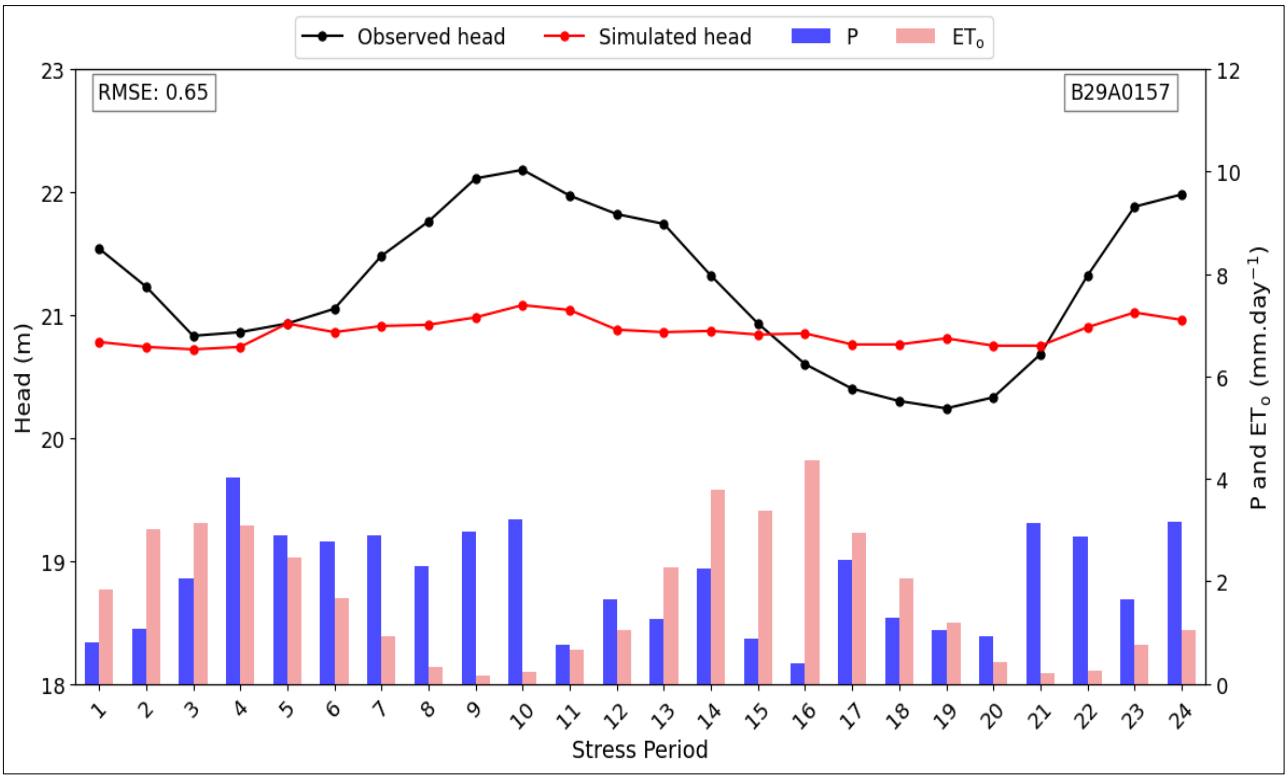
Observed head
Simulated head
P
ET$_o$
RMSE: 0.65
B29A0157
Head (m)
P and ET$_o$ (mm.day^{-1})
Stress Period

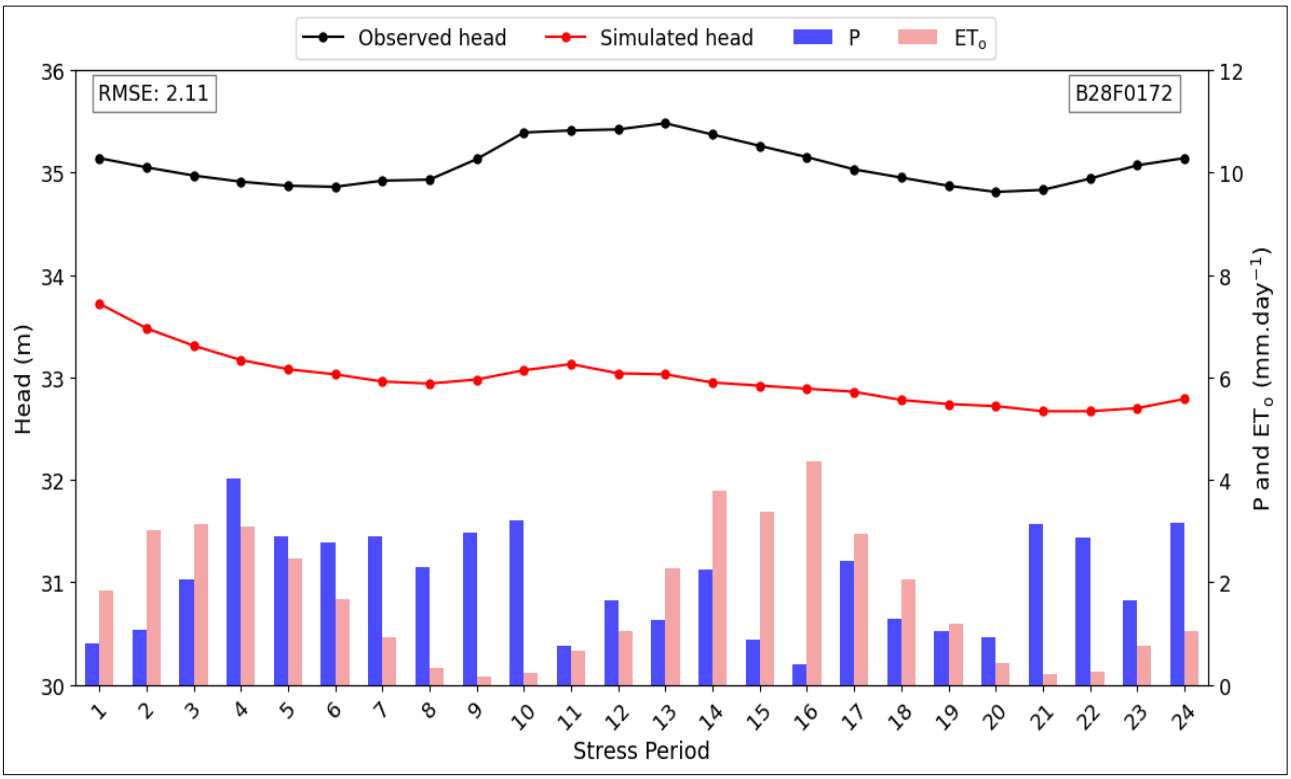
Observed head
Simulated head
P
ET$_o$
RMSE: 2.11
B28F0172
Head (m)
P and ET$_o$ (mm.day^{-1})
Stress Period

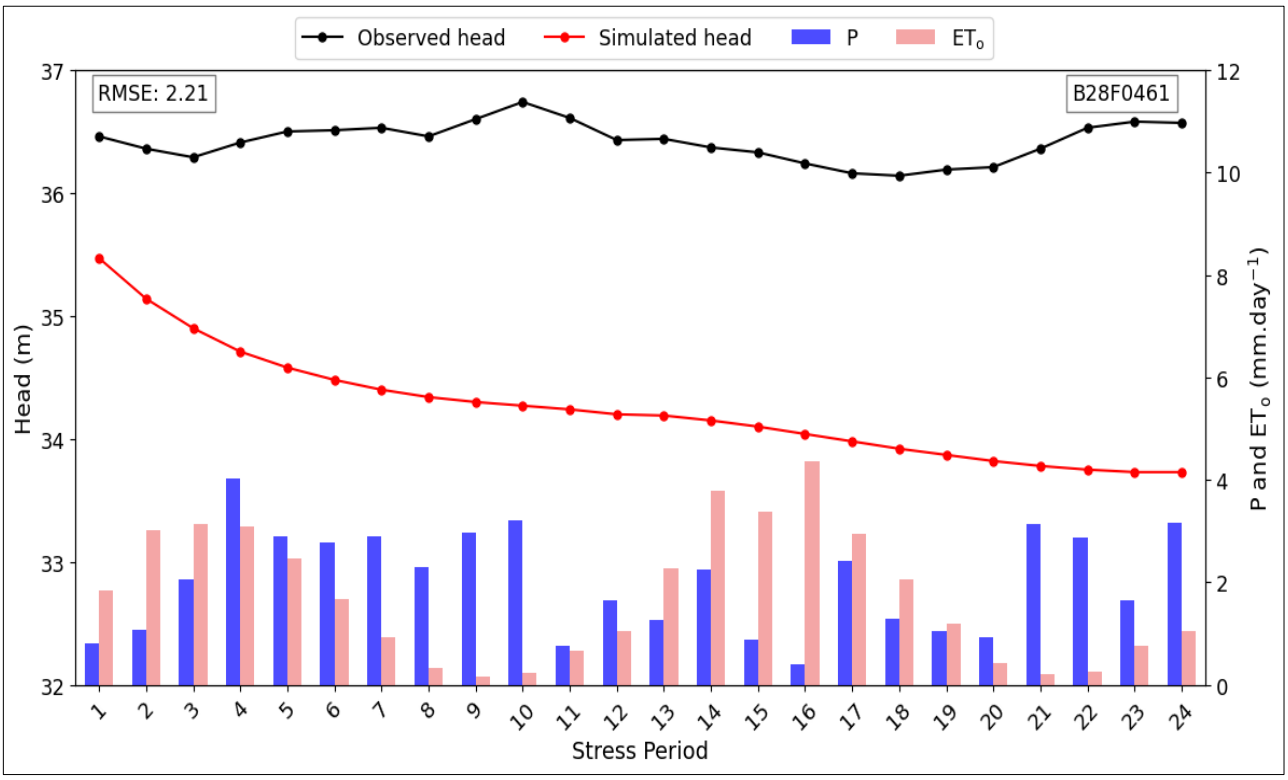
Observed head
Simulated head
P
ET$_o$
RMSE: 2.21
B28F0461
Head (m)
P and ET$_o$ (mm.day^{-1})
Stress Period

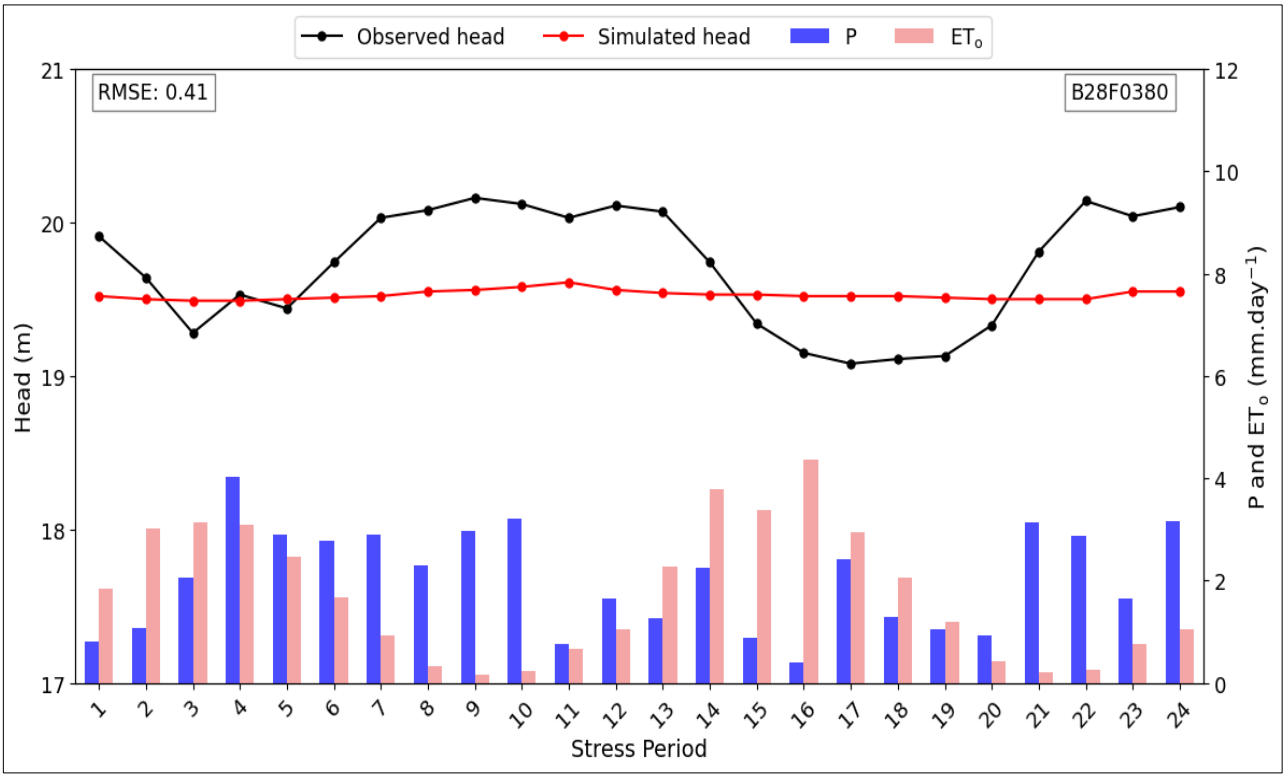
Observed head
Simulated head
P
ET$_o$
RMSE: 0.41
B28F0380
Head (m)
P and ET$_o$ (mm.day^{-1})
Stress Period

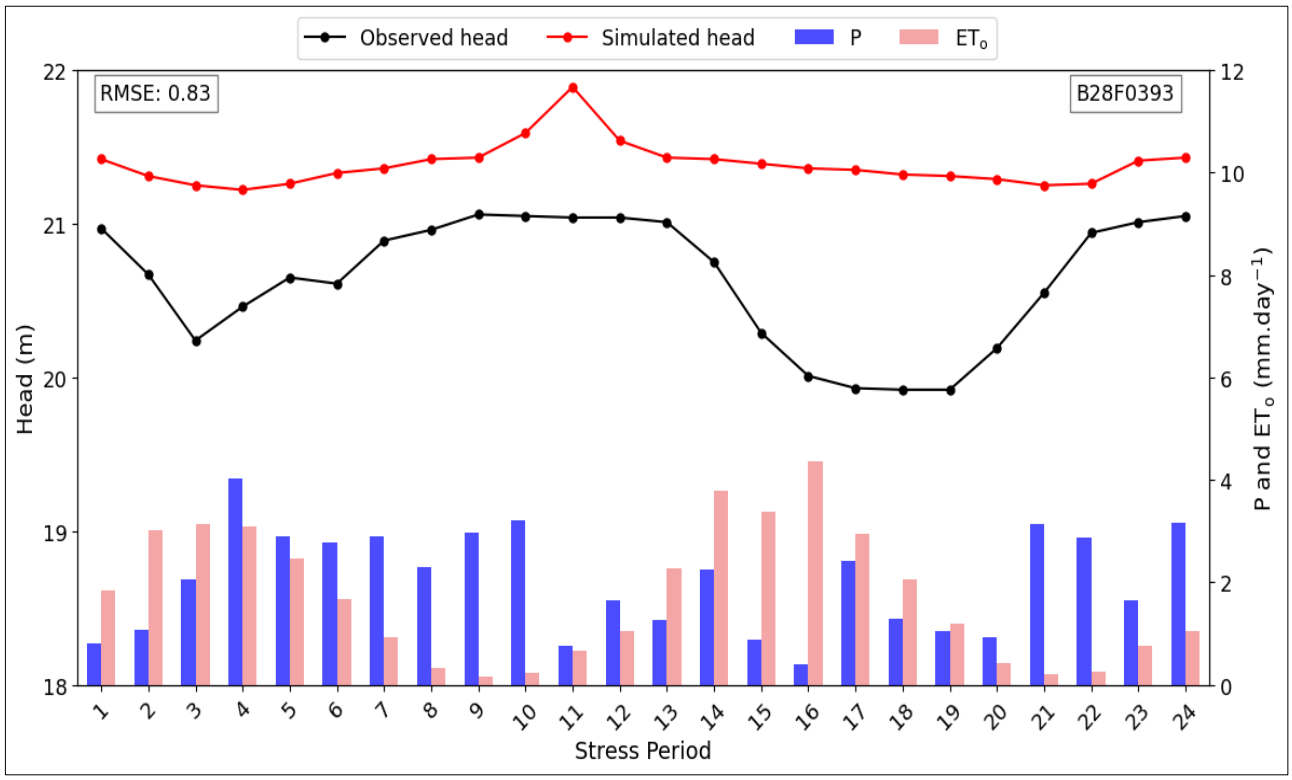

Figure 5.14. Observed versus simulated hydraulic head graphs for seven selected piezometers.

5.7.3. Comparison of wet and dry year predictive capability

There are 33 piezometers out of 61 that have measured hydraulic heads in both 2017 wet and 2018 dry years (Table 5.4). The wet and dry years predictive capability of the calibrated steady-state model has been compared using spatial distribution of error matrices (Figure 5.15) and histogram of the error metrices (Figure 5.16). The spatial distribution of ME, MAE and RMSE maps show that there are no clear differences in the spatial distribution of error metrices between 2017 wet and 2018 dry years. In all the error metrices, smaller values have been observed around the central part of the study area, however this pattern is common for both 2017 wet and 2018 dry years and not observed when all the 61 piezometers are displayed (not presented here). Both negative and positive ME values are also exhibit spatially distributed across the entire study area in both 2017 wet and 2018 dry years. Therefore, based on the spatial distribution of error metrices, the predictive capability of the calibrated steady-state groundwater model does not show distinct differences between 2017 wet and 2018 dry years. However, comparisons based on the maximum and minimum error metrices (see Figure 5.15, legend) between the 2017 wet and 2018 dry years depicts that maximum values are observed in 2018 dry year compared to the 2017 wet year in all the metrices. The maximum ME in 2017 wet year is 2.14. However, this figure demonstrated a notable increase for the dry year of 2018, reaching 2.68 meters. The minimum MAE and RMSE in 2017 wet year are 0.31 and 0.36 meters respectively, however those values for the 2018 dry year are 0.32 and 0.4 meters respectively. The maximum MAE and RMSE for 2017 wet year are 2.19 and 2.31 respectively, but those values for the dry year are 2.68 and 2.8 meters

respectively which demonstrated a notable increase. Therefore, based on the minimum and maximum error metrices assessment, the calibrated steady-state groundwater model of the Hollandse graven catchment exhibits superior predictive capabilities for the 2017 wet year compared to the 2018 dry year.

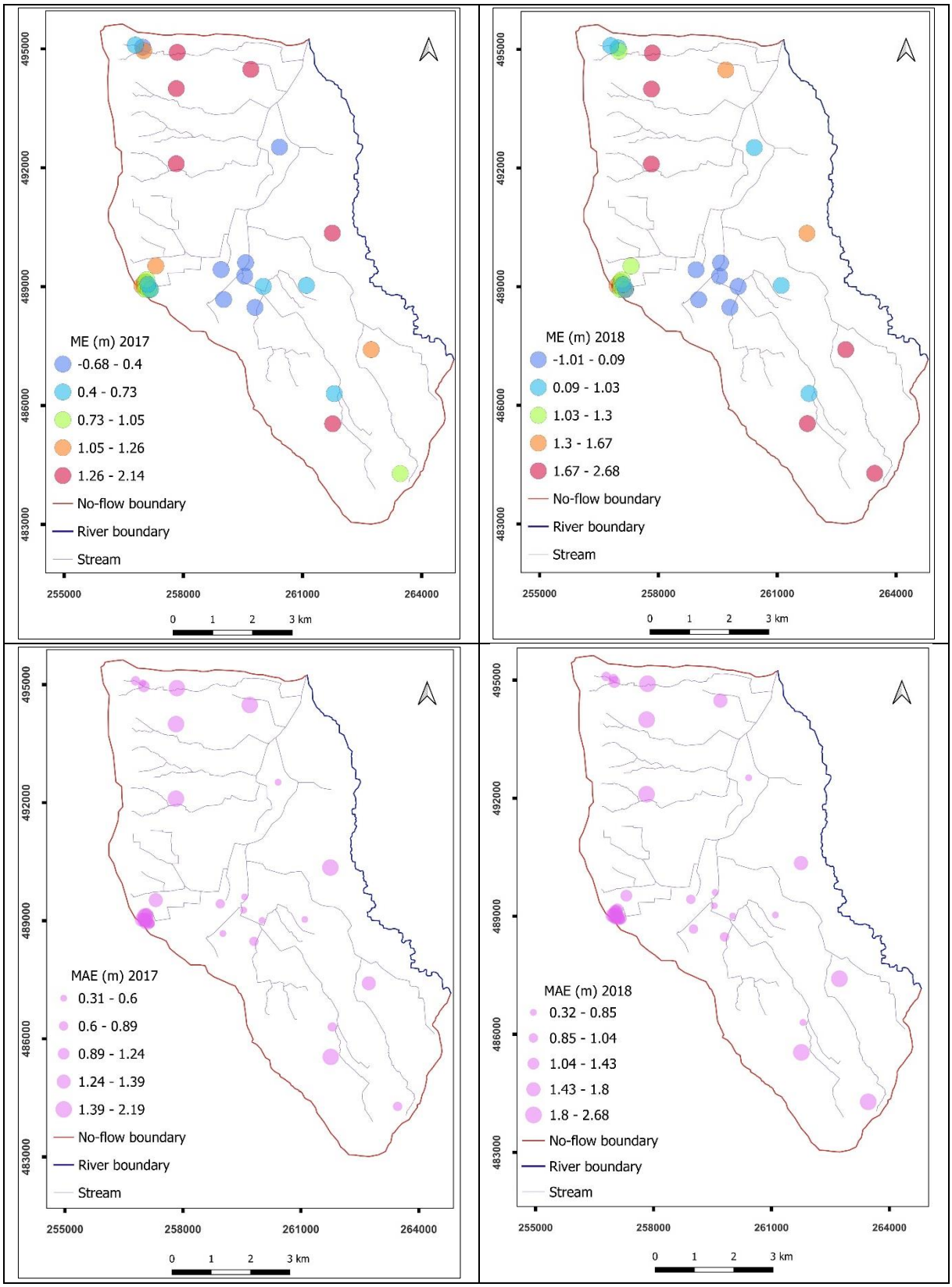

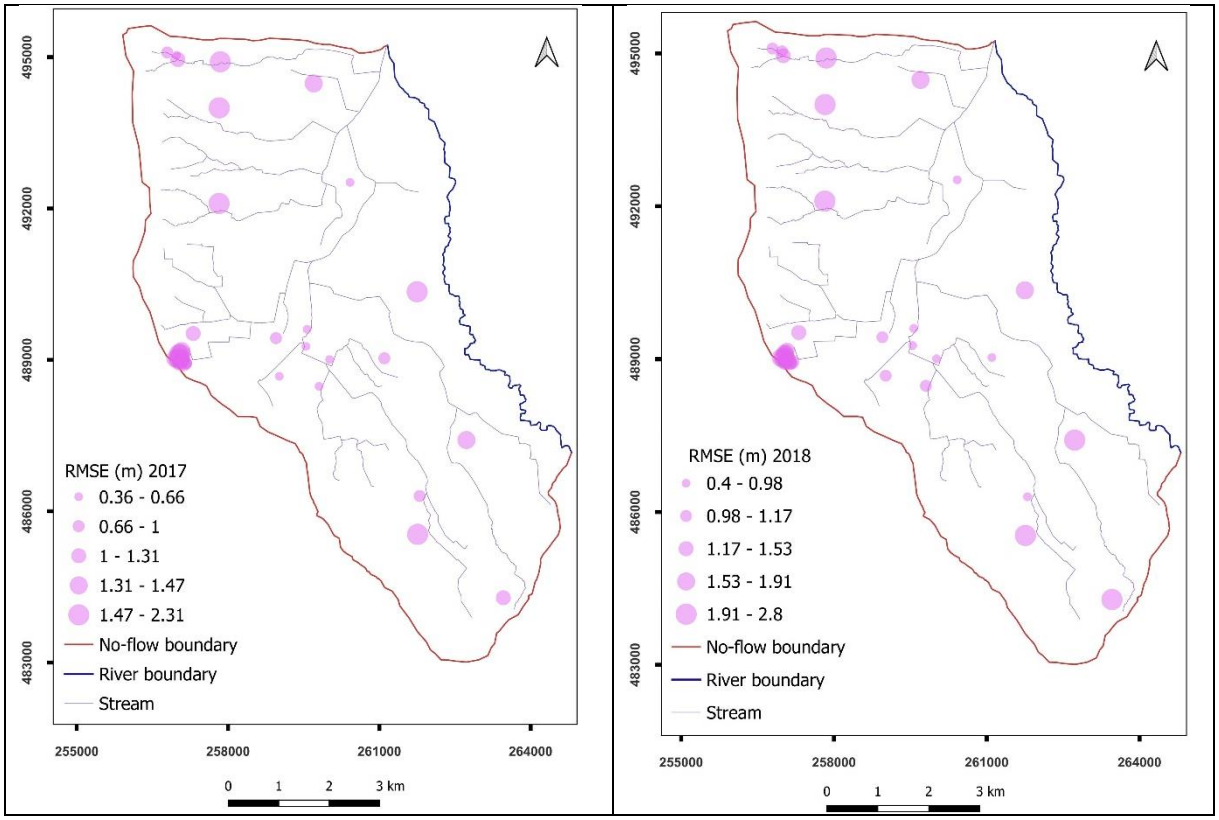

Figure 5.15. Illustrates the spatial distribution of ME, MAE and RMSE for 2017 wet and 2018 dry years computed from 33 piezometers that have available hydraulic head data for both years.

Histograms for ME, MAE and RMSE have also been constructed (Figure 5.16). In both 2017 wet and 2018 dry years, most of the piezometers have positive ME values; 30 (90.9%) and 28 (84.8%) piezometers out of 33 demonstrated positive ME values in the 2017 wet and 2018 dry years, respectively, which indicates that the model predictions are less than the measured hydraulic head for those common piezometers. Based on the ME histogram, the model is more biased for the prediction of 2017 wet hydrological year. While only 3 (9.1%) piezometers have an MAE of ≥ 1.89 meters in the 2017 wet year, it is 5 (15.2%) piezometers for the 2018 dry year. similarly, there is only 1 (3%) piezometer in the wet 2017 year which has an RMSE of > 2 meters, but there are 6 (18.2%) piezometers with an RMSE of > 2 meters in the 2018 dry year. Based on MAE and RMSE analysis, the calibrated steady state groundwater model predicts better for the 2017 wet year compared to the dry year of 2018.

The model being a better predictor for the 2017 wet year than the 2018 dry year based on the MAE and RMSE error metrics calculation is probably due to the precipitation and evapotranspiration of the calibration dataset being closer to the wet year than the dry year. The difference between precipitation of the wet year (834.33 mm. year^{-1}) and calibration years (788.4 mm. year^{-1}) is 45.93 mm. year^{-1} whereas, the difference in evapotranspiration of wet year (567.27 mm. year^{-1}) and calibration years (580.35 mm. year^{-1}) is 13.08 mm. year^{-1}. On the other hand, the difference between the precipitation of the dry year (650 mm. year^{-1}) and calibration years is 138.4 mm. year^{-1}, and their difference in evapotranspiration, 689.24 mm. year^{-1} for dry,

year is 108.89 mm. year^{-1}. In terms of both precipitation and reference evapotranspiration, the difference between the calibration dataset and 2017 wet year dataset is lower than that of the contrasting 2018 dry year.

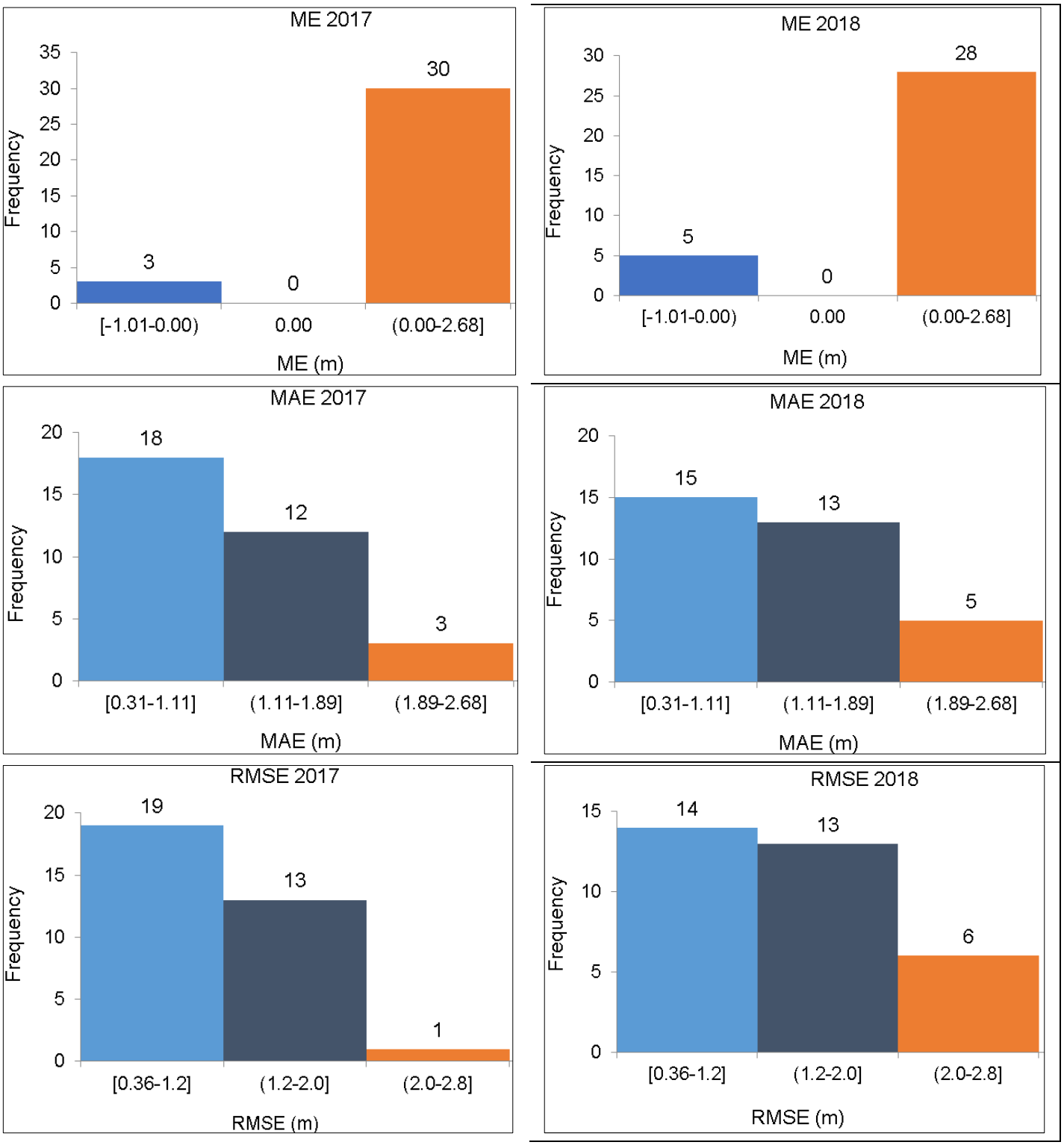

Figure 5.16. Histogram depicting the ME, MAE and RMSE values for 2017 wet and 2018 dry years constructed from 33 piezometers that have common hydraulic head data in both years.

6. CONCLUSION AND RECCOMMENDATION

6.1. Conclusion

Due to the less required data for calibration, computational efficiency, and easier model setup, steady-state groundwater models are often developed to simulate transient conditions. Hence, it is crucial to understand the capability of steady state groundwater models in predicting hydrological system regimes in transient mode under specific conditions. The Hollandse graven catchment, located in the eastern Netherlands, is charachterizd dominantly by sandy soils and grass land cover classes. The catchment is found to be appropraite to test the predictive capability of steady-state calibrated groundwater models in transient mode under 2017 wet and 2018 dry climatic conditions, due to the available time series precipitation, reference evapotranspiration and groundwater level measurments. To test the predictive capability of the steady-state groundwater model of the Hollandse graven catchment, first a MODFLOW 6-based steady state groundwater model with six years of hydrological data was developed. Second, model assessment and model validation were performed and finally, model testing in transient mode with twenty-four stress periods has been conducted.

Detailed representation of the subsurface hydrogeology and reliable boundary conditions reduces model uncertainity in the development of numerical hydrogeological models. A hydrogeological model, accounting nine units have been identified based on their hydrogeological characteristics, clay and sand, obtained from the REGIS II hydrogeological model of the Netherlands. The identification of those high number of distinct hydrogeological units contributes significantly for the representation of hydrological system hetrogenity in model prediction. Forthermore, the establishement of the boundary conditions of the Hollandse graven catchment using available physical feature- river boundary in the east and applying the conceptual framework of groundwater streamlines based on isohypses which provide no flow boundary on the remaining perimeters strengthen the reliability of the conceptual hydrological model.

Calibrating a groundwater model with high number of hydrogeological units using trial and error method of calibration takes time since it involves adjustment of the hydraulic conductivity for all hydrogeological units. Through meticulous trial and error method of calibration, a promising result has achieved for a steady-state groundwater model of the Hollandse graven catchment. The remarkable agreement between the forty-four observed and the simulated hydraulic heads indicate the robustness of the calibrated model. Moreover, the model error metrices calculations: Mean error (ME) of zero could indicate the unbiased calibration of the model, MAE and RMSE of 0.34 and 0.42 meters, respectively, demonstrated the model being calibrated sufficiently.

From the calculation of water balance of predictive groundwater model, the unsaturated zone evapotranspiration is the highest: 33.99% and 53.18% of their respective effective precipitation for 2017 wet and 2018 dry years. This dominant unsaturated zone evapotranspiration in the model testing shows the importance of the unsaturated zone evapotranspiration in the Hollandse graven catchment. This high percentage of unsaturated zone evapotranspiration could be due to the adequate available water at the unsaturated zone that satisfies the water needs of ET.

The steady-state model predictive capability assessment was conducted for the overall simulation period using 1) overall simulated versus observed hydraulic head 2) error metrices: ME, MAE and RMSE and 3) observed versus simulated hydraulic heads of individual piezometers. There are reasonable agreements between observed and simulated heads. This underscores that the overall model residual errors are not excessively high. This is one of an important aspect of error assessment where the observed and simulated hydraulic heads do not significantly deviate from each other. Therefore, the steady state calibrated model predictions could be taken as acceptable. Based on the second set of steady state model predictive capability assessment, 73.77% demonstrated the ME of $-1.25 \leq ME \leq 1.25$, 90.2 % with MAE of ≤ 1.71 and RMSE of ≤ 1.8 meters. Such error metrices from the steady-state model uncalibrated for transient conditions indicate acceptable predictions. The high percentage of piezometers being found in the indicated low range of error metrices is another indicator where residuals between observed and simulated heads are low. However, it is also important to note that from the analysis of ME, 54.1% of the model prediction heads are lower than the actual measured heads, hence the model could be taken as biased in its prediction which is also observed in both wet and dry years. From Figure 5.14, only one piezometer, from the selected seven, resembles the observed head. This challenge of accurately replicating the observed head could be due to the model being uncalibrated for the transient condition. Though the model is taken as acceptable based on the overall simulated versus observed hydraulic heads and error metrices: ME, MAE and RMSE, the comparison at selected piezometers shows deviations. Therefore, the main conclusion is that although the steady-state calibrated groundwater model of the Hollanse graven catchment is taken as acceptable based on error metrics, it still encounters challenges in replicating dynamically the hydraulic head across stress periods for the prediction of its hydrological system regimes under both wet and dry climatic conditions.

6.2. Reccomndation

The following points are the main recommendations of this research.

- Finer temporal and spatial discretization is recommended to reach at a more firm conclusion about the predictive capability of steady state groundwater models for transient simulations.

- Infiltration and evaporation of rejected infiltration and groundwater exfiltration are not conceptualized in the current groundwater model of the Hollandse graven catchment. It's recommended to conceptualize those processes in the model which could decrease the uncertainties of the model.

- The river boundary is taken as constant values (DTM) for monthly transient model prediction due to the absence of time series river stage records. Hence, it is recommended to test the model, with time variability of the river stage for the model prediction.

- The Almelo-Nordhorn canal has not been conceptualized in the current groundwater model calibration and prediction. Further investigation is recommended if there exist interactions of the canal water with the groundwater along the canal.

REFERENCES

Ala-aho, P., Rossi, P.M., Isokangas, E., Kløve, B., 2015. Fully integrated surface-subsurface flow modelling of groundwater-lake interaction in an esker aquifer: Model verification with stable isotopes and airborne thermal imaging. J. Hydrol. 522, 391–406. https://doi.org/10.1016/j.jhydrol.2014.12.054

Allen, R.G., Pereira, L.S., Raes, D., Smith, M., 1998. Crop evapotranspiration - Guidelines for computing crop water requirements - FAO Irrigation and drainage paper 56. FAO - Food and Agriculture Organization of the United Nations.Rome.

Anderson, M.P., Woessner, W.W., 1991. Applied groundwater modeling - simulation of flow and advective transport (4. pr.).

Anderson, M.P., Woessner, W.W., Hunt, R.J., 2015. Applied Groundwater Modeling—Simulation of Flow and Advective Transport, 2nd Editio. ed. Academic Press. https://doi.org/10.1111/gwat.12464

Awais, M., Arshad, M., Ahmad, S.R., Nazeer, A., Waqas, M.M., Aziz, R., Shakoor, A., Rizwan, M., Chauhdary, J.N., Mehmood, Q., Ahmad, M., 2023. Simulation of Groundwater Flow Dynamics under Different Stresses Using MODFLOW in Rechna Doab, Pakistan. Sustain. 15. https://doi.org/10.3390/su15010661

Bakke, S.J., Ionita, M., Tallaksen, L.M., 2020. The 2018 northern European hydrological drought and its drivers in a historical perspective. Hydrol. Earth Syst. Sci. 24, 5621–5653. https://doi.org/10.5194/hess-24-5621-2020

Bakker, M., Post, V., Langevin, C.D., Hughes, J.D., White, J.T., Starn, J.J., Fienen, M.N., 2016. Scripting MODFLOW Model Development Using Python and FloPy. Groundwater 54, 733–739. https://doi.org/10.1111/GWAT.12413

Barnett, B., Townley, L., Post, V., Evans, R., Hunt, R., Peeters, L., Richardson, S., Werner, A., Knapton, A., Boronkay, A., 2012. Australian groundwater modelling guidelines, Waterlines report, National Water Commission. Canberra. https://doi.org/10.5422/fordham/9780823263752.003.0009

Climate Change Knowledge Portal-https://climateknowledgeportal.worldbank.org/ [WWW Document], n.d. URL https://climateknowledgeportal.worldbank.org/ (accessed 3.1.23).

Corbett, E.S., Crouse, R.P., 1968. Rainfall interception by annual grass and chaparral . . . losses compared. U.S. For. Serv. Res. Pap. PSW zvzreport Berkeley, Calif., Pacific SW. Forest & R.

CORINE Land Cover- https://land.copernicus.eu/en/products/corine-land-cover [WWW Document], n.d. URL https://land.copernicus.eu/en/products/corine-land-cover (accessed 1.4.23).

Daoud, M.G., Lubczynski, M.W., Vekerdy, Z., Francés, A.P., 2022. Application of a novel cascade-routing and reinfiltration concept with a Voronoi unstructured grid in MODFLOW 6, for an assessment of surface-water/groundwater interactions in a hard-rock catchment (Sardon, Spain). Hydrogeol. J. 30, 899–925. https://doi.org/10.1007/s10040-021-02430-z

Dassargues, A., 2019. Hydrogeology: Groundwater Science and Engineering, Groundwater.

de Jong, S.M., Jetten, V.G., 2007. Estimating spatial patterns of rainfall interception from remotely sensed vegetation indices and spectral mixture analysis. Int. J. Geogr. Inf. Sci. 21, 529–545. https://doi.org/10.1080/13658810601064884

Di Salvo, C., 2022. Improving Results of Existing Groundwater Numerical Models Using Machine Learning Techniques: A Review. Water (Switzerland) 14. https://doi.org/10.3390/w14152307

DINO counter-Stratigraphic Nomenclator-https://www.dinoloket.nl/stratigrafische-nomenclator [WWW Document], n.d. URL https://www.dinoloket.nl/stratigrafische-nomenclator (accessed 1.15.23).

Dinoloket-https://www.dinoloket.nl/ [WWW Document], n.d. URL https://www.dinoloket.nl/ (accessed 1.25.23).

El-Zehairy, A.A., Lubczynski, M.W., Gurwin, J., 2018. Interactions of artificial lakes with groundwater applying an integrated MODFLOW solution. Hydrogeol. J. 26, 109–132. https://doi.org/10.1007/s10040-017-1641-x

Fan, X., Vrieling, A., Muller, B., Nelson, A., 2020. Winter cover crops in Dutch maize fields: Variability in quality and its drivers assessed from multi-temporal Sentinel-2 imagery. Int. J. Appl. Earth Obs. Geoinf. 91, 102139. https://doi.org/10.1016/j.jag.2020.102139

Farrick, K.K., Price, J.S., 2010. Ericaceous shrubs on abandoned block-cut peatlands: Implications for soil water availability and Sphagnum restoration. Ecohydrology 130, 126–130. https://doi.org/10.1002/eco

Finlayson, M., Everard, M., Irvine, K., McInnes, R.J., Middleton, B.A., van Dam, A.A., Davidson, N.C., 2018. The Wetland Book: Surface Water and the Maintenance of Hydrological Regimes, Springer, Dordrecht. https://doi.org/10.1007/978-90-481-9659-3

Foxx, T.S., Tierney, G.D., Williams, J.M., 1984. Rooting depths of plants relative to biological and environmental factors 26.

Francés, A.P., Reyes, L., Balugani, E., Tol, C. van der, Lubczynski, M.W., 2011. Assessment of catchment water balance using distributed and transient coupled models of the unsaturated and saturated zones, in: Proceedings of the ModelCare 2011 Conference. University of leipzig, Leipzig, Germany, p. 2.

Ghazavi, R., Ebrahimi, H., 2019. Predicting the impacts of climate change on groundwater recharge in an arid environment using modeling approach. Int. J. Clim. Chang. Strateg. Manag. 11, 88–99. https://doi.org/10.1108/IJCCSM-04-2017-0085

Groundwater-https://www.grondwatertools.nl/gwsinbeeld/ [WWW Document], n.d. URL https://www.grondwatertools.nl/gwsinbeeld/ (accessed 3.17.23).

Hassan, S.M.T., Lubczynski, M.W., Niswonger, R.G., Su, Z., 2014. Surface-groundwater interactions in hard rocks in Sardon Catchment of western Spain: An integrated modeling approach. J. Hydrol. 517, 390–410. https://doi.org/10.1016/j.jhydrol.2014.05.026

Heinen, M., Mulder, H.M., Bakker, G., Wösten, J.H.M., Brouwer, F., Teuling, K., Walvoort, D.J.J., 2022. The Dutch soil physical units map: BOFEK. Geoderma 427.

https://doi.org/10.1016/j.geoderma.2022.116123

Hendriks, D.M.D., Kuijper, M.J.M., van Ek, R., 2014. L'impact des eaux souterraines sur le besoin environnemental en eau des rivières des bassins versants sableux des Pays-Bas. Hydrol. Sci. J. 59, 562–577. https://doi.org/10.1080/02626667.2014.892601

Jetten, V.G., 1996. Interception of tropical rain forest: Performance of a canopy water balance model. Hydrol. Process. 10, 671–685. https://doi.org/10.1002/(sici)1099-1085(199605)10:5<671::aid-hyp310>3.0.co;2-a

Kaandorp, V.P., de Louw, P.G.B., van der Velde, Y., Broers, H.P., 2018. Transient Groundwater Travel Time Distributions and Age-Ranked Storage-Discharge Relationships of Three Lowland Catchments. Water Resour. Res. 54, 4519–4536. https://doi.org/10.1029/2017WR022461

Kozak, J.A., Ahuja, L.R., Green, T.R., Liwang, M., 2007. Modelling crop canopy and residue rainfall interception effects on soil hydrological components for semi-arid agriculture. Wiley Intersci. 21, 2267–2274. https://doi.org/10.1002/hyp.6235

Kuijper, M.J.M., Goorden, N., Vermeulen, P.T.M., 2012. Update Grondwatermodel Waterschap Regge en Dinkel. Deltares Rep. 1–91.

Langevin, C.D., Hughes, J.D., Banta, E.R., Niswonger, R.G., Panday, S., Provost, A.M., 2017. Documentation for the MODFLOW 6 Groundwater Flow Model. US Geol Surv Tech. Methods 6-A55 197. https://doi.org/https://doi.org/10.3133/tm6A55

Mohammed, K.S., Shabanlou, S., Rajabi, A., Yosefvand, F., Izadbakhsh, M.A., 2023. Prediction of groundwater level fluctuations using artificial intelligence-based models and GMS. Appl. Water Sci. 13, 1–14. https://doi.org/10.1007/s13201-022-01861-7

Moore, C.R., Doherty, J., 2021. Exploring the Adequacy of Steady-State-Only Calibration. Front. Earth Sci. 9, 1–17. https://doi.org/10.3389/feart.2021.692671

NHI -https://data.nhi.nu/ [WWW Document], n.d. URL https://data.nhi.nu/ (accessed 5.15.23).

NISTOR, M.-M., 2018. Projection of Annual Crop Coefficients in Italy Based on Climate Models and Land Cover Data. Geogr. Tech. 13, 97–113. https://doi.org/10.21163/GT_2018.132.08

Obergfell, C., Bakker, M., Maas, K., 2019. Identification and Explanation of a Change in the Groundwater Regime using Time Series Analysis. Groundwater 57, 886–894. https://doi.org/10.1111/gwat.12891

PDOK-https://www.pdok.nl/introductie/-/article/basisregistratie-gewaspercelen-brp- [WWW Document], n.d. URL https://www.pdok.nl/introductie/-/article/basisregistratie-gewaspercelen-brp- (accessed 7.1.23).

Philip, S.Y., Kew, S.F., Van Der Wiel, K., Wanders, N., Jan Van Oldenborgh, G., Philip, S.Y., 2020. Regional differentiation in climate change induced drought trends in the Netherlands. Environ. Res. Lett. 15. https://doi.org/10.1088/1748-9326/ab97ca

Pokhrel, P., Zhou, Y., Smits, F., Kamps, P., Olsthoorn, T., 2023. Numerical simulation of a managed aquifer recharge system designed to supply drinking water to the city of Amsterdam, The Netherlands. Hydrogeol. J. 31, 1291–1309. https://doi.org/10.1007/s10040-023-02659-w

Post, D.A., Jones, J.A., 2001. Hydrologic regimes of forested, mountainous, headwater basins in New Hampshire, North Carolina, Oregon, and Puerto Rico. Adv. Water Resour. 24, 1195–1210. https://doi.org/10.1016/S0309-1708(01)00036-7

Pouwels, J., de Louw, P., Hendriks, D., Hunink, J., Pouwels, J., de Louw, P., Hendriks, D., Hunink, J., 2020. Water system recovery after two consecutive years of extreme droughts. EGU Gen. Assem. 2020.

Reilly, T.E., Harbaugh, A.W., 2004. Guidelines for Evaluating Ground-Water Flow Models: Scientific Investigations Report 2004-5038. USGS Sci. Investig. Rep. 2004-5038 30.

Sahoo, S., Jha, M.K., 2013. Groundwater-level prediction using multiple linear regression and artificial neural network techniques: A comparative assessment. Hydrogeol. J. 21, 1865–1887. https://doi.org/10.1007/s10040-013-1029-5

Soil map of the Netherlands-https://www.tudelft.nl/en/library/collections/map-room/map-collection/thematic-maps/soil-map-of-the-netherlands-150000 [WWW Document], n.d. URL https://www.tudelft.nl/en/library/collections/map-room/map-collection/thematic-maps/soil-map-of-the-netherlands-150000 (accessed 5.14.23).

Soil Physical Units Map - WUR-https://www.wur.nl/nl/show/bodemfysische-eenhedenkaart-bofek2020.htm [WWW Document], n.d. URL https://www.wur.nl/nl/show/bodemfysische-eenhedenkaart-bofek2020.htm (accessed 12.12.23).

Sophocleous, M., Townsend, M.A., Vogler, L.D., McClain, T.J., Marks, E.T., Coble, G.R., 1988. Experimental studies in stream-aquifer interaction along the Arkansas River in Central Kansas - Field testing and analysis. J. Hydrol. 98, 249–273. https://doi.org/10.1016/0022-1694(88)90017-0

Spanoudaki, K., Stamou, A.I., Nanou-Giannarou, A., 2009. Development and verification of a 3-D integrated surface water-groundwater model. J. Hydrol. 375, 410–427. https://doi.org/10.1016/j.jhydrol.2009.06.041

Stafleu, J., Van der Meulen, M.J., Gunnink, J.L., Maljers, D., Busschers, F.S., Schokker, J., Vernes, R.W., Den Dulk, M., Ten Veen, J.H., 2019. Chapter 17: Systematic 3D Subsurface Mapping in the Netherlands. AER/AGS 179–190.

Trapp, H., Geiger, L.H., 1986. Three-dimensional steady-state simulation of flow in the sand-and-gravel aquifer, southern Escambia County, Florida. https://doi.org/10.3133/wri854278

Van Der Velde, Y., Rozemeijer, J.C., De Rooij, G.H., Van Geer, F.C., Torfs, P.J.J.F., De Louw, P.G.B., 2011. Improving catchment discharge predictions by inferring flow route contributions from a nested-scale monitoring and model setup. Hydrol. Earth Syst. Sci. 15, 913–930. https://doi.org/10.5194/hess-15-913-2011

Van Huijgevoort, M.H.J., Voortman, B.R., Rijpkema, S., Nijhuis, K.H.S., Witte, J.P.M., 2020. Influence of climate and land use change on the groundwater system of the veluwe, the netherlands: A historical and future perspective. Water (Switzerland) 12, 1–16. https://doi.org/10.3390/w12102866

Winston, R., 2019. ModelMuse Version 4: A Graphical User Interface for MODFLOW 6, U.S. Geological

Survey:Scientific Investigations Report 2019–5036. https://doi.org/10.3133/sir20195036

Winter, T.C., Harvey, J.W., Franke, O.L., Alley, W.M., 1999. Ground Water and A Single Resource Surface Water. U.S. Geological Survey, Denver, Colorado. https://doi.org/https://doi.org/10.3133/cir1139

Wolfert, H.P., Hommel, P.W.F.M., Prins, A.H., Stam, M.H., 2002. The formation of natural levees as a disturbance process significant to the conservation of riverine pastures. Landsc. Ecol. 17, 47–57. https://doi.org/10.1023/A:1015229710294

Zaadnoordijk, W.J., Bus, S.A.R., Lourens, A., Berendrecht, W.L., 2019. Automated Time Series Modeling for Piezometers in the National Database of the Netherlands. Groundwater 57, 834–843. https://doi.org/10.1111/gwat.12819

Zhou, Y., Dong, D., Liu, J., Li, W., 2013. Upgrading a regional groundwater level monitoring network for Beijing Plain, China. Geosci. Front. 4, 127–138. https://doi.org/10.1016/j.gsf.2012.03.008